Characteristics of Solar Activity at 4 and 8.6 millimeters

From May 1, 1965 to July 1, 1966

FINAL REPORT

Contract No. NASW-1118

JULY, 1966

Prepared For

Office Of Space Sciences And Applications
Physics And Astronomy Programs
NASA Headquarters – Washington, D.C.

EWEN KNIGHT

Doc. # 1158

Copy # _____

CHARACTERISTICS OF SOLAR ACTIVITY AT 4 AND 8.6 MILLIMETERS FROM MAY 1, 1965 TO JULY 1, 1966

FINAL REPORT
CONTRACT NO. NASW-1118
JULY, 1966

PREPARED FOR:

OFFICE OF SPACE SCIENCES AND APPLICATIONS
PHYSICS AND ASTRONOMY PROGRAMS
NASA HEADQUARTERS
WASHINGTON, D.C.

TABLE OF CONTENTS

ABSTRACT

A dual frequency millimeter solar radio telescope was assembled for the purpose of obtaining a measure of the average solar flux intensity and burst activity at wavelengths of 8.6 and 4 millimeters. The patrol instrument was placed in operation on 1 May 1965. Observational data was accumulated on a nearly continuous basis for a period of one year at a wavelength of 8.6 mm. Operational difficulties were encountered with the 4 mm system, primarily with the reliability of the mixer crystal used in the superheterodyne mode of operation. Consequently, only three months of data were accumulated at a 4 mm wavelength. The days of observation were broadly scattered throughout the year. A reliable mixer-crystal mount was assembled during the spring of 1966 and placed in operation during May of that year.

The quiet sun flux intensity at 8 mm was measured by direct comparison with the known flux intensity of the moon. The measured brightness temperature is 8,000°K corresponding to a flux intensity of 2×10^{-19} watts/m^2/Hz (2,000 flux units). Similar measurements were attempted at the 4 millimeter wavelength. The sensitivity of the instrument at the time of observation precluded a significant result.

A gradual increase in solar activity was noted during the observational period from 1 May 1965 to 1 May 1966 at a wavelength of 8.6 millimeters. A slowly varying component was easily detected. The first detection of burst activity at 8.6 mm was noted in the spring of 1966. Three types of burst phenomena were recorded: (a) gradual rise and fall; (b) sudden intense burst; and (c) extremely short bursts.

During the 90 day period from 1 March 1966 to 1 July 1966, several sudden intense bursts were recorded at 8.6 mm. Several were in near coincident time with events at wavelengths of 10cm or greater. A sudden intense burst on April 12, 1966 was correlated with events observed only at 6.5 cm, and this burst showed a pronounced increase in flux intensity with increasing frequency.

In addition to the short term burst activity noted above, continuous complex activity was first noted during the month of June 1966. This phenomena, not previously observed, consists of a combination of all three types of events and occurs over the period of several hours, and in some cases, several days. Correlation of this phenomena with events at other frequencies over a longer time base was in the process of analysis at the time of report preparation.

Correlation of sudden intense bursts and complex solar activity at 8.6 mm with activity at 4 mm was first obtained in June 1966. The sparse nature of the 4 mm data is inadequate to arrive at significant conclusions at this time.

1.0 INTRODUCTION

The prime objective of the program was to obtain a measure of the characteristics of solar activity at wavelengths of 8.6 and 4 mm, to aid in an understanding of the relationship of millimeter wave solar characteristics to various solar phenomena observed throughout the electromagnetic spectrum. The effort was in large part suggested by the prior work of R.J. Coates[1,2,3] and the analysis of Tanaka and Kakinuma[4] that the millimeter wave brightness of a plage area might serve as an indicator of an impending solar flare.

The one-year observing period beginning in May 1965 was in near coincidence with the period of quiet sun activity, hence a significant objective was to obtain a measure of the quiet sun level.

The first phase of the program effort was the assembly of a dual frequency radio telescope. Original design objectives and measured performance characteristics are discussed in Section 3.0. The second phase of the effort was devoted to one year of observation, commencing on 1 May 1965.

A high degree of reliability was obtained with the 35 GHz (8.6 mm) radiometer system. Essentially, continuous daily solar patrol data was obtained throughout the entire year at this frequency. Considerable difficulty was experienced with the 75 GHz system particularly in the area of mixer crystal reliability. Several design approaches were investigated leading to reliable conversion unit operation based on a Sylvania diode, Type D5252.

The program is indebted to the Electronic Research Center of NASA for their generous support in providing crystals and klystron local oscillators for evaluation.

Results obtained under the program include:

1. A precise measure of quiet solar flux intensity at a wavelength of 8.6 mm.
2. Measurement of the characteristics of the slowly varying solar component.

3. Identification of 3 types of solar burst activity at a wavelength of 8.6 mm.

4. Correlation of 8.6 mm actually with simultaneous observations at 4 mm.

A discussion of the observational data is included in Section 2.0

Failure to achieve reliable operation at 4 mm until very late in the program was the greatest disappointment. This did, however, highlight the need for greater concentration of effort on improved component reliability at frequencies above 35 GHz. An in-house supported effort was undertaken to identify those approaches which appear most promising in the achievement of the desired reliability. Considerable progress was made in this direction. As a result, the present "RF head" configuration of the 4 mm system represents a marked improvement over what was considered to be a conventional state-of-the-art approach undertaken at the outset of the program.

The significance of this research effort is considerably enhanced by the marked increase in solar burst activity recently observed at both 8.6 mm and 4 mm. Recommendations for continuation of the program are included as an addendum to this report.

---

1. R.J. Coates, J.E. Gibson, and J.P. Hagen, "The 1954 Eclipse Measurement of the 8.6 mm Brightness Distribution," Astrophysical Journal, Vol. 128, pp. 406-415, September 1958.

2. R.J. Coates, "A Model of the Chromosphere From Millimeter Wavelength Observations," Astrophysical Journal, Vol. 128, pp. 83-91, July 1958.

3. R.J. Coates,"Measurements of Solar Radiation and Atmospheric Attenuation at 4.3 Millimeters Wavelength," Proc. IRE, Vol. 46, pp. 122-126, January 1958.

4. H. Tanaka and T. Kakinuma, "The Relation Between the Spectrum of Slowly Varying Component of Solar Radio Emission and Solar Proton Event," Rept. Ionosphere Space Res. Japan, Vol. 18, pp. 32-44, No. 1, 1964.

2.0 RESULTS AND DISCUSSION OF DATA

2.1 8.6 mm Observations

Observational objectives included:

Measurement of the quiet sun flux intensity

Characteristics of the slowly varying component

Burst Characteristics

Quiet Sun Flux Intensity

The conventional method for measurement of flux intensity is predicated on a detailed knowledge of antenna aperture characteristics. The engineering detail needed for measurements of this type frequently requires a large number of antenna pattern observations. An alternate technique is to calibrate a new telescope with one previously calibrated. This requires observations by both on a common time base over a sufficient period of time to assign a flux level to the observed antenna temperature.

The technique employed under this program represents a minor modification of the simultaneous comparison method. Since a well calibrated telescope was not available for comparison of measured flux intensity at 8.6 mm, the comparison was made between the measured antenna temperature obtained when observing the moon to that obtained when observing the sun. The relatively large dynamic range required precise calibration of the radiometer detector law. Several observations of both sources were made, under similar atmospheric conditions and on several occasions within a time difference of only one or two hours in order to minimize the effect of variations in atmospheric attenuation.

If the main beam of the antenna is significantly larger than the solid angle subtended by the sun, the observed antenna temperature (assuming the atmospheric reradiation term is cancelled by antenna beam comparison) may be expressed in the form:

$$T(\Theta) = K T_s \, e^{-\gamma} e^{-\tau \sec \Theta} \qquad (2\text{-}1)$$

where:

K	=	constant depending on the antenna pattern and solar diameter
T_S	=	solar brightness temperature (^oK)
γ	=	radome loss
τ	=	atmosphere zenith opacity
Θ	=	solar zenith angle

Since the observation procedure consists of recording the output voltage of the radiometer in terms of the deflection $D_S(\Theta)$ when observing the sun, followed by a measure of the output deflection produced by an internal noise calibration source D_C, $T(\Theta)$ may be expressed in the form:

$$T(\Theta) = \frac{D_s(\Theta)}{D_C} T_C \qquad (2\text{-}2)$$

where T_C is the effective temperature of the internal noise calibration source.

Note that the technique does not require a precise knowledge of T_C.

Referring to Equation (2-2), we may define a parameter r_i in the generalized form:

$$r_i = \frac{D_s(\Theta_i)}{D_C} = K \frac{T_S}{T_C} e^{-\gamma} e^{-\tau_j \sec \Theta_i} \qquad (2\text{-}3)$$

For lunar observations with the identical instrument, the general form of r_i is:

$$r_i = \frac{K T_M e^{-\gamma}}{T_C} e^{-\tau_j \sec \Theta_i} \qquad (2\text{-}4)$$

where $T_M(\phi)$ is the integrated brightness temperature of the moon at the optical phase of observation ϕ. By selecting the time of observation with care, variations in the parameter $e^{-\tau_i \sec \Theta_i}$ can be minimized or at least known to a high degree of precision, since τ_i depends on air mass conditions and τ_i on the zenith angle of observation.

All other parameters of r_i with the exception of T_M are common to the value of r_i obtained in a solar observation except, of course, of $T_{M(\phi)}$. By this simple argument, it can be seen that the brightness temperature of the sun is obtained directly from the observed ratio of antenna temperatures (sun:moon) and the known brightness temperature of the moon at the optical phase of the observation.

The determination of the mean brightness temperature of the moon can be derived from the assumption that the brightness temperature of any region of the moon with coordinates (η, λ) is approximately described by:

$$T_{\eta,\lambda}(\phi) = A + B \cos(\phi - \Psi) \tag{2-5}$$

where ϕ is the optical phase of the region and Ψ is the empirically determined radio phase lag for the region. T_M is then:

$$T_M = \frac{\int_{Moon} T_{\eta,\lambda}(\phi) F(\eta,\lambda) d\Omega}{\int_{4\pi} F(\eta,\lambda) d\Omega} \tag{2-6}$$

where $F(\eta,\lambda)$ is the antenna receiving pattern function expressed in lunar coordinates. Noting that $d\Omega$ can be approximated by $d\eta\, d\lambda$, Equation (2-6) may be written in the form:

$$T_M(\phi) \cong \frac{\iint T_{\eta,\lambda}(\phi) F(\eta,\lambda) d\eta\, d\lambda}{\iint F(\eta,\lambda) d\eta\, d\lambda} \tag{2-7}$$

Since ϕ is the optical phase of the subterrestrial point at the time of observation and the latitude dependence of T_M is negligible, we may let $F(\lambda,\eta) = f(\lambda)\ g(\eta)$ and rewrite Equation (2-7) in the form:

$$T_M(\phi) \cong \frac{\int_{-\pi/2}^{\pi/2} f(\lambda)\, d\lambda \int_{\pi/2}^{\pi/2} \left(A + B\cos(\phi - \Psi + \eta)\right) g(\eta)\, d\eta}{\int_{-\pi/2}^{\pi/2} f(\lambda)\, d\lambda \int_{\pi/2}^{\pi/2} g(\eta)\, d\eta} \qquad (2\text{-}8)$$

Three approximations to the form of the antenna pattern will be considered:

Case I

$$f(\lambda) = 1 - \frac{\pi}{2} \le \lambda \le \frac{\pi}{2}$$

$$g(\eta) = 1 - \frac{\pi}{2} \le \eta \le \frac{\pi}{2}$$

$$T_M(\phi) \cong A + \frac{\pi}{2} B\cos(\phi - \Psi) \qquad (2\text{-}9)$$

Case II

$$\left.\begin{aligned} f(\lambda) &= \cos^2 \lambda/2 \\ g(\eta) &= \cos^2 \eta/2 \end{aligned}\right\} -\frac{\pi}{2} \le \lambda, \eta \le \frac{\pi}{2}$$

$$T_M(\phi) \cong A + \frac{\pi+4}{2\pi+4} B\cos(\phi - \Psi) \qquad (2\text{-}10)$$

Case III

$$\left.\begin{aligned} f(\lambda) &= \cos\lambda \\ g(\eta) &= \cos\eta \end{aligned}\right\} -\frac{\pi}{2} \le \lambda, \eta \le \frac{\pi}{2}$$

$$T_M(\phi) = A + \frac{\pi}{4} B\cos(\phi - \Psi) \qquad (2\text{-}11)$$

Thus, the mean lunar temperature can be expressed:

$$T_M(\phi) = A + \alpha B\cos(\phi - \Psi) \qquad (2\text{-}12)$$

where:

$\alpha = 2/\pi$ for Case I - Square antenna pattern

$\frac{\pi+4}{2\pi+4}$ for Case II - $\cos^2 \lambda/2$ antenna pattern

$\pi/4$ for Case III - $\cos \lambda$ antenna pattern

The antenna performance characteristics of the dual frequency solar telescope are best represented by the Case II distribution given above. (Note also that Case II is close to the average of the 3 cases considered.)

Utilizing an average of the constant and first harmonic temperatures measured by J. Copeland,[5] Expression (2-12) takes the form:

$$T_M(\phi) = (197 + 22 \cos(\phi - 35°)\,°K \qquad (2\text{-}13)$$

The first series of observational measurements to establish the quiet sun level were undertaken during the month of November 1965. The observations made on three days during that month are summarized in Table 2-1.

TABLE 2-1

Date	Sec Θ_z	Weather	Lunar Signal Deflection	Calibration Signal Deflection
November 2, 1965	2.2	Clear	6.0 ± 0.5 mm	129.0 mm
			9.0 ± 0.5	192.5
November 4, 1965	1.6	Clear	9.5 ± 0.5	183.5
			9.0 ± 0.5	185.0
			10.0 ± 0.5	187.5
November 19, 1965	1.5	Clear	11.2 ± 0.5	215.0
			10.8 ± 0.5	215.0
			11.0 ± 0.5	215.0

The mean lunar temperatures, calculated from Equation (2-13) for the optical phase at the times of observation are given in Table 2-2.

TABLE 2-2

Date	Optical Phase	Microwave Phase	$T_M(\phi)$
November 2, 1965	292°	257°	192°K
November 4, 1965	316°	281°	201°K
November 19, 1965	137°	102°	190°K

Assuming a nominal value of τ of 0.03, the actual values of the system constant $Ke^{-\gamma}/T_c$ were calculated (using Equation (2-5)). The numerical values obtained are shown in Table 2-3.

TABLE 2-3

Date	$\frac{Ke^{-\gamma}}{T_c}$ ($°K^{-1}$)
November 2, 1965	
Scan 1	2.57×10^{-4}
Scan 2	2.58×10^{-4}
November 4, 1965	
Scan 1	2.66×10^{-4}
Scan 2	2.55×10^{-4}
Scan 3	2.76×10^{-4}
November 19, 1965	
Scan 1	2.83×10^{-4}
Scan 2	2.74×10^{-4}
Scan 3	2.78×10^{-4}

The mean system constant is $2.68\ (+0.15, -0.13) \times 10^{-4}\ (^{\circ}K)^{-1}$, based on the average of the values given in Table 2-3.

The solar observational data (sun to calibration level ratio) was converted to apparent brightness temperature corresponding to various "deflection ratio" values are summarized in Table 2-4. The absolute error in these values is estimated at slightly greater than 5%, assuming "no error" in the value of T_M, 5% in the value of r and 2% in the value of the atmospheric correction.

TABLE 2-4

Deflection Ratio*, r'	Solar Brightness Temperature, °K
1.0	3,740
1.2	4,480
1.4	5.230
1.6	5,980
1.8	6,720
2.0	7,460
2.2	8,220
2.4	8,960
2.6	9,700
2.8	10,400
3.0	11,200

* Corrected for atmospheric attenuation.

The average brightness temperature of the sun at 8.6 mm during the 3-month period from 1 September 1965 through 31 December 1965 (the quiet period noted during all observations) was 8,000°K ± 400°K, corresponding to a flux intensity of 2×10^{-19} watts/sq. meter/Hz (2,000 flux units).

5. J. Copeland, "Radio Observations of the Moon and Venus at 8.6 mm Wavelength", Ewen Knight Corporation Doc. #1088, Contract No. NASw-593.

Slowly Varying Component

As a consequence of atmospheric effects, the burst phenomena which follows a typical gradual rise and fall is more easy to detect than the slowly varying component. The slowly varying component is best obtained by plotting the average solar intensity (appropriately corrected for atmospheric attenuation) on a day-to-day basis obtained during the period of $\pm$ one hour about the meridian. Graphical plots of this type are shown in Figures 2-1 and 2-2. (Note that Figure 2-1 covers the period from September 1, 1965 through February, 1965 and Figure 2-2 provides a four-month overlap covering the six-month time period from November 1, 1965 to April 30, 1966). These figures provide a comparison of the observed brightness temperature of the sun at 35 GHz with the reported flux level at 3 GHz for each day of observation. The 3 GHz data includes significant flares as well as the average sun level. The 8.6 mm data is plotted at the top of each figure. Data points shown with a clear circle refer to clear days of observation. Those shown as a black dot refer to days of heavy overcast. The differentiation between clear and overcast conditions is important since the atmospheric correction was made without including consideration for cloud attenuation. Hence, the data points shown as black dots would, in fact, be representative of a higher intensity than indicated on the graph.

Referring to Figures 2-1 and 2-2, the following features are worthy of note:

1. The average brightness temperature of the sun at 8.6 mm during the months of October through February was 8,000°K corresponding to 2,000 flux units.
2. There appears to be a strong correlation between periods of intense solar activity at 3 GHz and an increase in the average brightness temperature observed at 35 GHz.
3. The scatter in the average intensity level at 35 GHz appears to increase during periods corresponding to flare activity at 3 GHz.

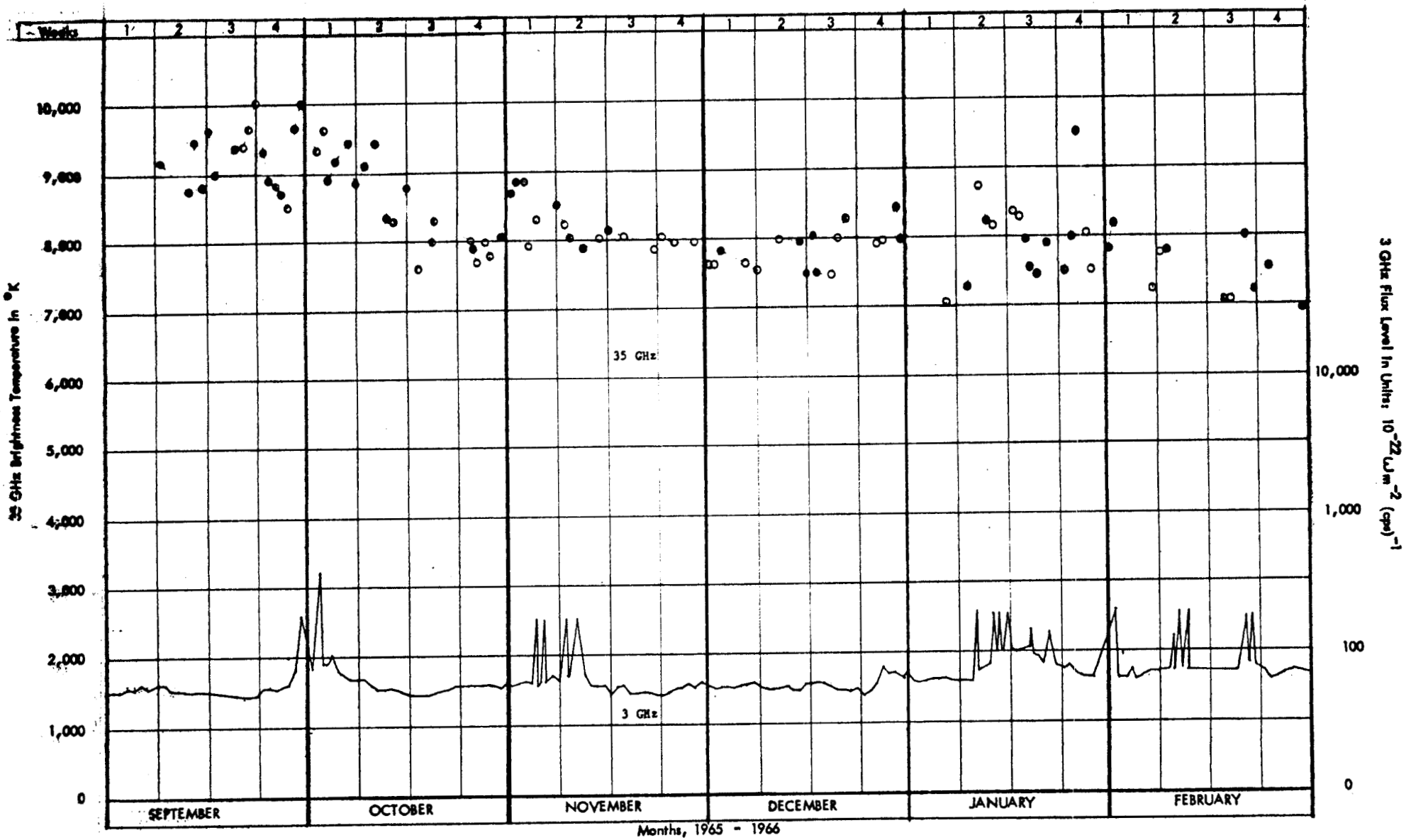

COMPARISON OF SOLAR ACTIVITY

NASW-1118

FIGURE 2-1

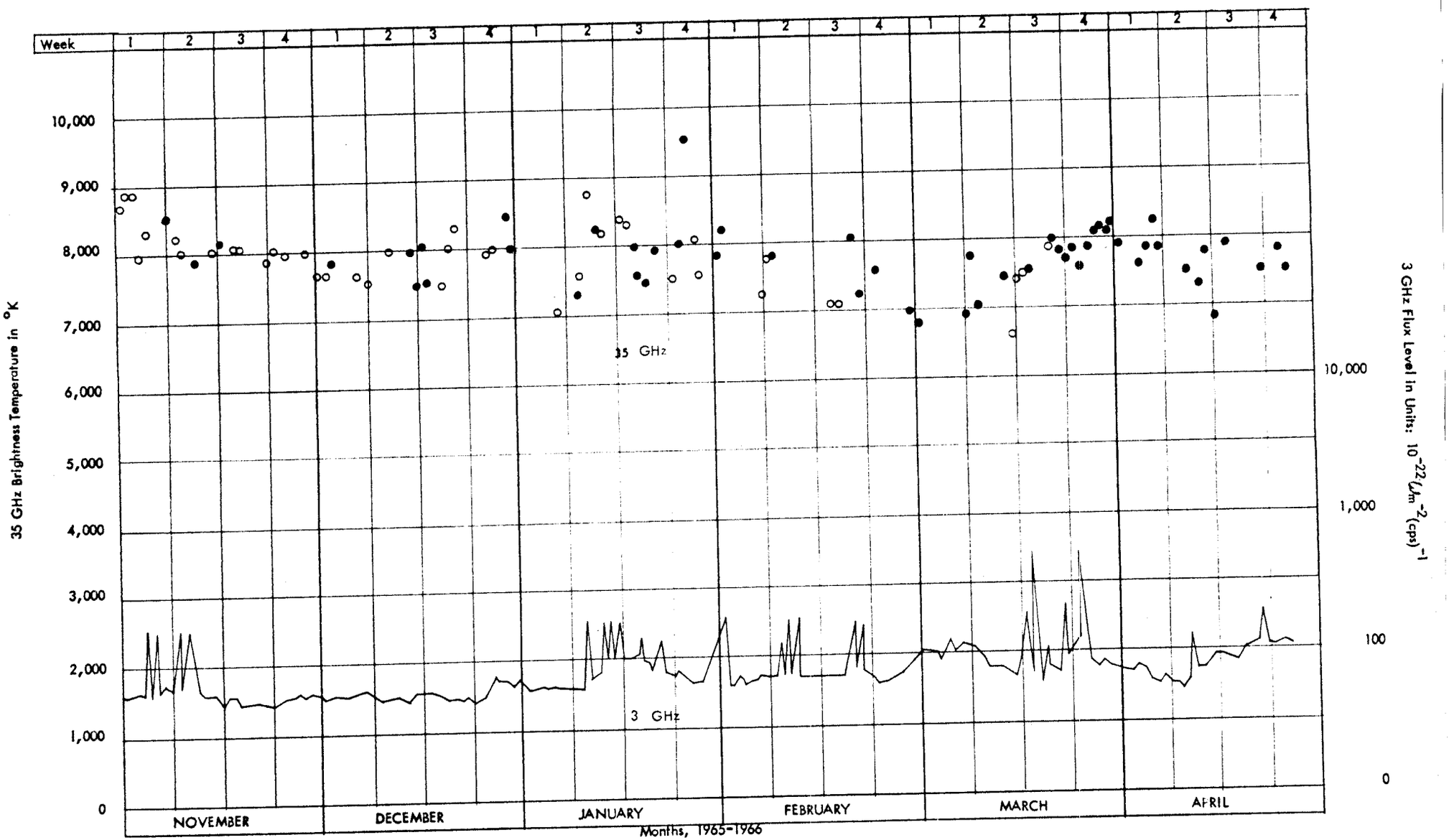

COMPARISON OF SOLAR ACTIVITY

NASW-1118

FIGURE 2-2

4. An apparent decrease in the average brightness temperature of the sun during the months of March and April of 1966 is most likely related to the poor observing conditions during that period. An appropriate correction for cloud attenuation would reduce the level of scatter and increase the average intensity noted on the graph. This correction was not introduced since appropriate values are not as yet well defined.

Burst Characteristics

Recorded burst activity at 8.6 mm was divided into three classes: gradual rise and fall, sudden intense and extremely short. In addition, combinations of these three extending over long periods of time (frequently more than one day) were observed as a relatively new phenomena early in June 1966.

Identification of the gradual rise and fall type of burst phenomena requires relatively clear, stable weather conditions to minimize confusion with variations in atmospheric attenuation. The intensity of this phenomena appears to have a mean value of approximately 3% above the quiet sun level (50 to 60 flux units). Bursts of this type became relatively common after January 1, 1966 and usually occurred over periods of one to two hours.

The sudden intense bursts is most easily recognized. It is frequently preceded by a gradual increase in solar intensity though this is not always the case. It is equally probable that the burst will be followed by a reduction in average solar intensity, to a few tens of flux units higher than the flux intensity prior to the burst. The level then slowly decays typical of the "fall" portion of a "gradual rise and fall" burst characteristic.

The sudden intense burst usually lasts for a period of one or two minutes, and demonstrates either considerable structure, i.e., several intense bursts in rapid sequence or an individual pronounced burst showing a sharp rise followed by a more gradual decay.

Typical sudden intense bursts recorded during the months of March and April 1966 are shown in Figure 2-3 through 2-9. The following features are worthy of note in reference to the recordings of these events:

1. The dual burst which occurred on 15 March at 18:04 U.T. and 18:05 U.T. was preceded by an abrupt increase in the average flux intensity approximately 4 minutes prior to the first burst. This abrupt increase was preceded by a gradual increase corresponding to approximately 60 flux units over a period of one hour. Following the dual burst, the plateau of the average solar intensity continued at approximately 120 flux units above the quiet sun level for a period of 4 minutes and then abruptly decreased to approximately 70 flux units and gradually decayed over a period of two hours. (Figure 2-3).
2. Two sudden intense bursts occurred on March 16 at 19:03 U.T. and 19:10 U.T. These bursts were on the "fall" portion of a gradual rise and fall type of burst which had reached its peak approximately 30 minutes prior to the first sudden intense burst. (Figure 2-4).
3. The single intense burst of March 18, which occurred at 14:12 U.T. was preceded by a gradual rise and fall and occurred on the "fall" portion. The quiet sun level immediately following the burst was 60 flux units below the level immediately preceding the burst. (Figure 2-5).
4. The sudden intense burst of March 24 consisted of three major outbursts at 15:20, 15:28, and 15:28:20 U.T. Each bursts was more intense than the one preceding. (Figure 2-6).
5. A pair of sudden intense bursts occurred on April 6 at 15:52 and at 15:52:40 U.T. The bursts were followed within 10 minutes by a complex structure of increased solar intensity lasting for a period of 20 minutes at a mean level of 120 flux units above the average solar flux for that day of observation. (Figure 2-7).

6. The sudden intense burst which occurred on April 12 at 17:18 U.T. consisted of an initial outburst with a peak intensity of 200 flux units followed within one minute by a second burst of approximately 60 flux units. The first peak occurred at 17:18:40 U.T. -- duration, 20 seconds. The burst decayed to 3% above the quiet sun level at 17:19 U.T., and immediately followed by the second burst which lasted for a period of 10 to 15 seconds with the peak occurring at 17:19:10 U.T. The entire recording of the event above the average sun level for the day of observation lasted for a time period of approximately two minutes. (Figure 2-8).

The burst was coincidently observed at the same wavelength (8.6 mm) by the Prospect Hill Radio Telescope (30-foot diameter) while operating in a raster scan patrol of solar activity. The burst was observed near the solar equator on the western limb. The apparent disk diameter of the sun as measured by the high resolution patrol instrument increased 12.8% during the time of the burst as measured directly by the scan of the antenna "pencil beam" (4 arc minutes) across the burst phenomena.

This burst was also observed at the AFCRL Sagamore Hill Radio Observatory which is instrumented for daily solar patrols at 606, 1415, 2695, 4995 and 8800 MHz. The flare was observed only at 4995 and 8800 MHz at the Sagamore Hill Observatory. The burst intensity showed a marked increase with frequency. The measured peak intensity of the burst at 8800 MHz was 123.8 flux units and at 35 GHz, 200 flux units. (Figure 2-9).

We are indebted to J. Castelli of the Sagamore Hill Observatory for Figure 2-9 which is a record of the April 12 burst observed at 4995 and 8800 MHz.

Just prior to the first detection of sudden intense burst activity, the daily records showed extremely short burst activity. When first detected, this phenomena was considered to be equipment difficulty or possibly RFI. Attempts to trace the source of difficulty to equipment were unsuccessful. The phenomena consistently appeared on the record only

during those times when the antenna was directed toward the sun.

The extremely short bursts appear as individual spikes on the output recording with a maximum duration of ten seconds. This phenomena was difficult to detect at first since the chart speed throughout the program had been set at a nominal value of 2.5 mm per minute. The time markers are spaced at this interval on Figures 2-3 through 2-8.

Extremely short bursts typical of those observed during March and April 1966 are shown in Figure 2-10 through 2-16.

The extremely short burst (ESB) shown in Figure 2-10 may be difficult to observe on the copy of the record shown in the figure. This event is more easily seen on the original data recording.

The negative going square-wave pulse on the record of April 4 is a calibration signal (Figure 2-12).

Five ESB were observed on April 13. (Figure 2-13, 14 and 15) note that on the expanded scale (lower record) the general level of solar activity shows fluctuations of the order of $\pm$ 10 flux units with a definite indication of complex structure in addition to ESB.

The three bursts noted on the record shown on Figure 2-14 are difficult to sort from other possible complex disturbances, both prior to and following those events designated on the record as ESB.

The time coincidence of the ESB on 25 April (Figure 2-16) with a 3 GHz flare beginning approximately 40 seconds later clearly points out the difficulty previously experienced in detection of bursts of this type. The ESB more easily identified on the expanded scale available through the use of a 6-channel strip chart recorder provided on loan by NASA-ERC.

Following the identification of ESB as a solar event, the recording system was adjusted to provide a chart speed of 25 mm per minute. The expanded scale factor at 75 GHz was set at 2:1; at 35 GHz, 5:1. In addition, the integration time constant at 75 GHz was reduced from 10 seconds to 3 seconds and at 35 GHz from 3 seconds to 1 second. With these equipment changes, the ESB are more easily detected.

A fourth characteristic of solar activity at 8.6 mm was noted beginning early in May 1966 and continuing through June. This characteristic is best described as a combination of all three previously described burst phenomena: gradual rise and fall, sudden intense bursts, and extremely short bursts. We have had relatively brief experience with this type of activity, insufficient to analyze in detail their significance relative to other solar phenomena. This type of complex solar activity lasts for periods of several hours and frequently continues for several days. The onset of this complex structure is relatively abrupt and continues for a minimum time period of three or four hours. The activity noted on May 2 is typical of this complex structure. Selected segments of the record obtained on May 2 are shown in Figure 2-17. A summary of the times of specific events is presented in Figure 2-18.

Referring to Figure 2-17, note the general complexity of the structure, though only one burst event at 1745, has been tabulated. It is apparent that a series of very complex events was in process throughout the complete time period shown on the record.

Of particular interest (Figure 2-17) are the series of ESB preceding the ESB at approximately 13:39 U.T. (May 2, 1966) which is coincident with a flare observed at 3 GHz.

On the following day, May 3, the general level of activity had subsided, however, complex structure interspersed with ESB was readily apparent on the record (Figure 2-19).

In summary a marked change in the character of solar activity at a wavelength of 8.6 mm became apparent shortly after the quiet period in the fall of 1965. The complexity of the observed activity increased from separate sudden intense bursts to a far greater number of extremely short bursts and ultimately to long periods of complex combinations of both phenomena interspersed with gradual changes in the average solar flux level.

Date	Frequency	No. of Events For the Day	U. T. Begin	U. T. End	Burst Amplitudes % 35 GHz	Other
15 Mar 66	35GH$_z$	2	18:04	18:04:20	2.8	
			18:04:40	18:05	2.8	
	3GH$_z$	2	15:20	15:23		
			19:11	19:14		
	.5GH$_z$	1	01:07	01:11		6-9x Median Flux

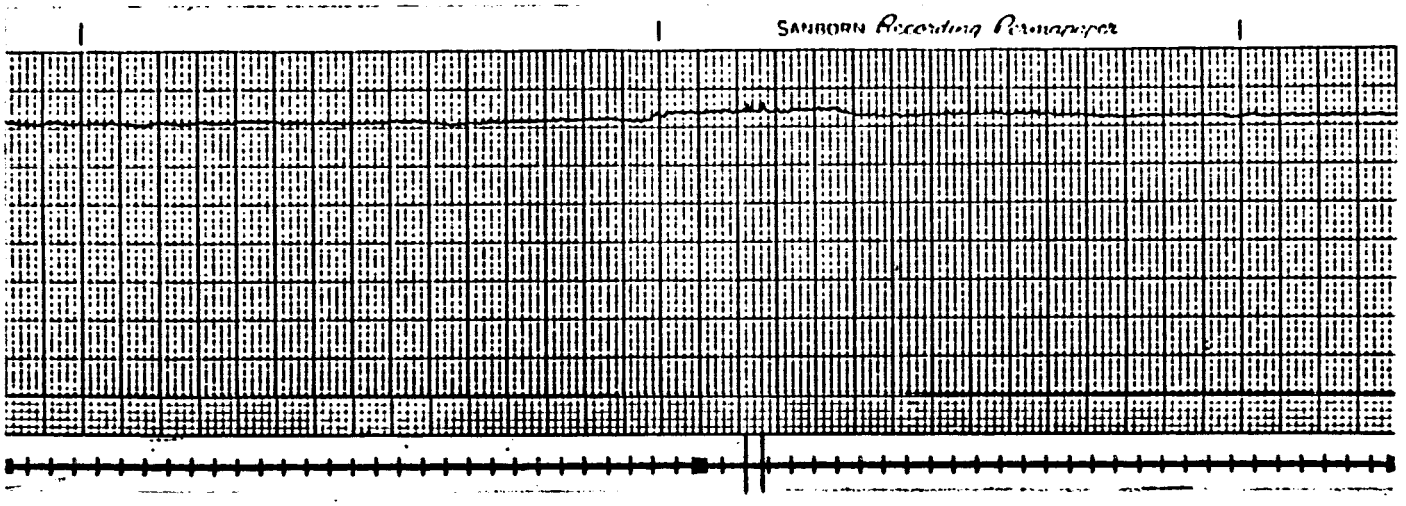

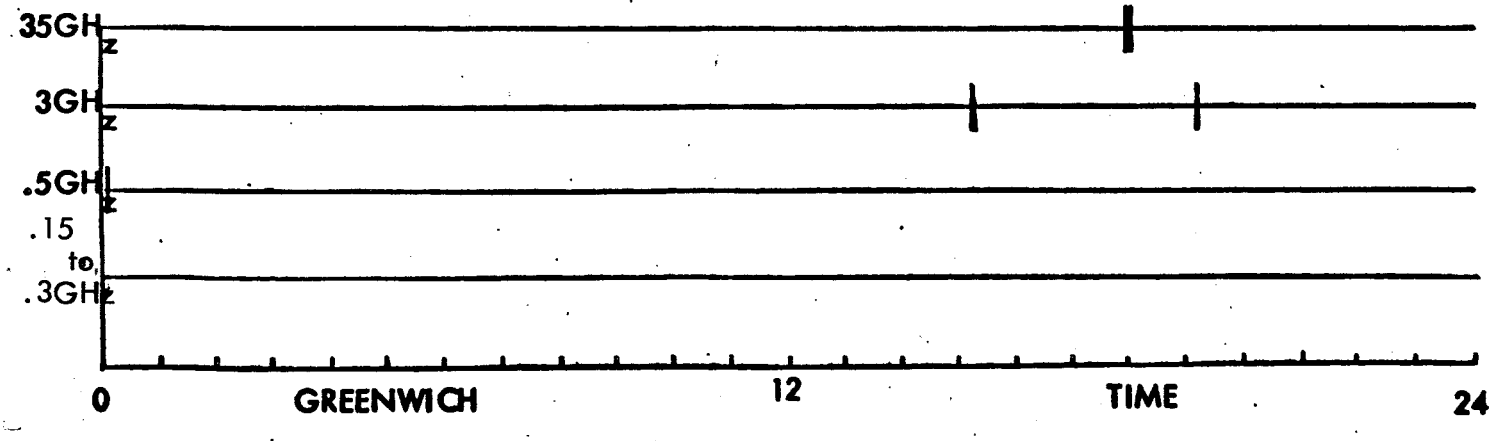

FIGURE 2-3

Date	Frequency	No. of Events For the Day	U. T. Begin	U. T. End	Burst Amplitudes % 35 GHz	Other
16 Mar 66	35GH$_z$	2	19:03:20	19:04	15	
			19:09:10	19:09:50	15	
	3GH$_z$	1	15:14	15:19		
	.5GH$_z$					
	.15-.3GH$_z$	1	22:55	22:58		> 39x Median Flux

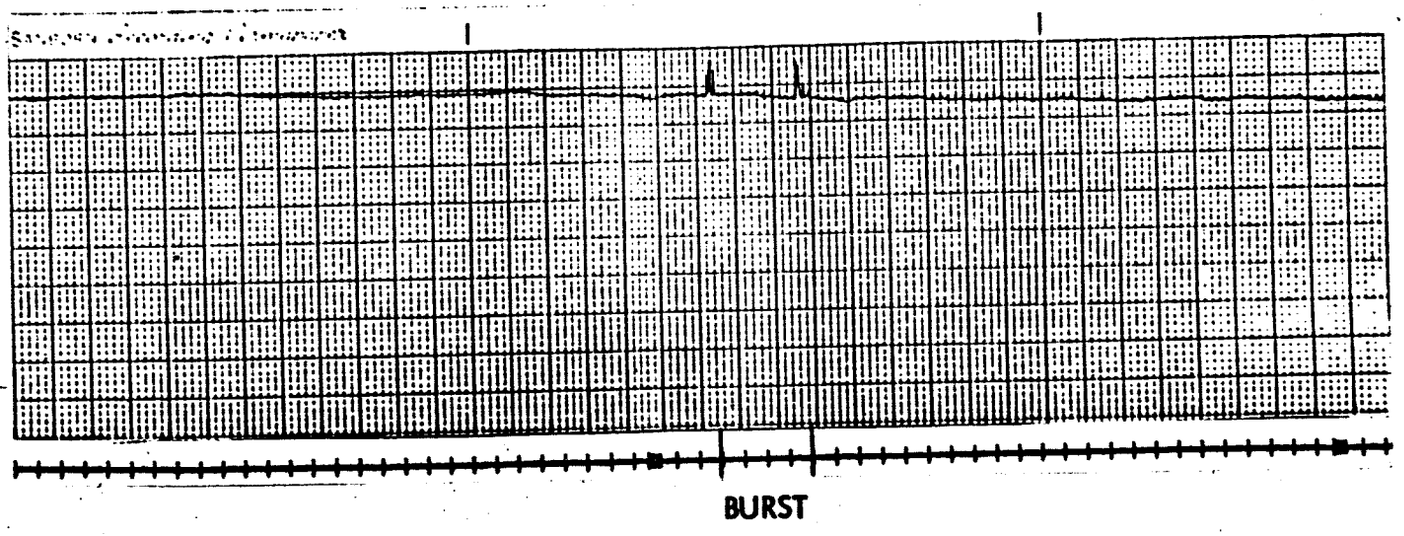

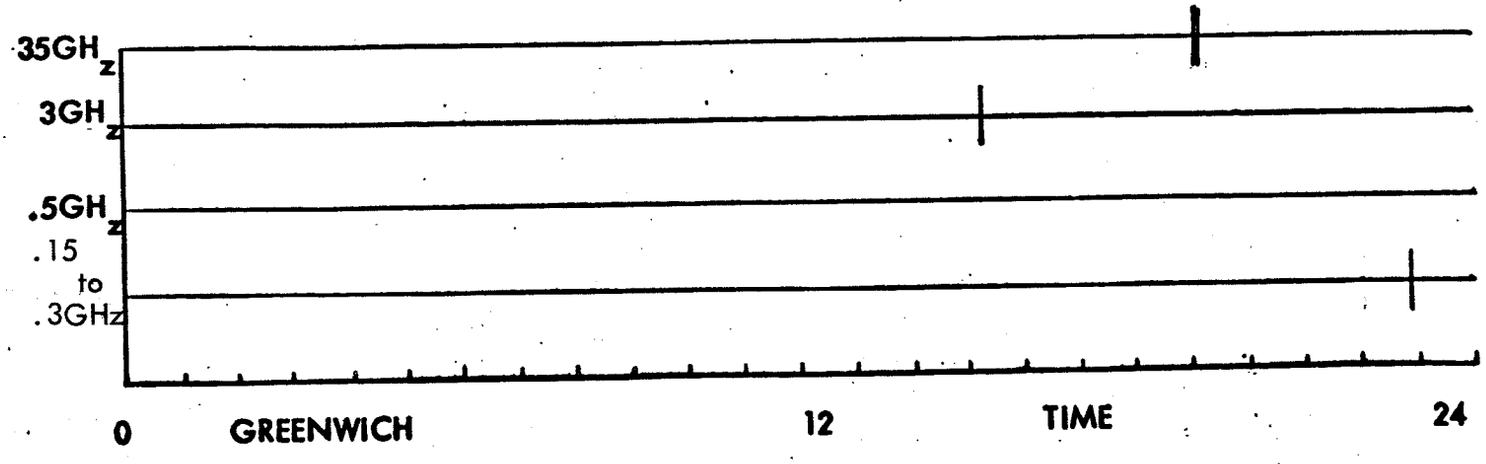

FIGURE 2-4

Date	Frequency	No. Of Events For the Day	U. T. Begin	U. T. End	Burst Amplitudes %35 GHz	Other
18 Mar 66	35GH$_z$	1	14:12:20	14:13	34	
	3GH$_z$	2		14:45		
			19:05	22:08		
	.15-.3 GH$_z$	2	10:45	11:15		
			10:45	11:05		

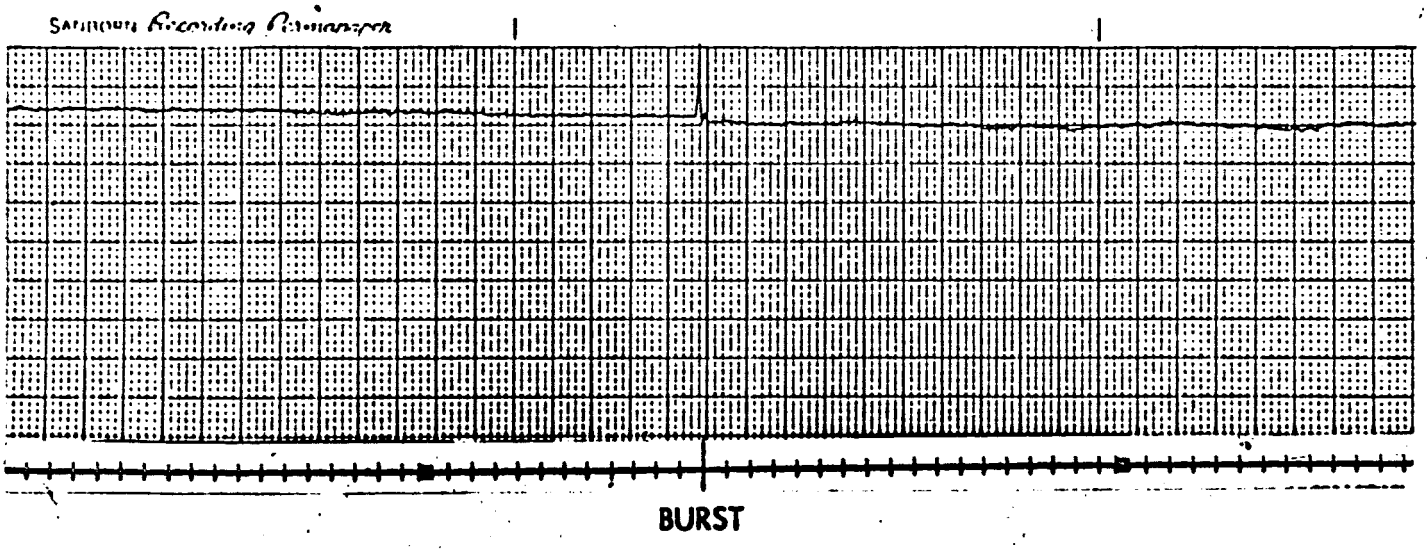

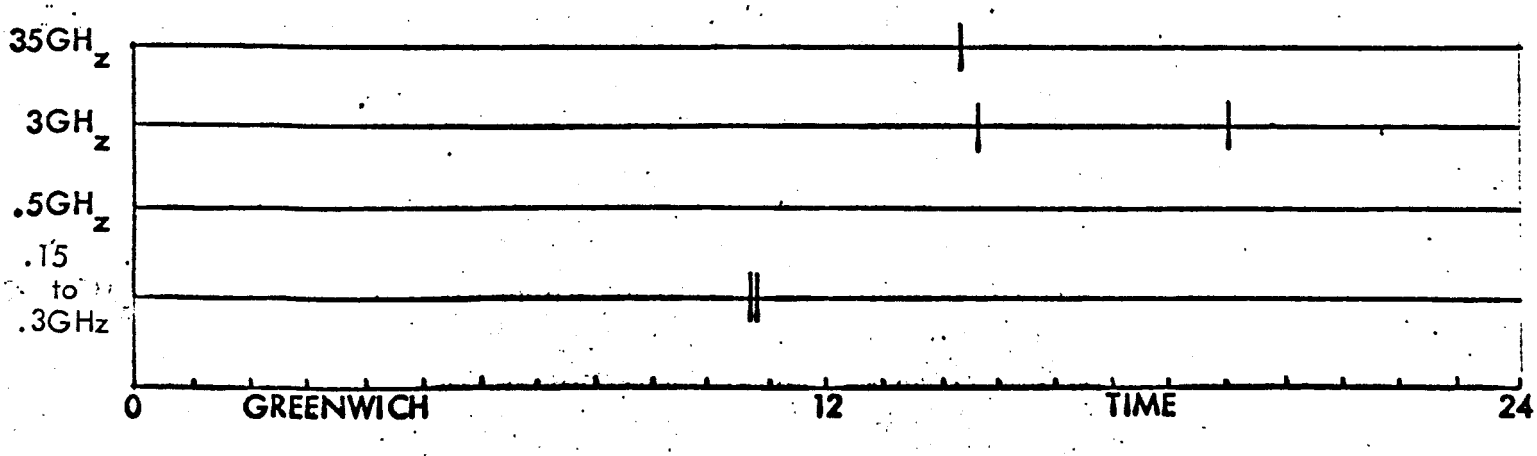

FIGURE 2-5

Date	Frequency	No. Of Events For the Day	U. T. Begin	U. T. End	Burst Amplitudes % 35 GHz	Other
24 Mar 66	35GH$_z$	3	15:27:20	15:27:40	1.8	
			15:28	15:28:20	36	
			15:28:20	15:28:40	≥36	
	3GH$_z$	1	09:55	10:03		
	.15-.3 GH$_z$	1	01:56	02:00		

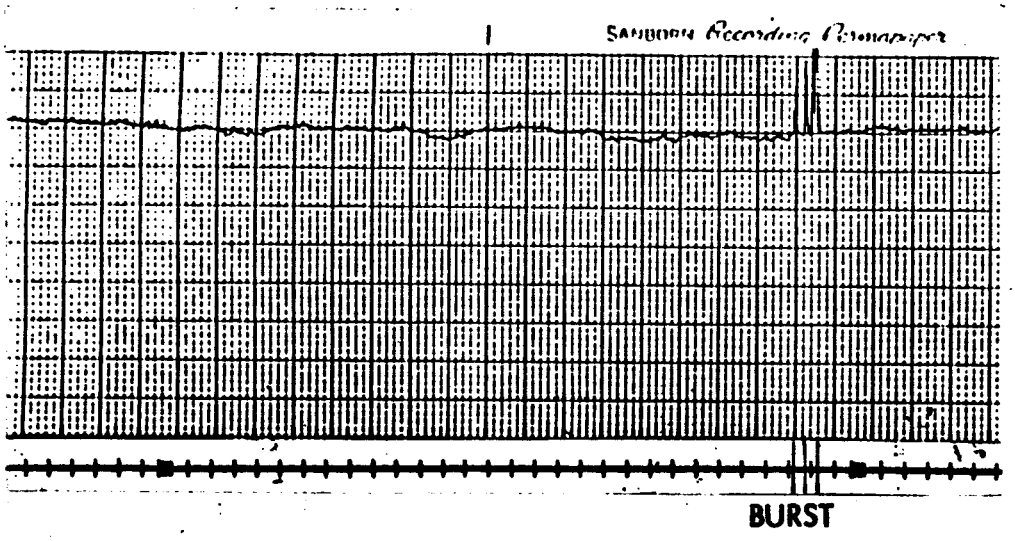

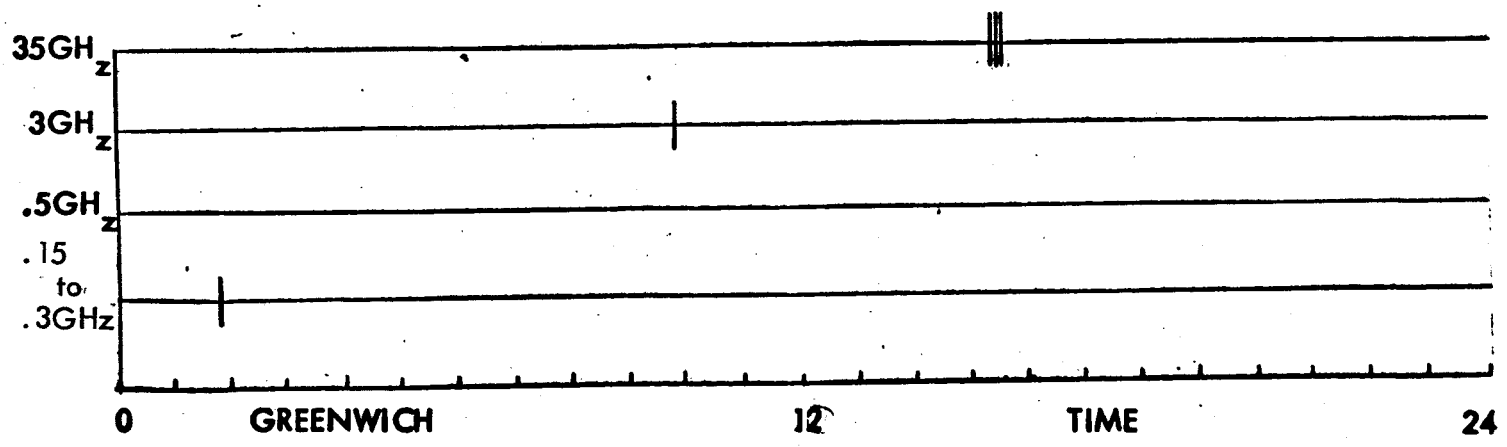

FIGURE 2-6

Date	Frequency	No. Of Events For the Day	U. T. Begin	U. T. End	Burst Amplitudes % 35 GHz	Other
6 Apr 66	35GH$_z$	2	15:52	15:52:15	≥48	
			15:52:40	15:53	47	
	3GH$_z$	1		15:39		
	.15-.3 GH$_z$					

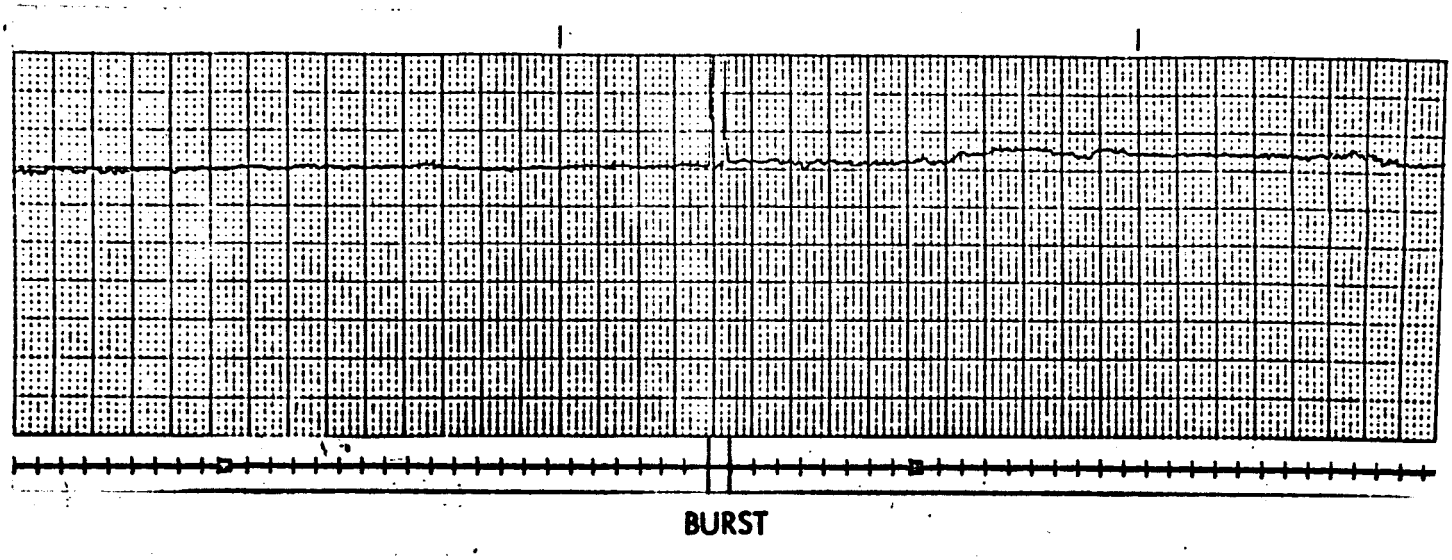

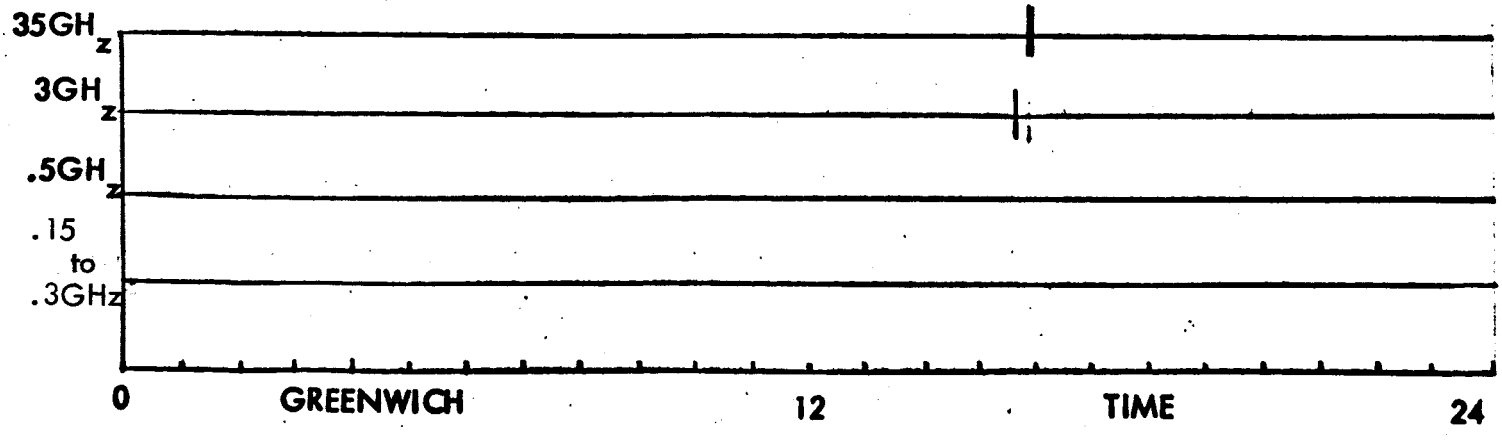

FIGURE 2-7

Date	Frequency	No. of Events For the Day	U. T. Begin	U. T. End	Burst Amplitudes % 35 GHz	Other
12 Apr 66	35GH$_z$	1	17:18	17:20	10	
	3GH$_z$	1	16:30	16:38		
	.5GH$_z$					
	.15-.3GH$_z$					

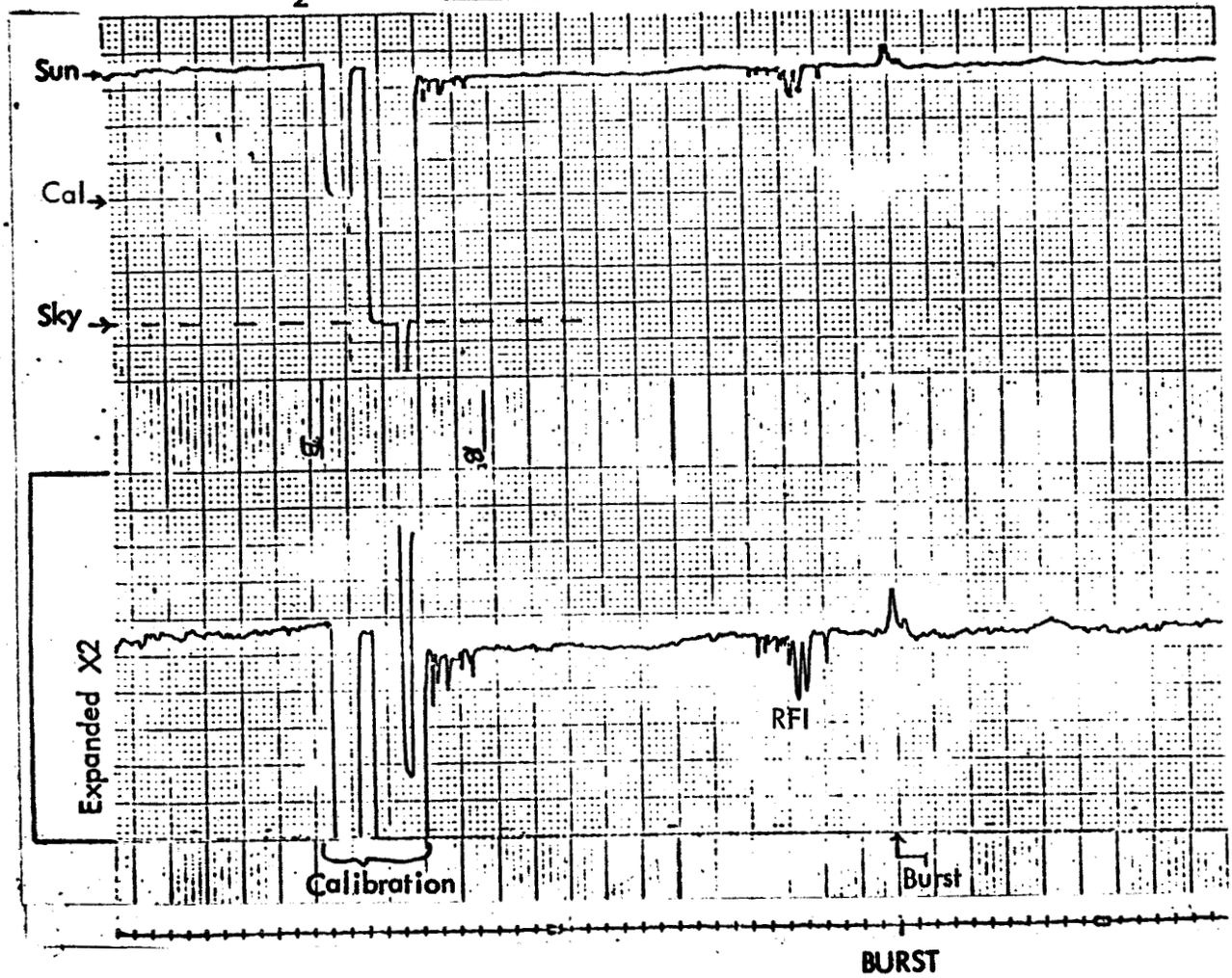

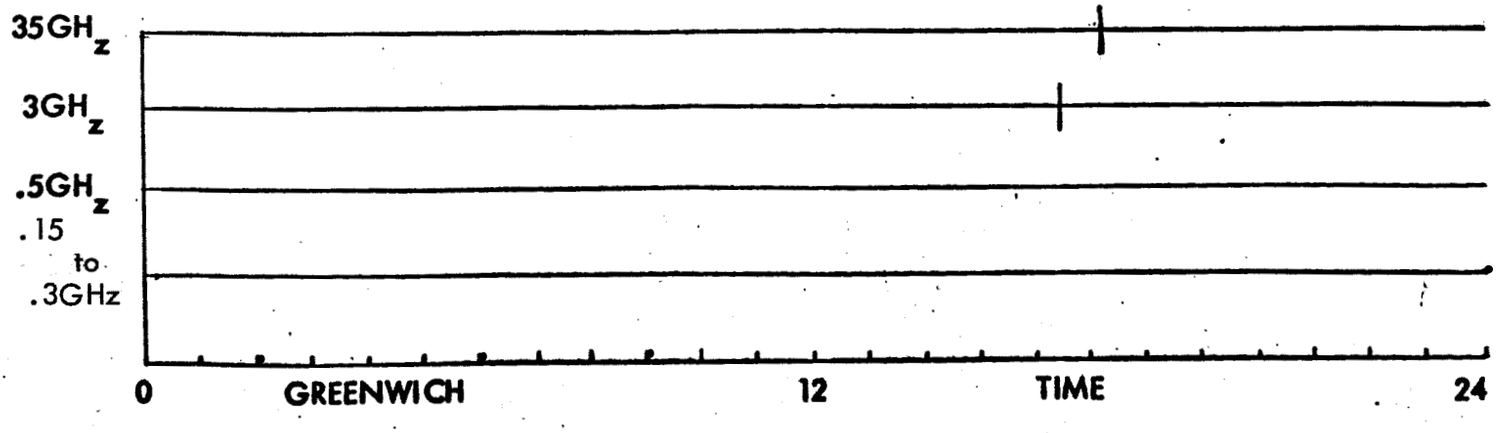

FIGURE 2-8

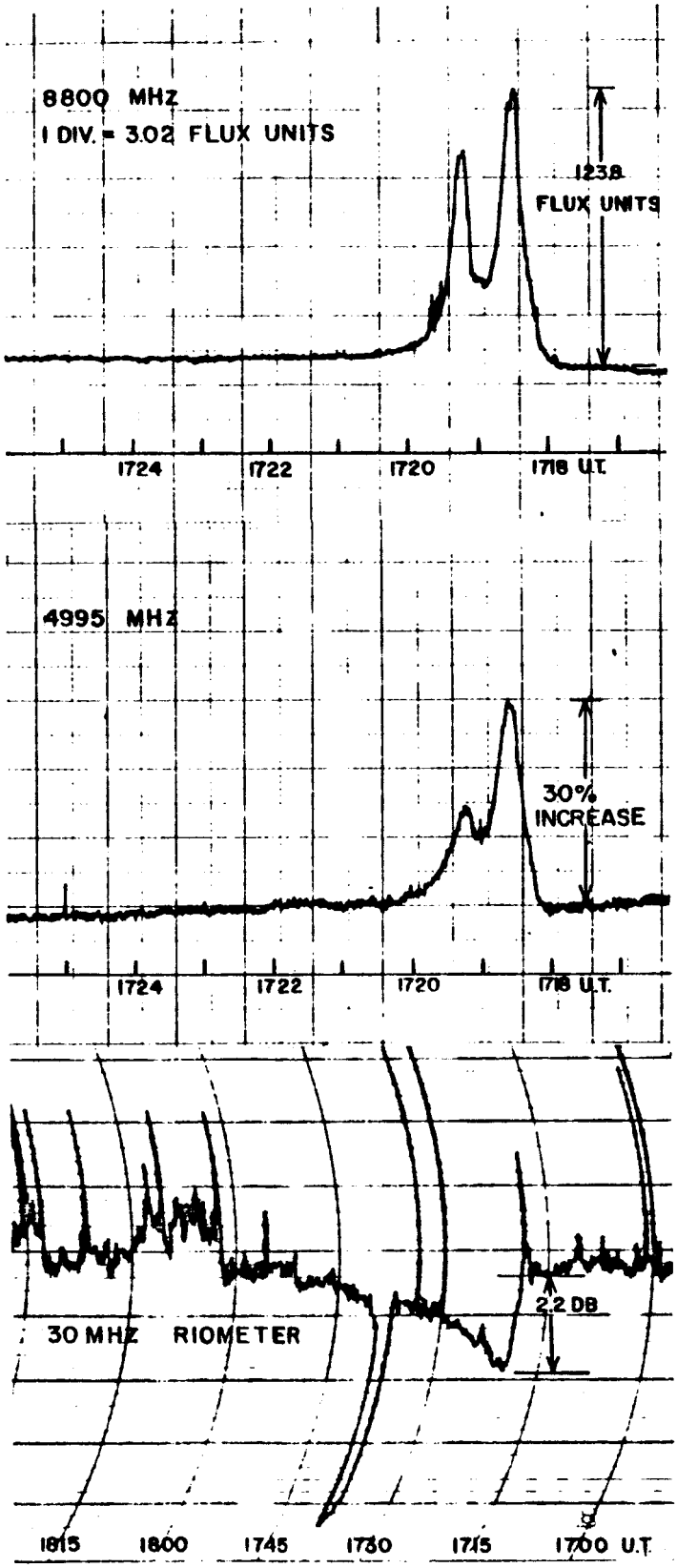

COMPLEX BURST OBSERVED AT APPROXIMATELY 1718 U.T.,
APRIL 12, 1966 AT AFCRL HAMILTON, MASS.
NO SIGNIFICANT FLUX INCREASE OBSERVED AT 2695, 1415, OR 606 MHz

Investigator - J. Castelli

FIGURE 2-9

Date	Frequency	No. Of Events For the Day	U. T. Begin	U. T. End	Burst Amplitudes % 35 GHz	Other
23 Mar 66	35GH$_z$	1	20:29:40	20:29:42	1.9	
	3GH$_z$	2	13:30	13:34		
			19:38	22:16		
	.15-.3 GH$_z$	1	20:31	21:45		6-9x Median Flux

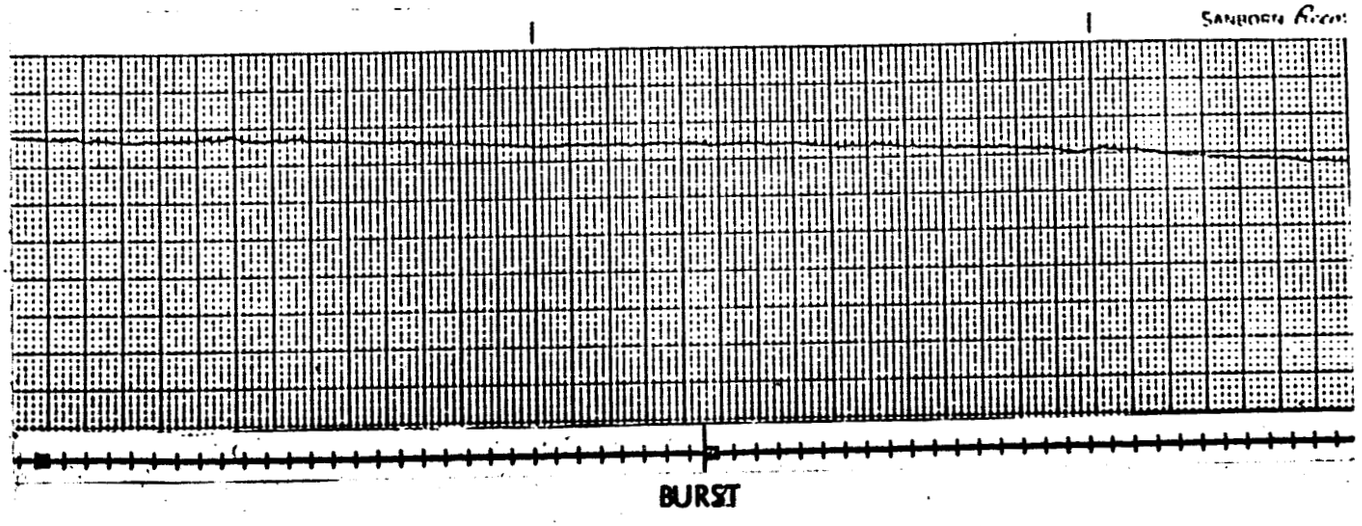

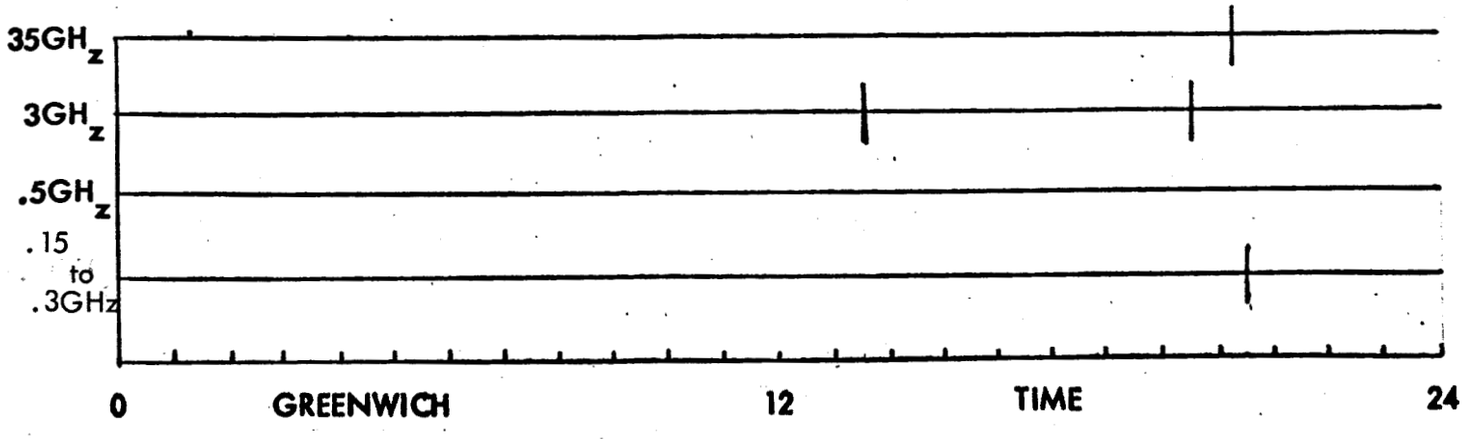

FIGURE 2-10

Date	Frequency	No. Of Events For the Day	U. T. Begin	U. T. End	Burst Amplitudes % 35 GHz	Other
31 Mar 66	35GH$_z$	1	19:16:30	19:16:34	3	
	3GH$_z$	2	12:36	13:44		
			22:44	19:00		
	.15-.3 GH$_z$					

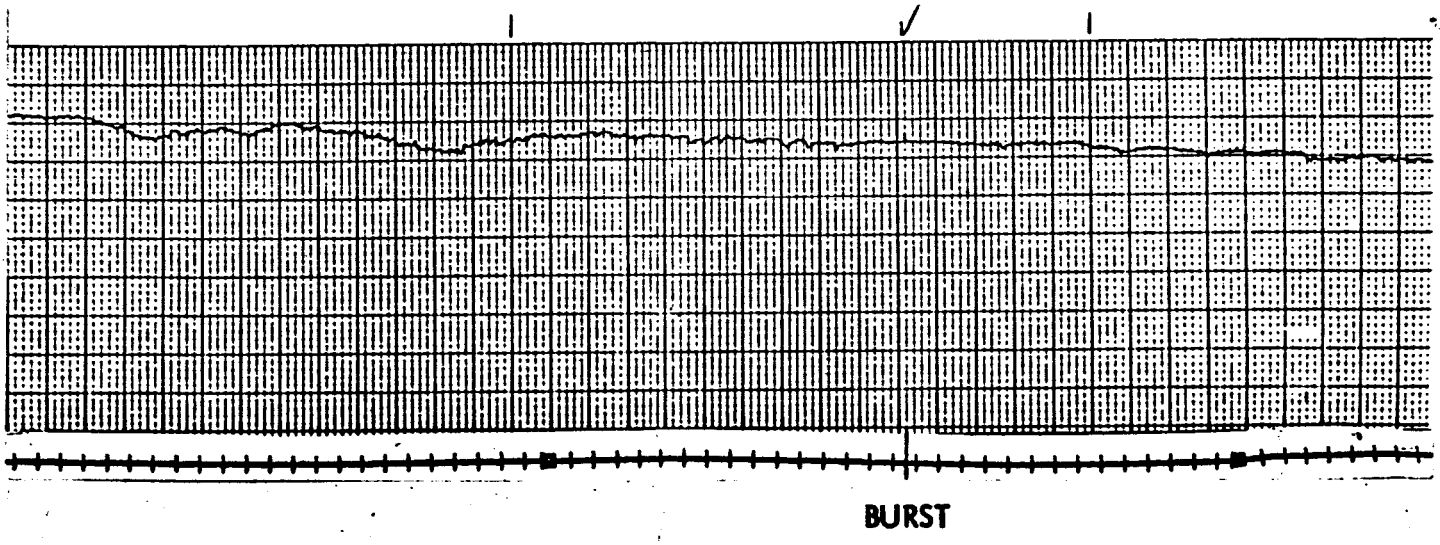

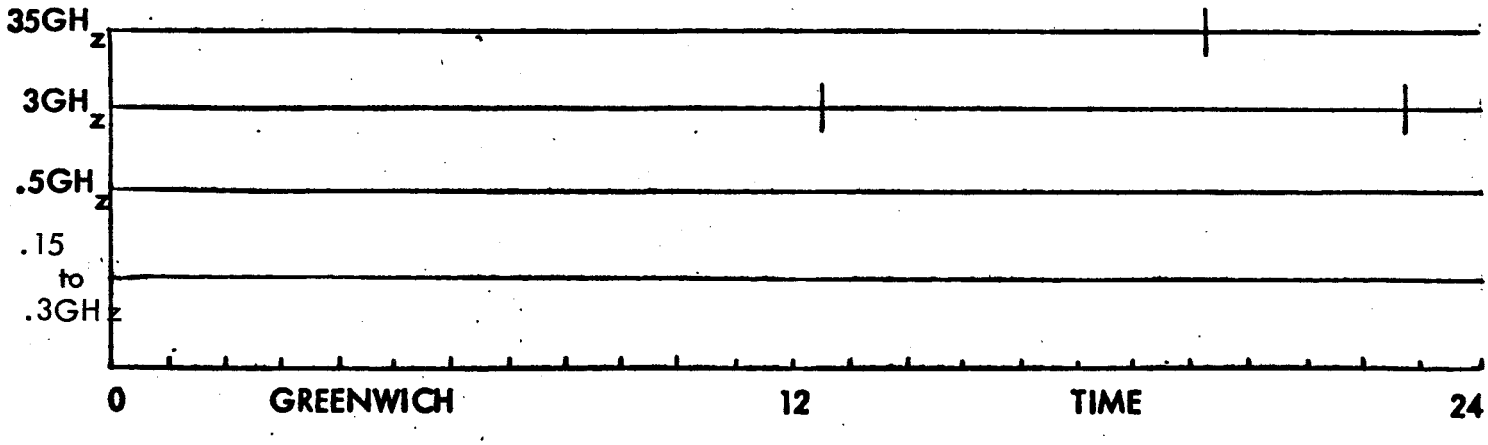

FIGURE 2-11

Date	Frequency	No. Of Events For the Day	U. T. Begin	U. T. End	Burst Amplitudes % 35 GHz	Other
4 Apr 66	35GH$_z$	2	15:25:20	15:25:25	3.3	
			15:41	15:41:20	4.8	
	3GH$_z$	2	14:57			
			18:36	21:08		
	.15-.3 GH$_z$					

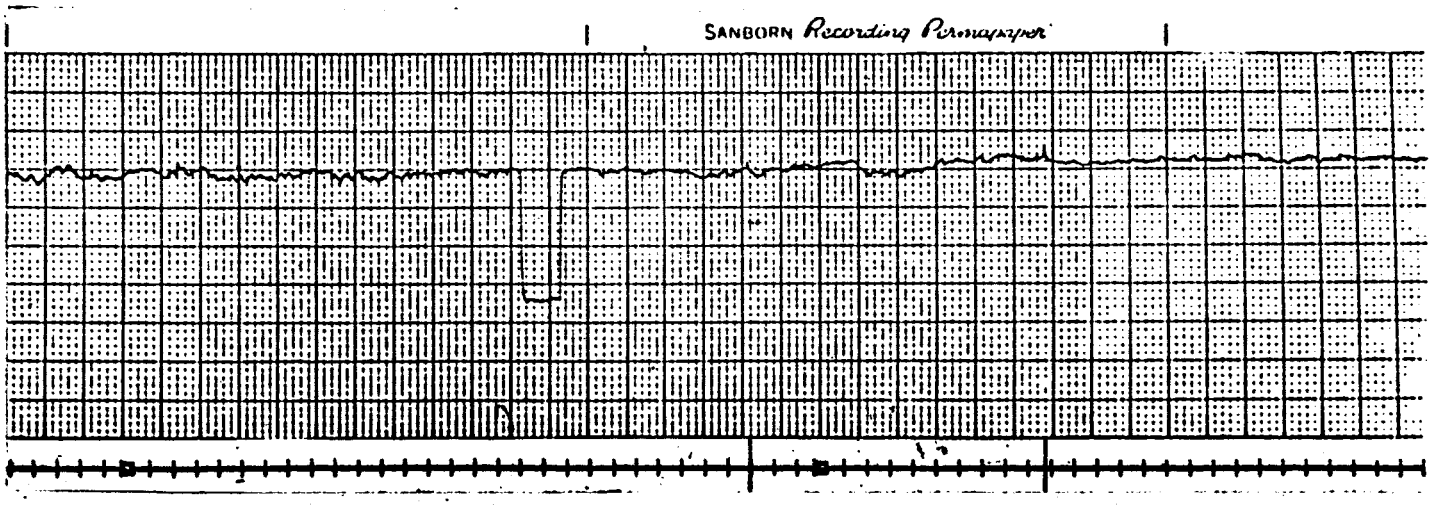

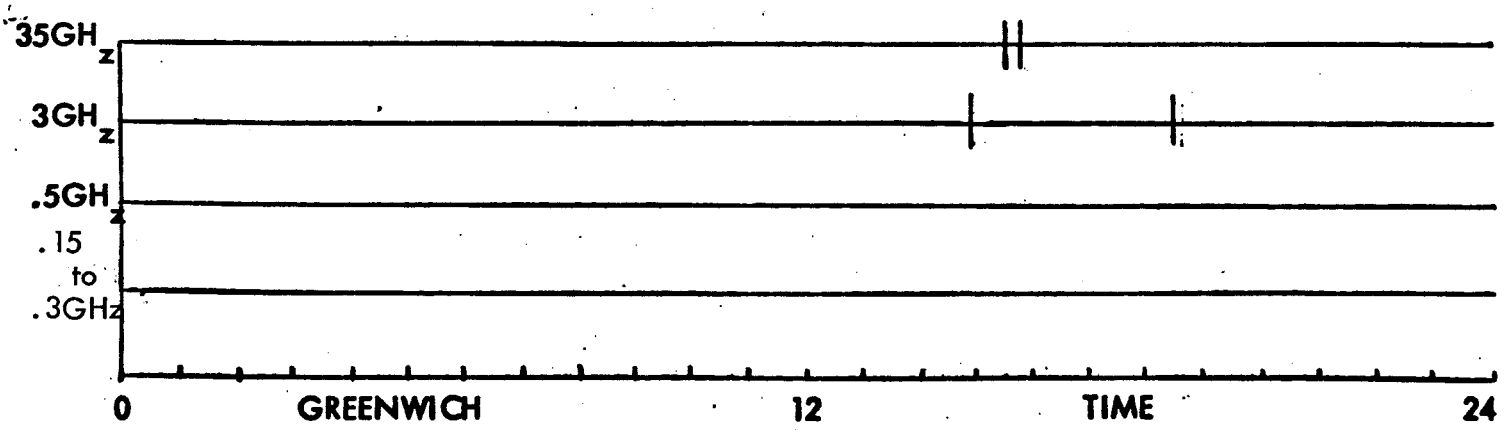

FIGURE 2-12

Date	Frequency	No. Of Events For the Day	U. T. Begin	U. T. End	Burst Amplitudes % 35 GHz	Other
13 Apr 66	35GH$_z$	5	14:10:20	14:10:40	1.5	
	3GH$_z$					
	.15-.3 GH$_z$					

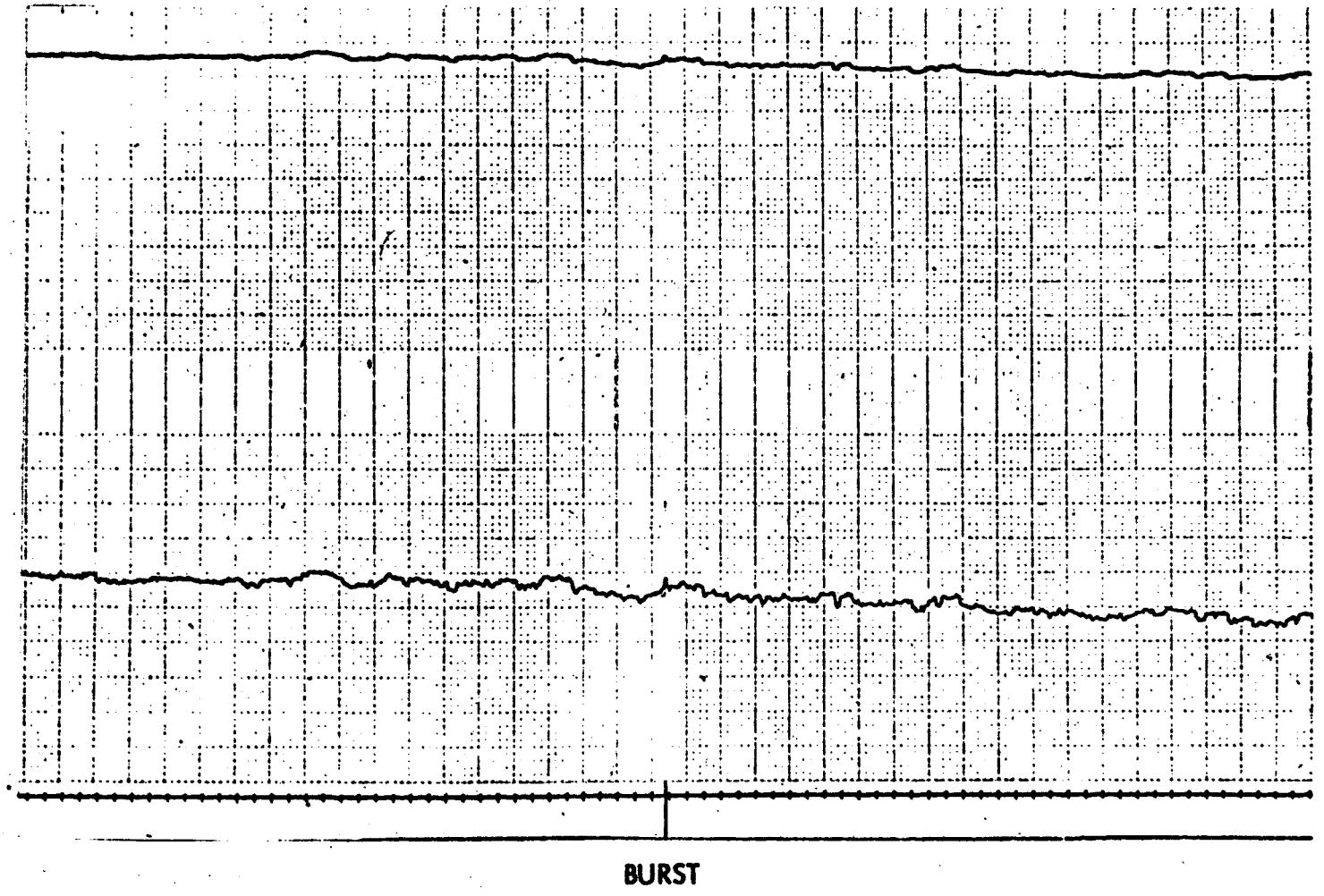

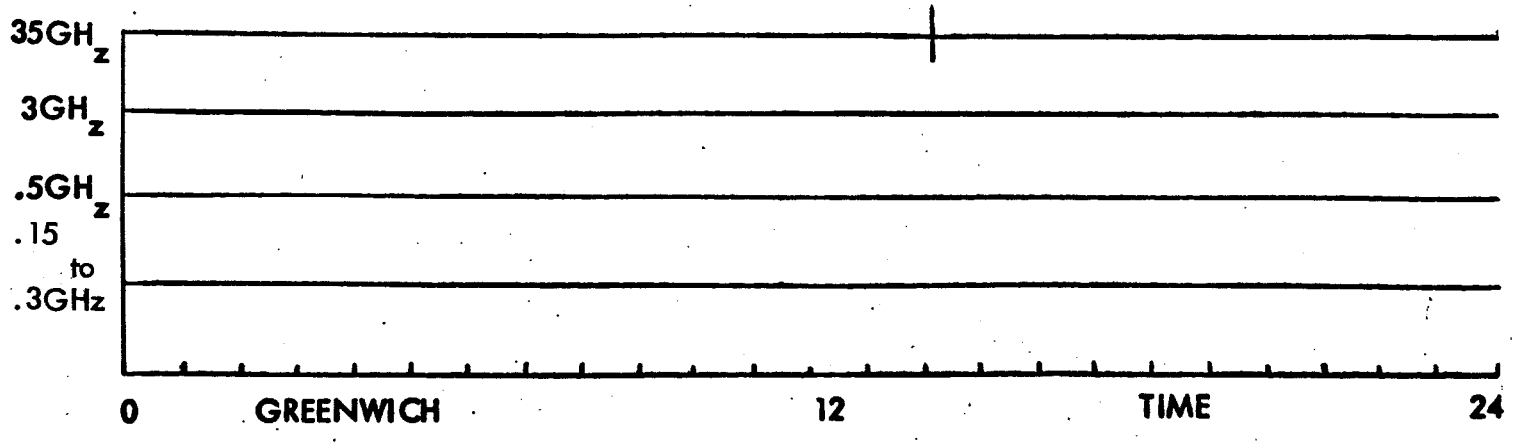

FIGURE 2-13

Date	Frequency	No. Of Events For the Day	U. T. Begin	U. T. End	Burst Amplitudes % 35 GHz	Other
13 Apr 66	35GH$_z$	5	16:22:50	16:23:10	1.5	
			16:25	16:25:30	3.0	
			16:28:20	16:31	3.0	
	3GH$_z$					
	.15-.3 GH$_z$					

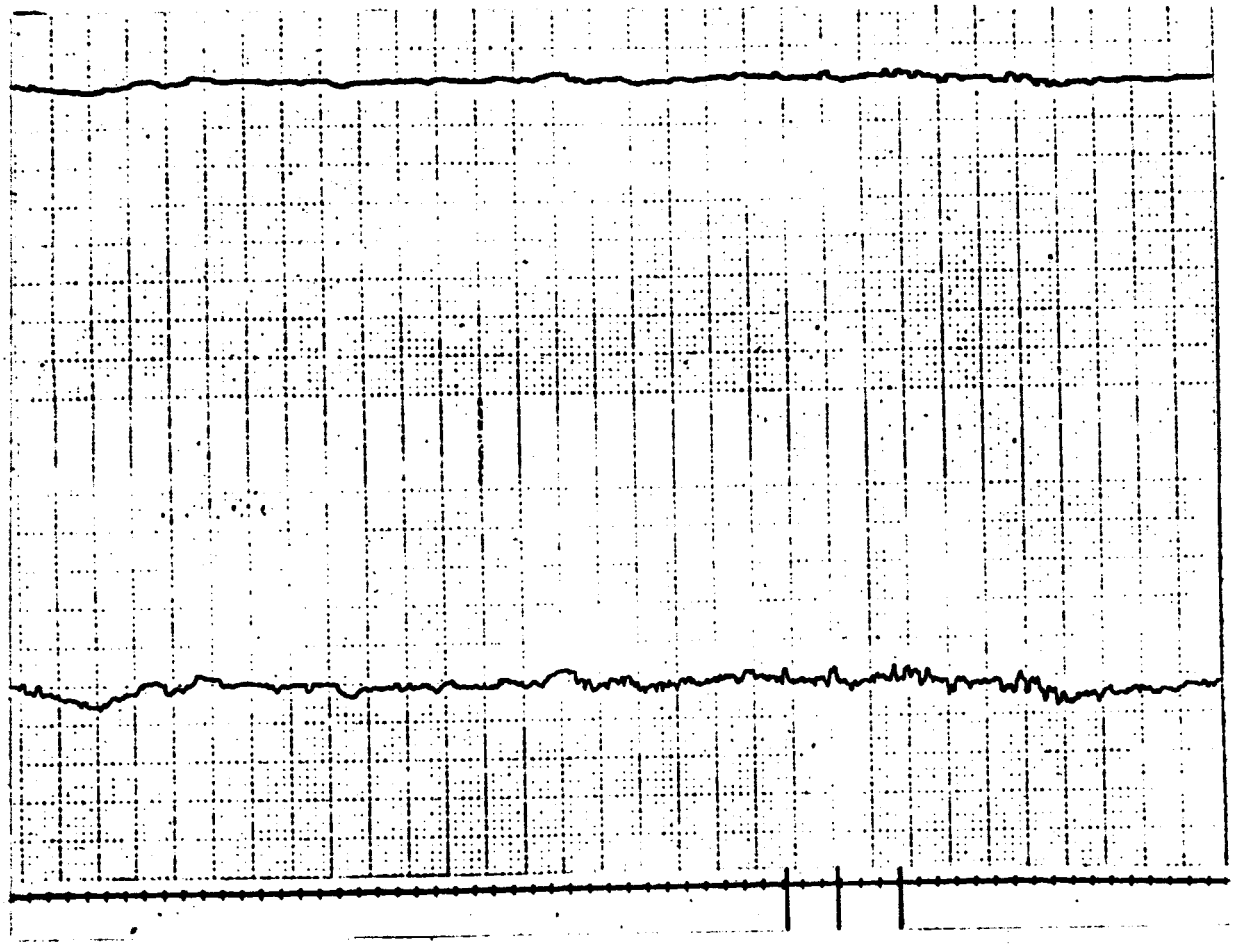

BURSTS

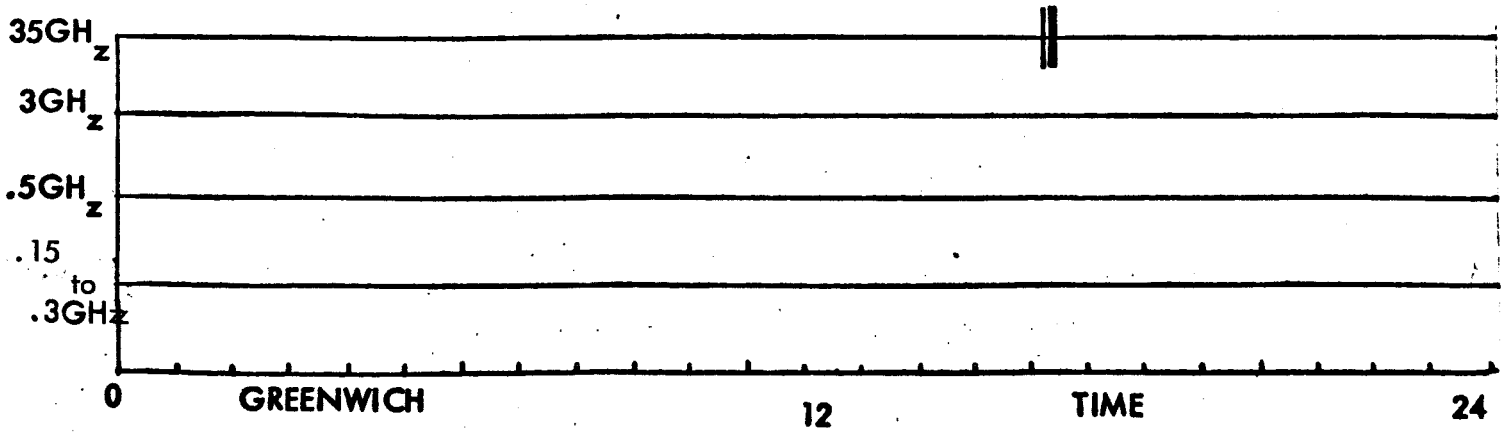

FIGURE 2-14

Date	Frequency	No. Of Events For the Day	U. T. Begin	U. T. End	Burst Amplitudes % 35 GHz	Other
13 Apr 66	35GH$_z$	5	18:07:20	18:07:40	1.5	
	3GH$_z$					
	.15-.3 GH$_z$					

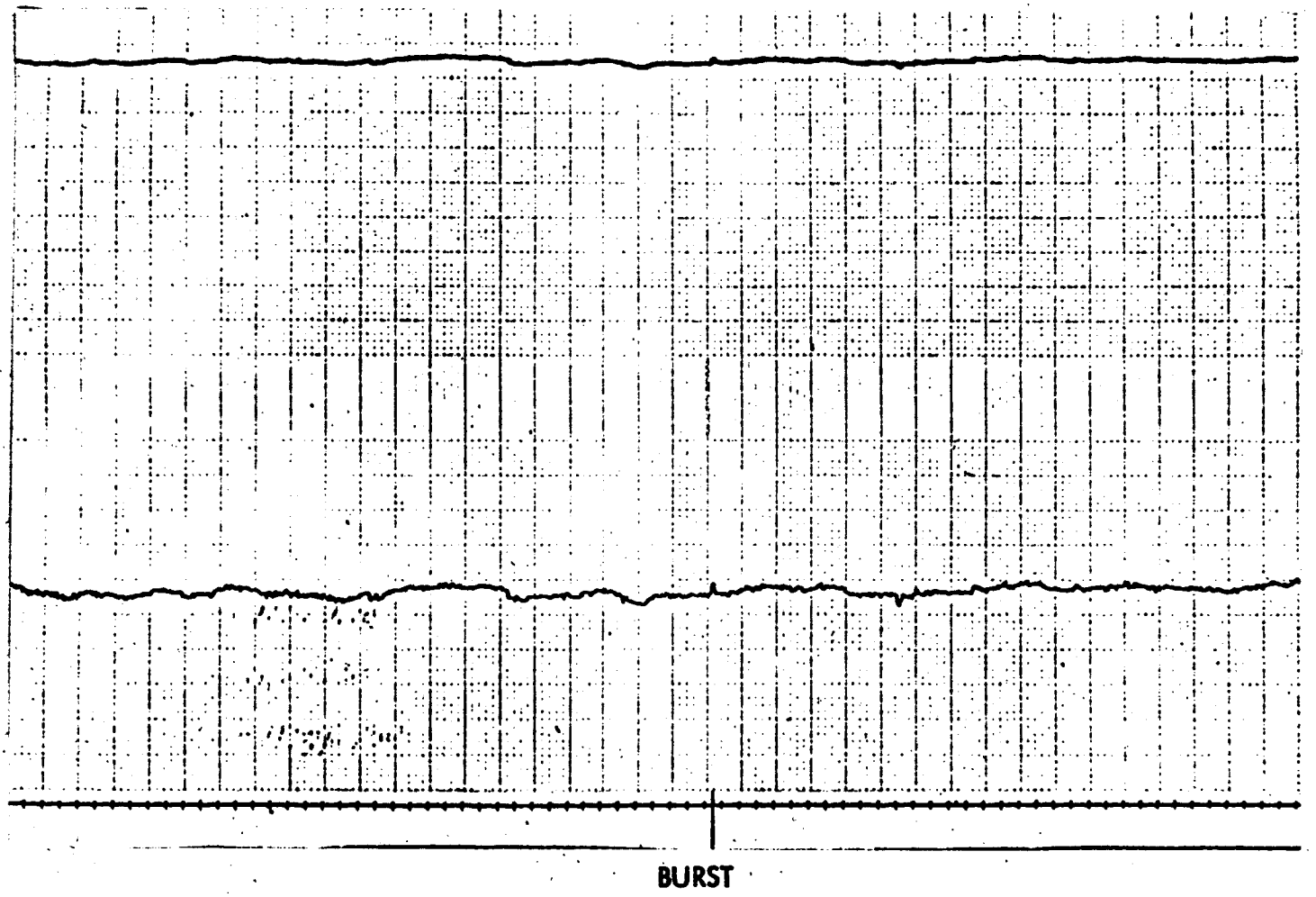

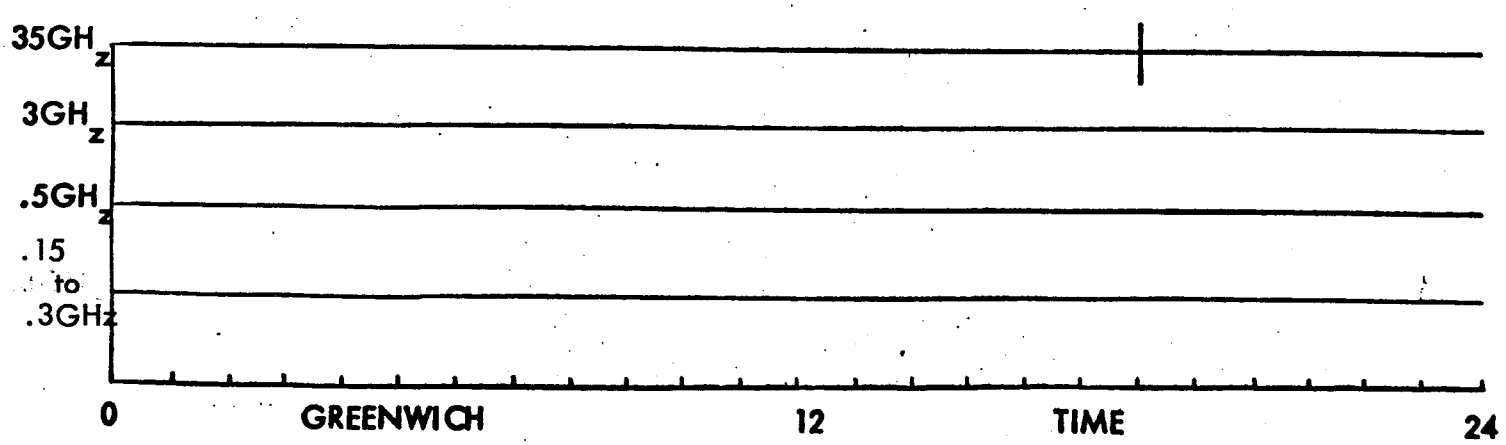

FIGURE 2-15

Date	Frequency	No. of Events For the Day	U. T. Begin	U. T. End	Burst Amplitudes % 35 GHz	Other
25 Apr 66	35GH$_z$	1	14:09:30	14:09:40	1.6	
	3GH$_z$	1	14:10			
	.5GH$_z$					
	.15-.3GH$_z$					

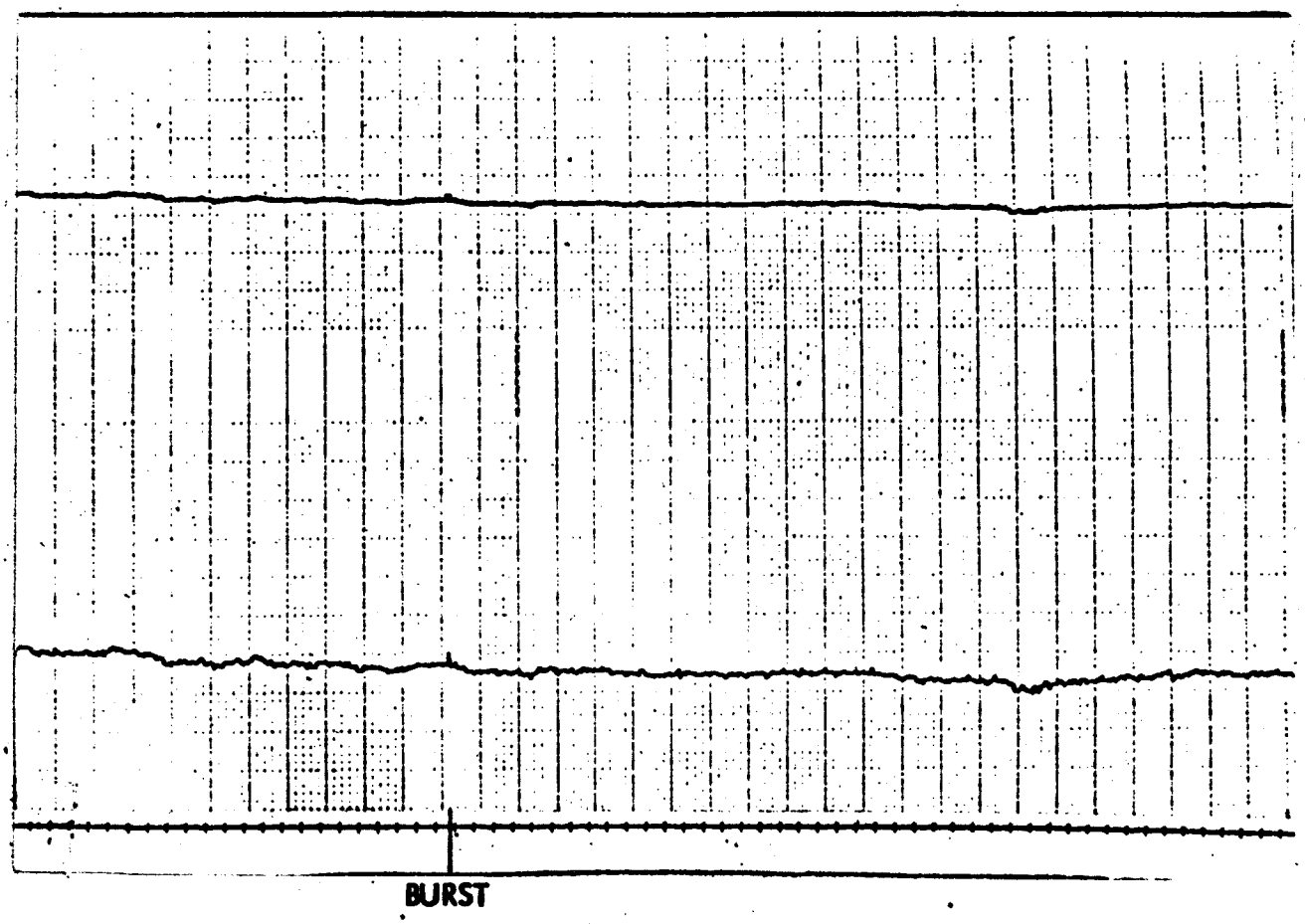

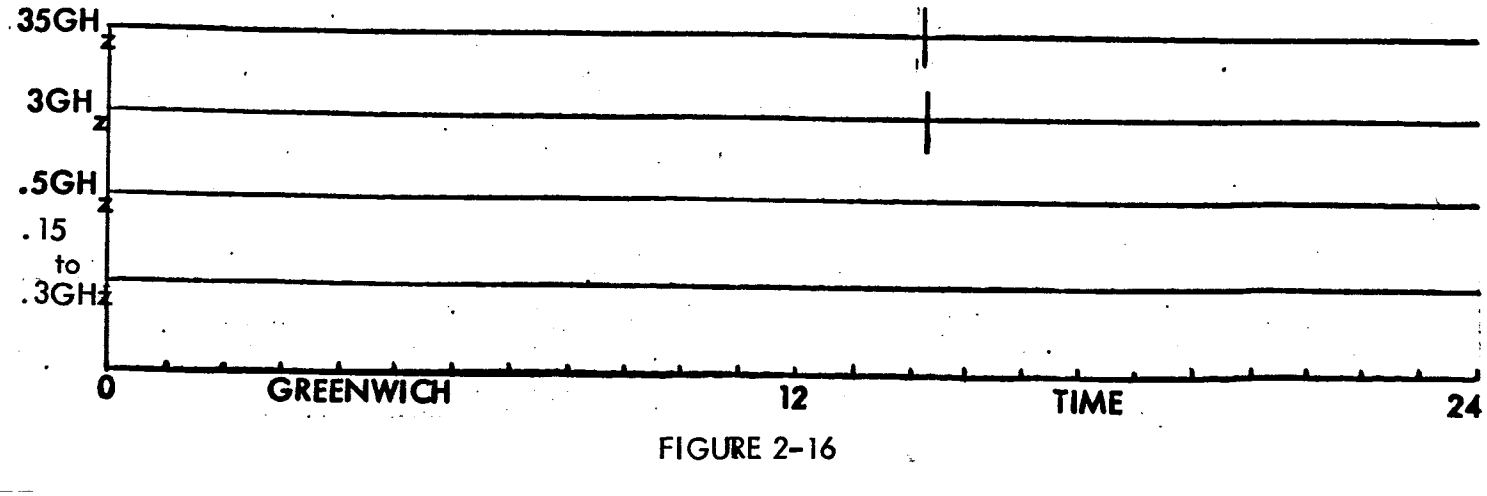

FIGURE 2-16

MAY 2, 1966 **35 GHz SOLAR ACTIVITY**

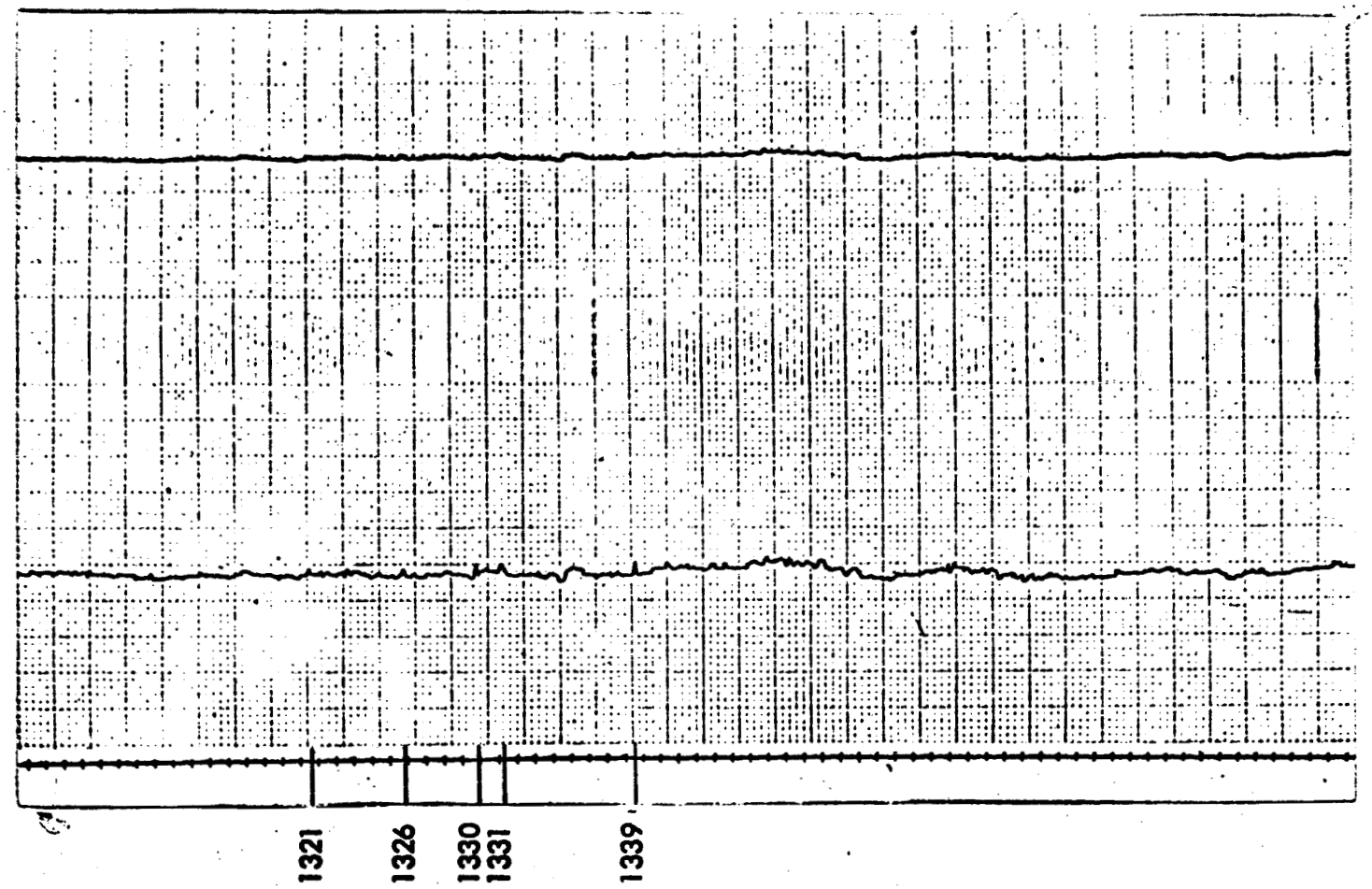

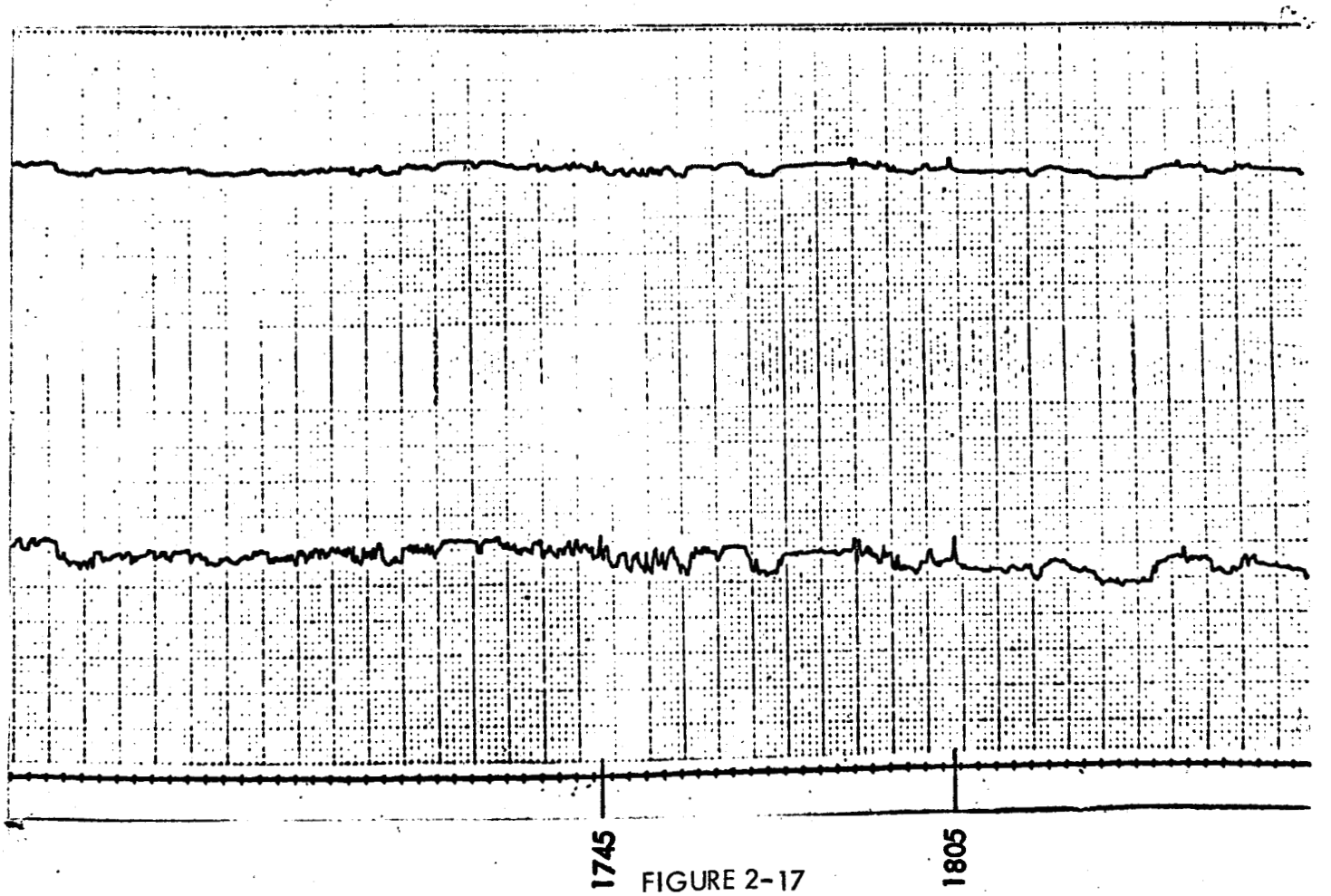

FIGURE 2-17

Date	Frequency	No. of Events For the Day	U.T. Begin	U.T. End	Burst Amplitude % 35 GHz	Other
2 May 66	35 GHz	7	13:20:50	13:20:52	< 1	
			13:25:40	13:25:50	< 1	
			13:29:50	13:30:00	< 1	
			13:31:00	13:31:30	< 1	
			13:38:40	13:38:50	2.5	
			17:45:25	17:45:55	3	
			18:05:30	18:05:45	5.5	
	3 GHz	1	13:36	13:39		
	0.15-0.3 GHz					

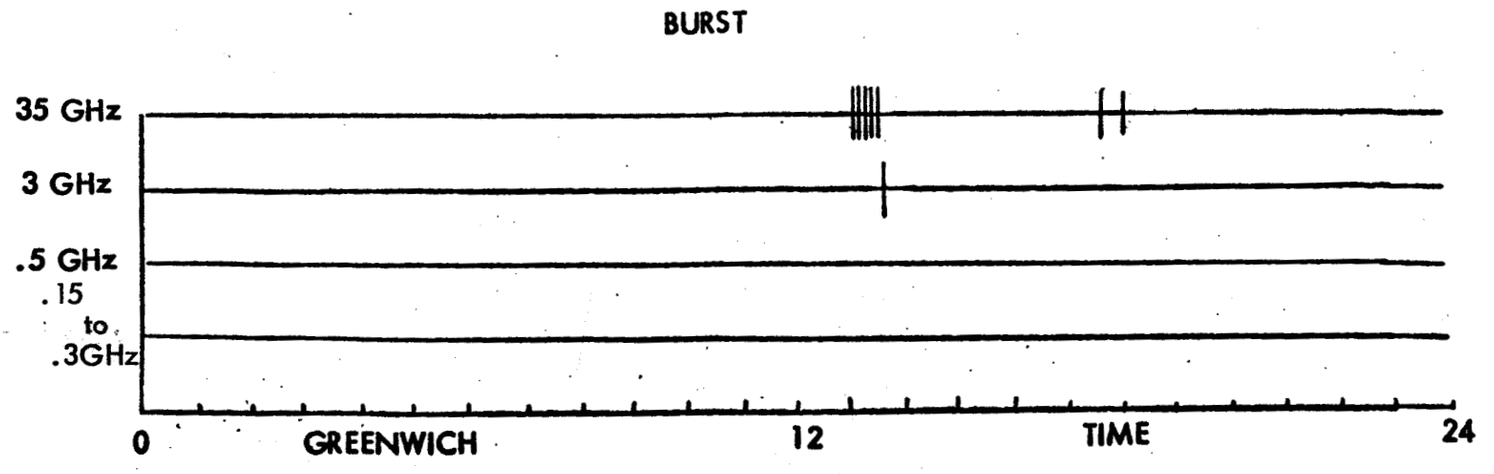

FIGURE 2-18

Date	Frequency	No. of Events For the Day	U. T. Begin	U. T. End	Burst Amplitudes % 35 GHz	Other
3 May 66.	35GH$_z$	4	17:24:20	17:24:50	4	
			17:35:20	17:35:50	1.5	
			17:46:20	17:46:30	1	
			17:48	17:48:15	1	
	.15-.3GH$_z$	1	01:52	01:53		Major Plus Burst

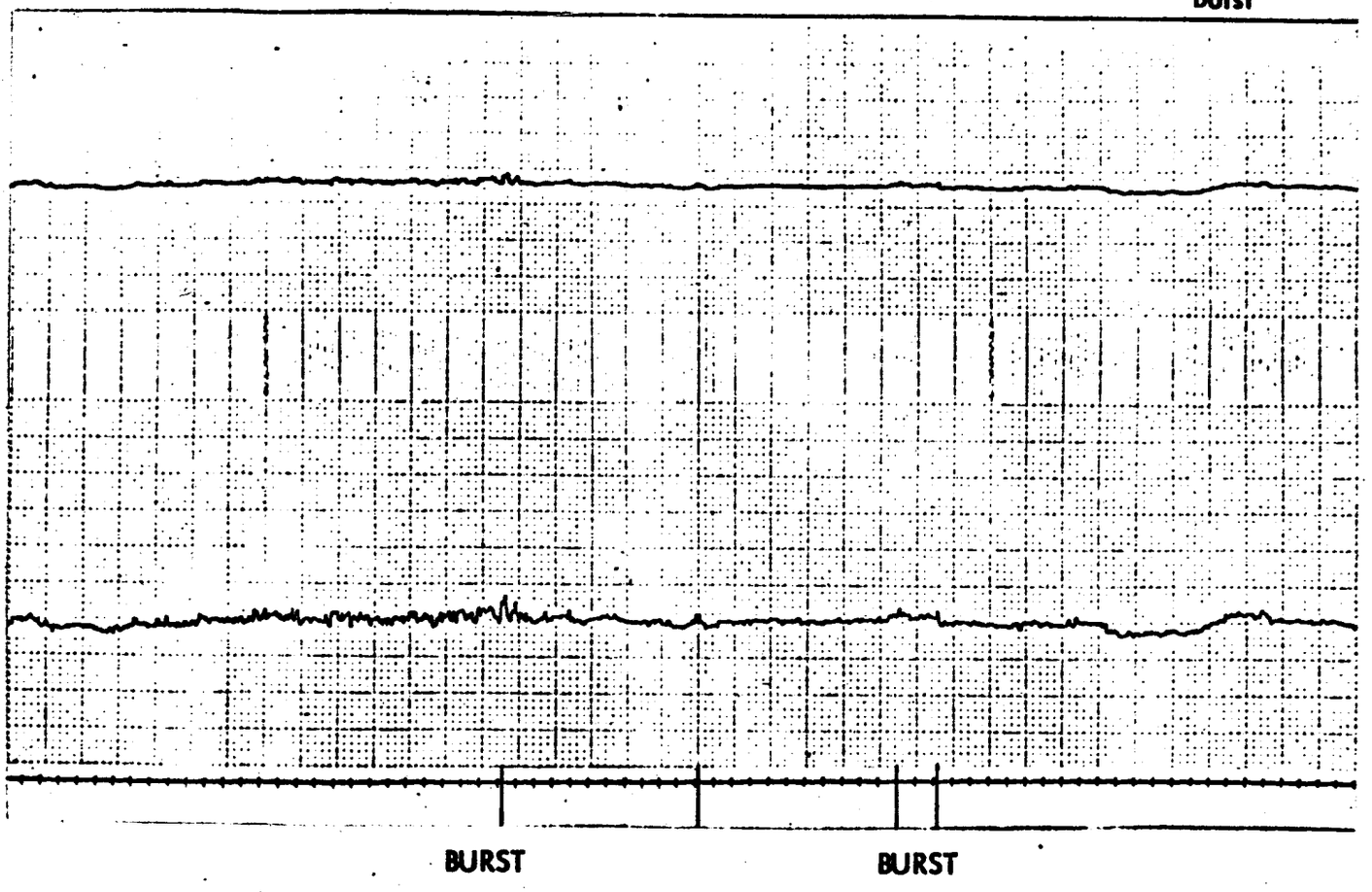

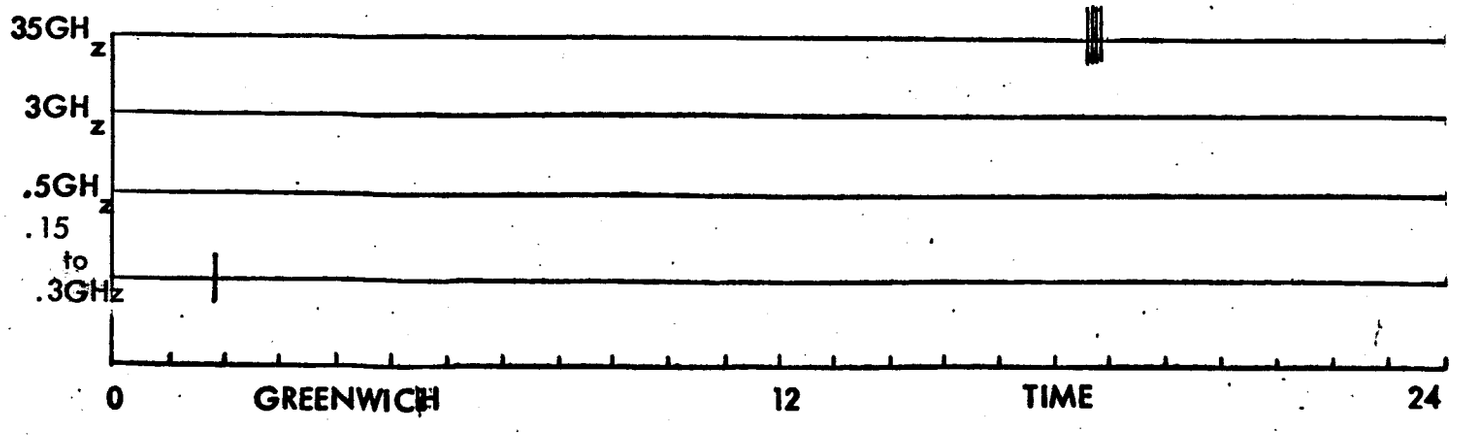

FIGURE 2-19

2.2 Solar Activity at a Wavelength of 4 Millimeters

Observational data obtained at a wavelength of 4 mm during the period from 1 May 1965 to 31 December 1965 showed no outstanding burst activity or structure. As noted previously, there were only 3 months of data obtained in total, and the days of observation were scattered throughout the 8-month period. Equipment difficulties precluded the possibility of obtaining continuous patrol data typical of the 8.6 mm records. A revised design approach to the RF Head for the 4 millimeter radiometer was completed early in the spring of 1966, and subjected to intensive laboratory testing as well as tests in the operational configuration during the months of March and April. The 4 mm channel was placed in full operation early in May and continuous patrol data was obtained through the month of June (at the time of report preparation).

The data was being analyzed at the time of report preparation. A detailed description of observed phenomena will be submitted as an Addendum to this report as soon as the analysis is complete.

The calibration of the flux intensity at 4 mm referenced to the measured lunar flux intensity will be repeated in the near future. Prior measurements indicated a brightness temperature of the order of 6,000°K with an uncertainty of $\pm$ 1,000°K. The flux intensity corresponding to a temperature of 6,000°K is 7,100 flux units.

Preliminary examination of the June record shows a most interesting phenomena beginning at 17:11:35 U.T., June 20 extending through June 24. On June 25 and 26, there was a heavy overcast with occasional light rain and fog. Variations in atmospheric attenuation were so severe that the expanded scale was not usable. Fluctuations on the "normal scale" were so great (50-60%) that it was not possible to separate atmospheric effects from solar activity.

The recorded activity beginning on June 20 was as follows:

June 20, 1966

Beginning at 17:11:40 (Figure 2-20) unusual activity was noted at 35 GHz. Approximately 10 seconds later, a complex phenomena of minor amplitude was noted at 75 GHz, consisting of differential absorption and emission. This relatively brief complex structure ceased at 17:12:40 as did the major complex activity at 35 GHz. This was followed by a gradual increase in intensity at both frequencies accompanied by a gradual undulating rise and fall noted at both 35 and 75 GHz.

At 12:24, an abrupt change in the character of the signal at both frequencies was noted (Figure 2-21) as the signal changed from a relatively smooth characteristic to one indicative of complex low level activity, less than 200 flux units peak-to-peak at 75 GHz and 70 flux units peak-to-peak at 35 GHz. This complex structure continued to increase in amplitude, and during the time period from 17:30 to 17:38, correlation of observed phenomena on both frequencies was clearly evident (Figure 2-22). Note the simultaneous increase with occurred at approximately 17:30:30 and the brief burst which lasted approximately four seconds beginning at 17:34:00.

Weather conditions were clear, hence, there was no confusion of this phenomena with atmospheric effects.

No significant activity was reported at other frequencies. (Washagi)

June 21, 1966

The complex activity which began at 17:11:40 on June 20 persisted through June 21. The amplitude of the structure at 75 GHz had increased slightly over that on the prior day of observation. The 35 GHz record showed occasional ESB (extremely short bursts). A typical portion of the June 21 record is shown in Figure 2-23. Note the ESB at 14:47:12 and 14:49:48.

Weather conditions were clear. No significant activity was reported at any other frequencies. (Washagi).

June 22, 1966

The level of complex activity continued to persist through June 22 and the phenomena of ESB increased in intensity and duration.

At 15:58:50 a "ramp" increase on the leading edge of an ESB was noted at 75 GHz followed approximately 3 seconds later by a similar phenomena of complex structure at 35 GHz. (Figure 2-24). The duration of the ESB was approximately 24 seconds, approaching the character of a sudden intense burst. Following this burst, the intensity increased in a complex fashion at 75 GHz and decreased at 35 GHz typical of an absorption phenomena at 35 GHz.

The record for the remainder of the day showed similar structure. On occasion a gradual increase and decrease over a period of three to four minutes was noted coincidently at both 75 GHz and 35 GHz. (Figure 2-25). Of particular interest on this record is the structure at 75 GHz in the period from 19:51:03 to 19:51:27 followed 3 seconds later by an ESB at 35 GHz. Note also the gradual increase and decrease in the average intensity at both frequencies occurring on a gradual increasing "ramp".

Weather conditions were clear throughout the period of observation.

No significant activity was reported at other frequencies.

June 23, 1966

The complex activity which began on Monday continued into Thursday with a noticeable increase in the ESB activity first noted on the afternoon (Wednesday June 22), A typical record of the activity on June 23 is shown in Figure 2-26. Note the series of extremely short bursts apparent on the 8.6 mm record. Activity at 75 GHz was quite complex, typical of the level of activity noted on the prior day.

Weather conditions were "scattered clouds." The optical monitor provided easy identification of those periods of observation when the sun was obscurred by a cloud.

No significant solar radio activity was reported at any other frequency (Washagi).

June 24, 1966

The activity persisted into Friday with evidence of greater complexity particularly at 8.6 mm as the ESB phenomena gradually changed to sudden intense bursts. Burst flux intensities reached a maximum of 150 flux units on that day. A typical record is shown in Figure 2-27.

Weather conditions were overcast but stable as indicated by the optical monitor. Under these conditions, there was no confusion of atmospheric effects with solar activity.

No significant radio solar activity was reported on this day at any other frequency (Washagi).

June 25, 1966

The weather in Boston was "heavy overcast, rain and fog". The expanded scale on both channels was reduced to a 1:1 ratio. The variability in cloud attenuation combined with moisture on the radome negated the possibility of separating solar activity from atmospheric effects.

At 15:28 U.T., fluctuations in solar intensity were reported at 3 GHz, ending at 16:10 U.T. (WASHAGI). Flux intensity levels ranged from 75 to 750 flux units. There was a definite post-burst increase noted after 16:10 U.T.

Station 33 (Boulder) reported a very dark Type III burst beginning at 15:36 U.T. and developing to Type IV (Washagi).

A major burst at 0.5 GHz was reported at 15:31, ending at 16:37 U.T. The flux level was not reported (WASHAGI).

A complex burst was reported at 10 GHz beginning at 15:33 and ending at 15:43 U.T. Flux intensity levels ranged from 7.5 to 75 flux units. A postburst increase beginning at 15:43 and ending at 16:33 U.T. was recorded at this frequency with a flux increase to 7.5 units (WASHAGI).

June 26, 1966

Weather conditions in Boston, typical of the prior day, persisted through Sunday June 26. Fluctuations associated with the high variability of attenuation and moisture on the radome negated separation of solar activity from atmospheric effects.

A simple Type III burst was reported at 3 GHz beginning at 15:05 U.T. and described as long-enduring or gradual rise and fall burst (WASHAGI). The intensity above the quiet sun level was in the range of 7.5 to 75 flux units.

June 27, 1966

The weather in Boston on Monday was "clear and dry". Observing conditions were excellent. No significant activity was noted at either 35 or 75 GHz. Of particular significance was the reduction in the fluctuation level typical of a quiet sun. The solar events which began at 17:11:40 U.T. on June 20 at both frequencies and recorded throughout the five-day period through the 24th were no longer apparent on the record. A portion of the record of June 27 typical of the entire day, with one exception, is shown in Figure 2-28.

From 13:50 to 13:56 U.T. minor complex activity was noted at both frequencies. The phenomena describable as a minor and gradual rise and fall combined with extremely short bursts and minor sudden intense bursts. This portion of the recording of June 27 is shown in Figure 2-29.

FIGURE 2-20

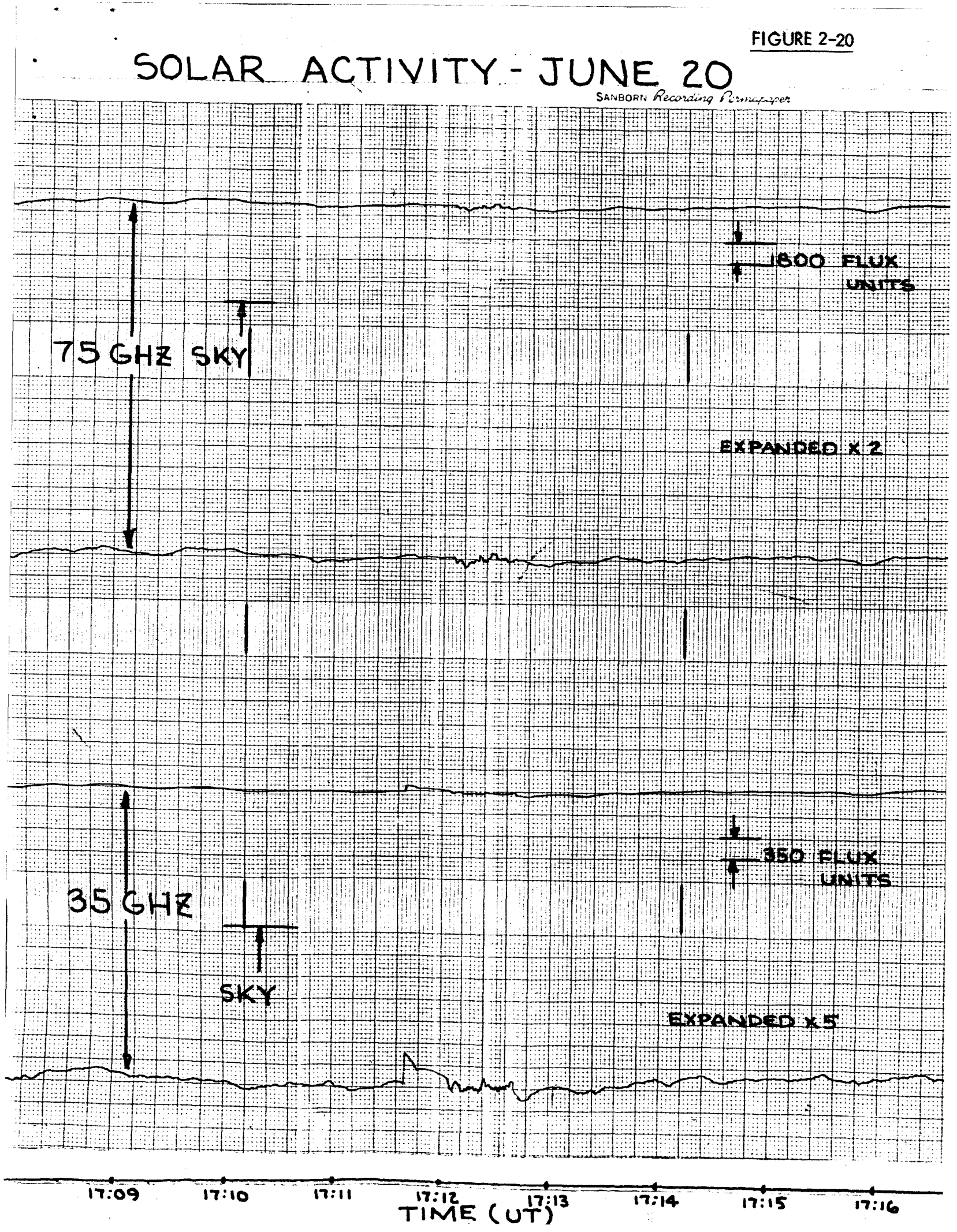
SOLAR ACTIVITY - JUNE 20
SANBORN Recording Permapaper
1800 FLUX UNITS
75 GHZ SKY
EXPANDED x 2
350 FLUX UNITS
35 GHZ
SKY
EXPANDED x 5
17:09
17:10
17:11
17:12
17:13
17:14
17:15
17:16
TIME (UT)

SOLAR ACTIVITY - JUNE 20

FIGURE 2-21

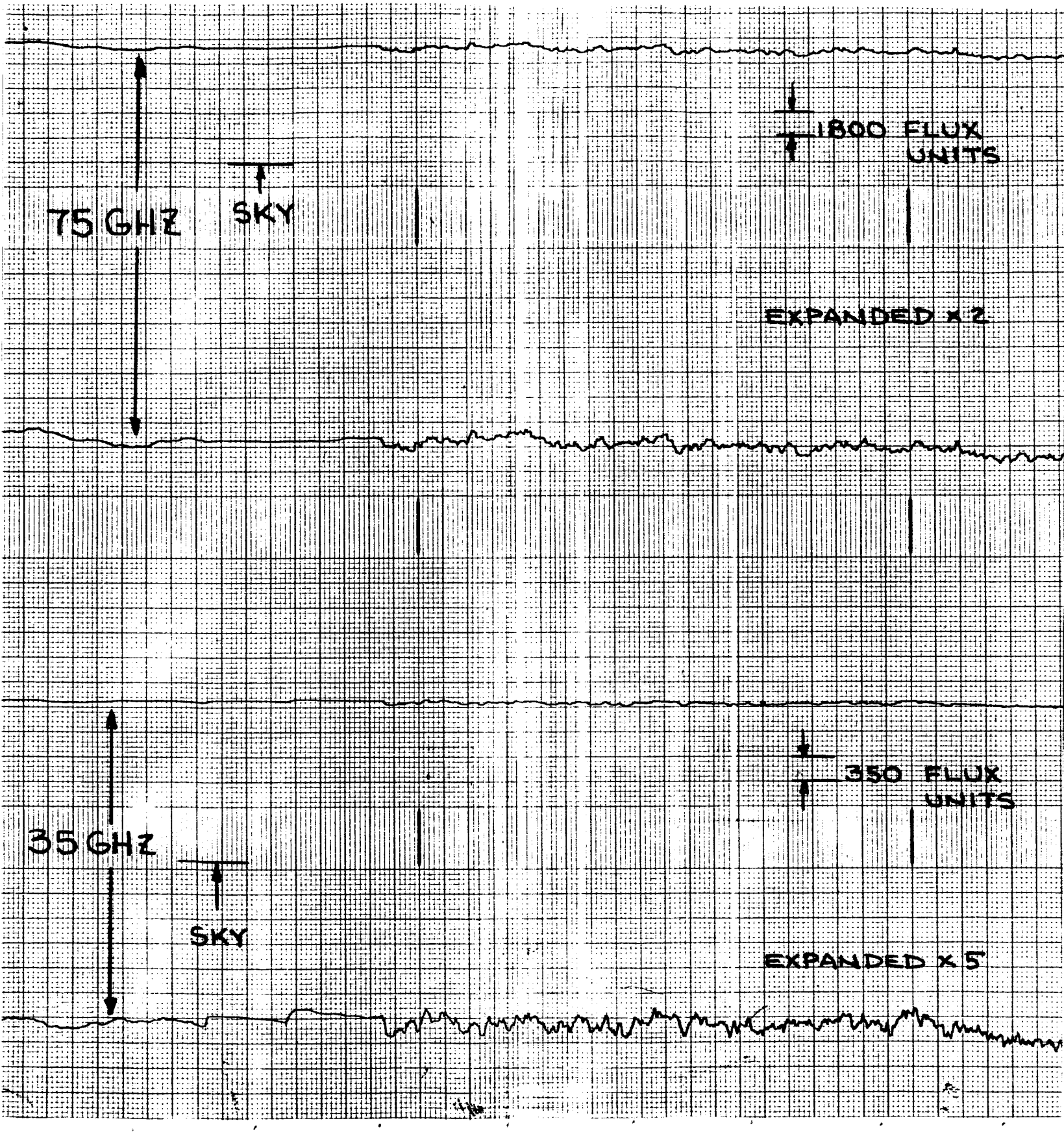

SOLAR ACTIVITY - JUNE 20

FIGURE 2-22

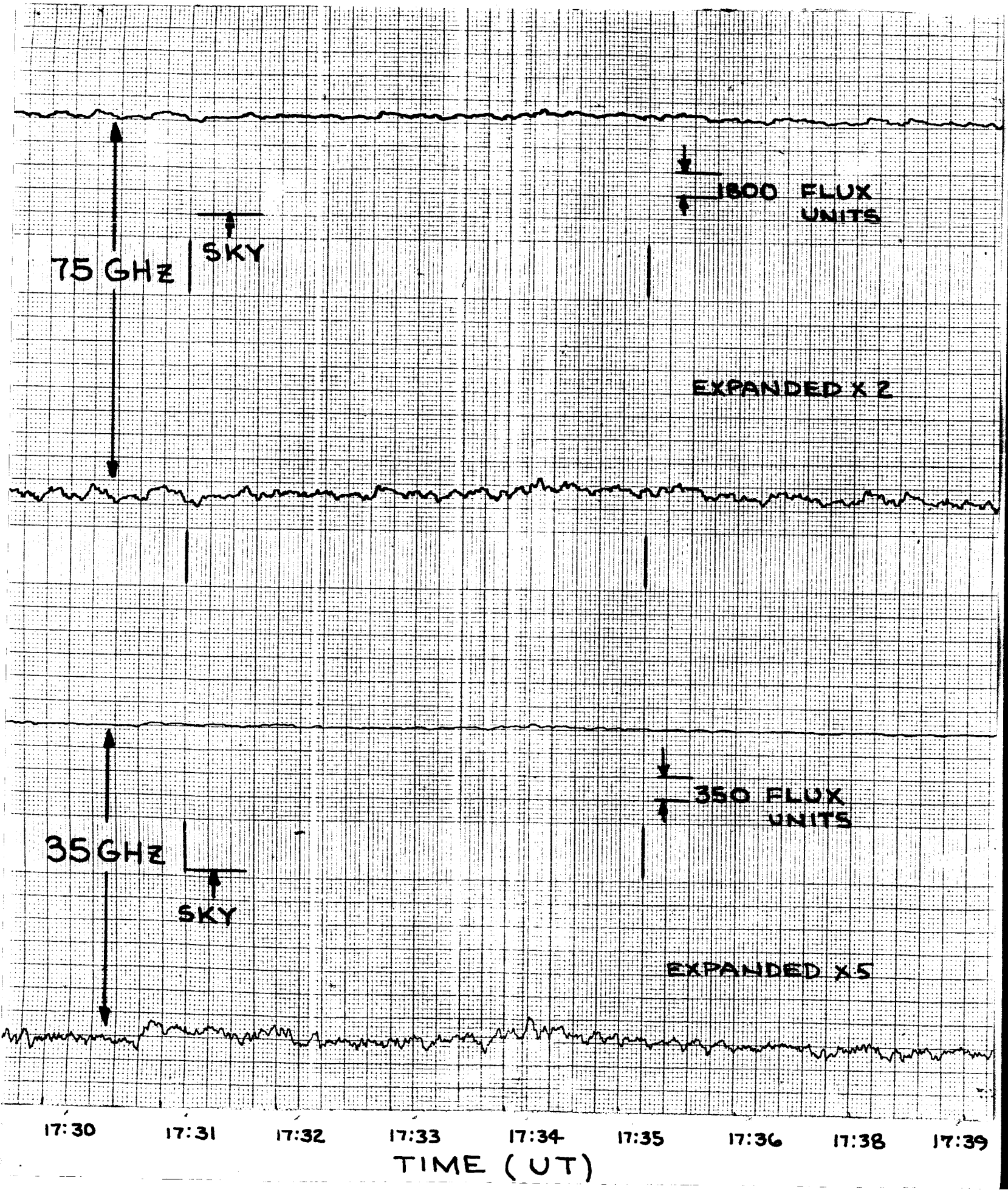

SOLAR ACTIVITY - JUNE 21

FIGURE 2-23

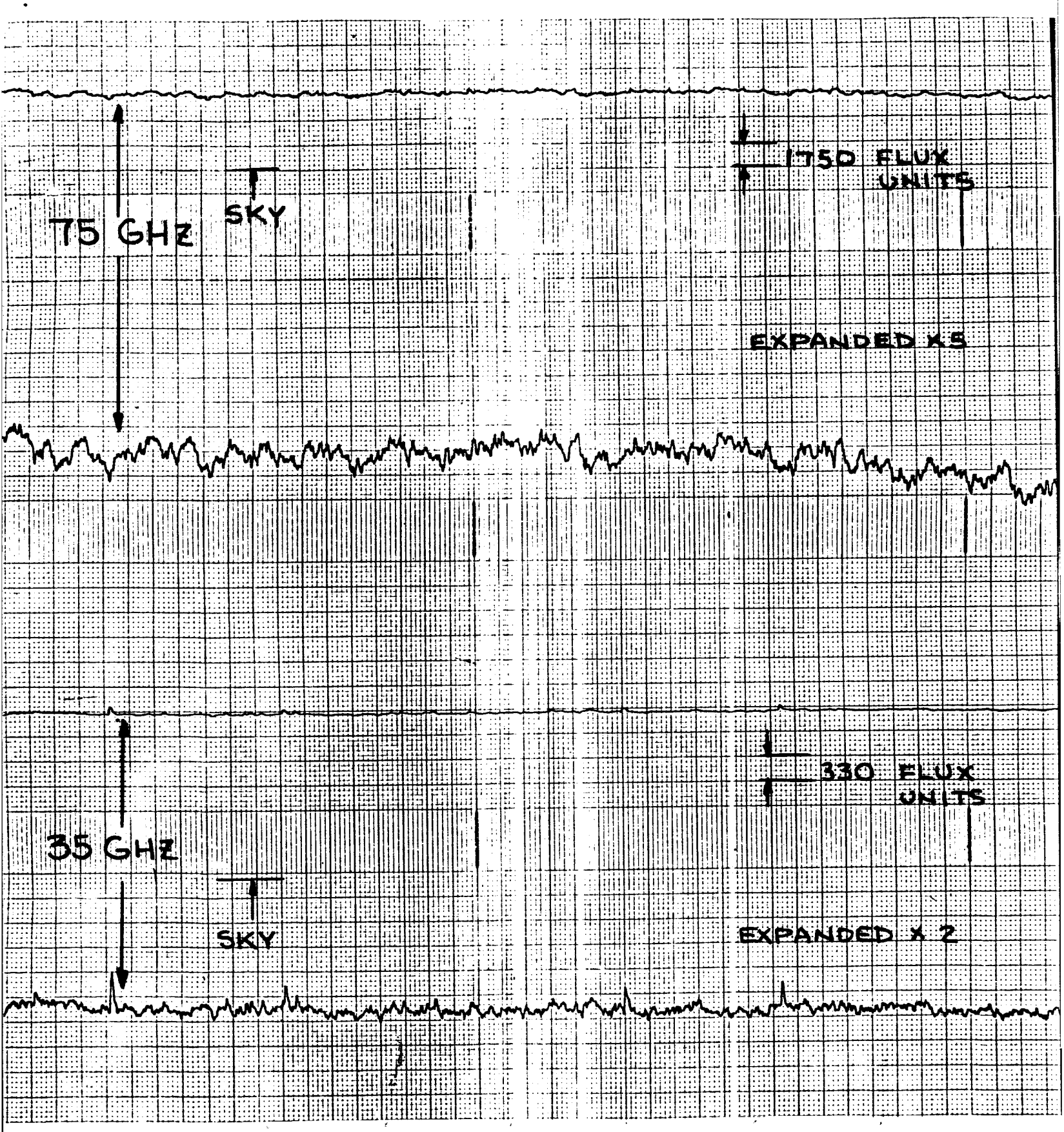

FIGURE 2-24

SOLAR ACTIVITY - JUNE 22

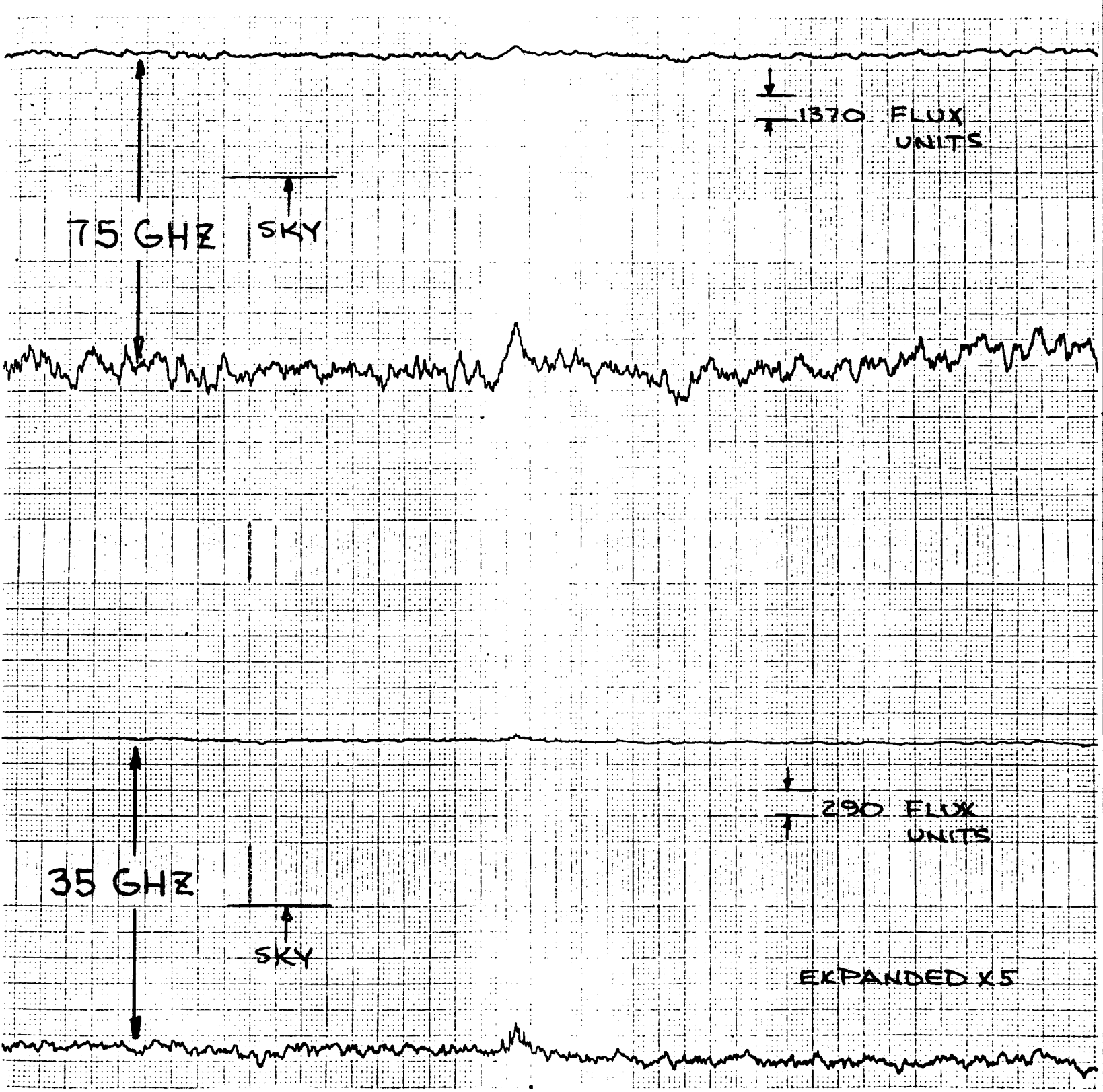

FIGURE 2-25

SOLAR ACTIVITY - JUNE 22

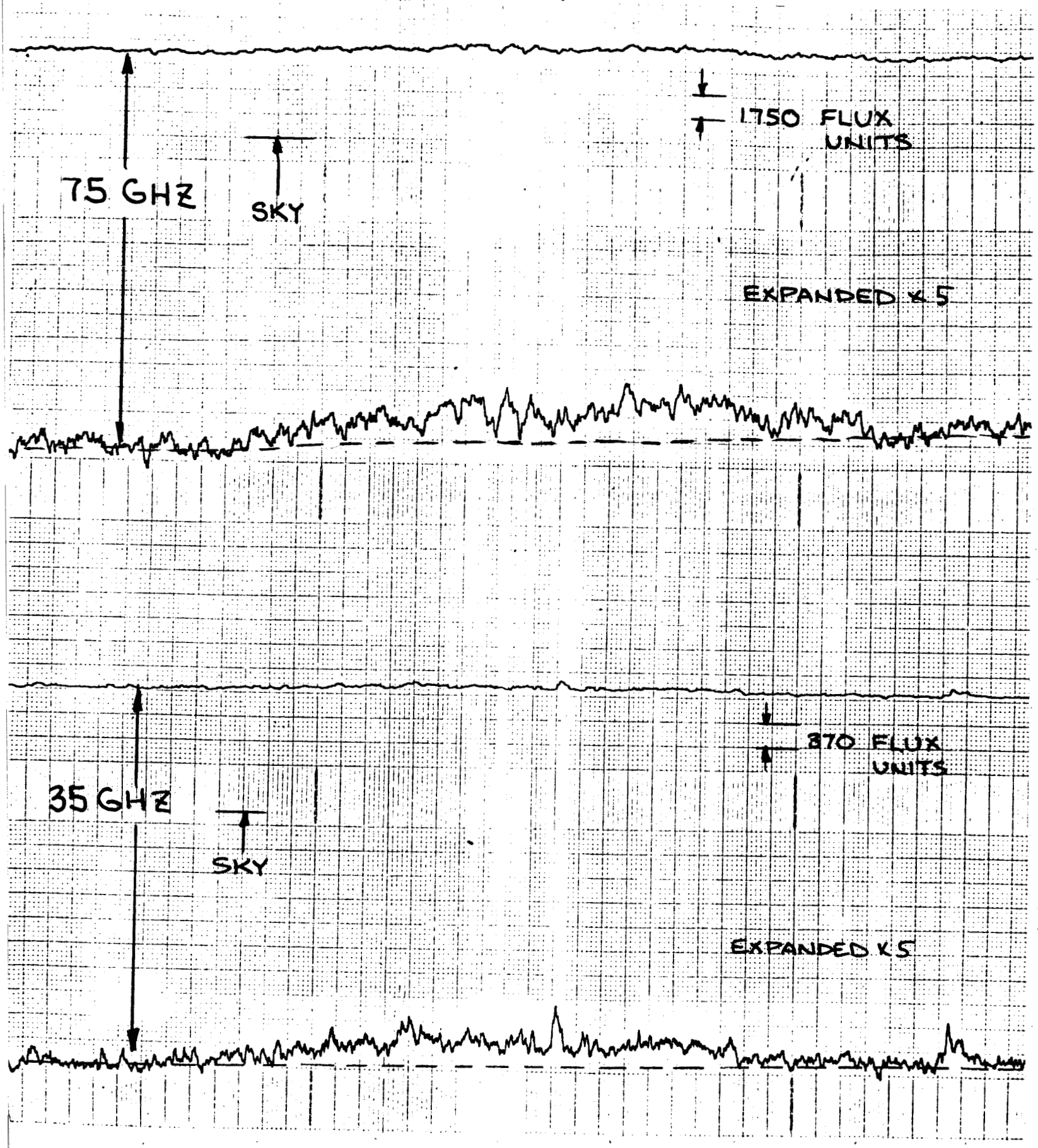

FIGURE 2-26

SOLAR ACTIVITY - JUNE 23

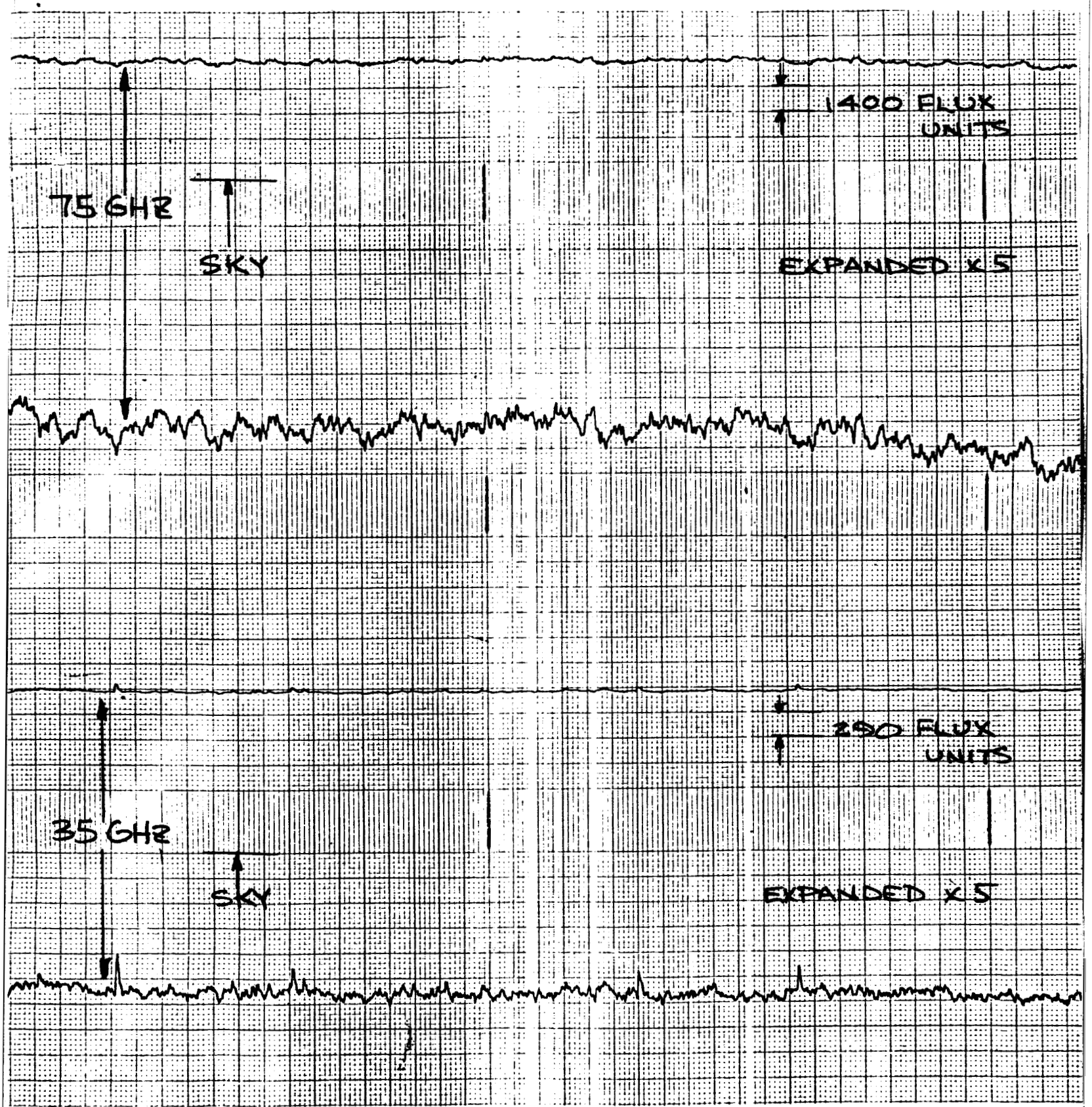

FIGURE 2-27

SOLAR ACTIVITY - JUNE 24

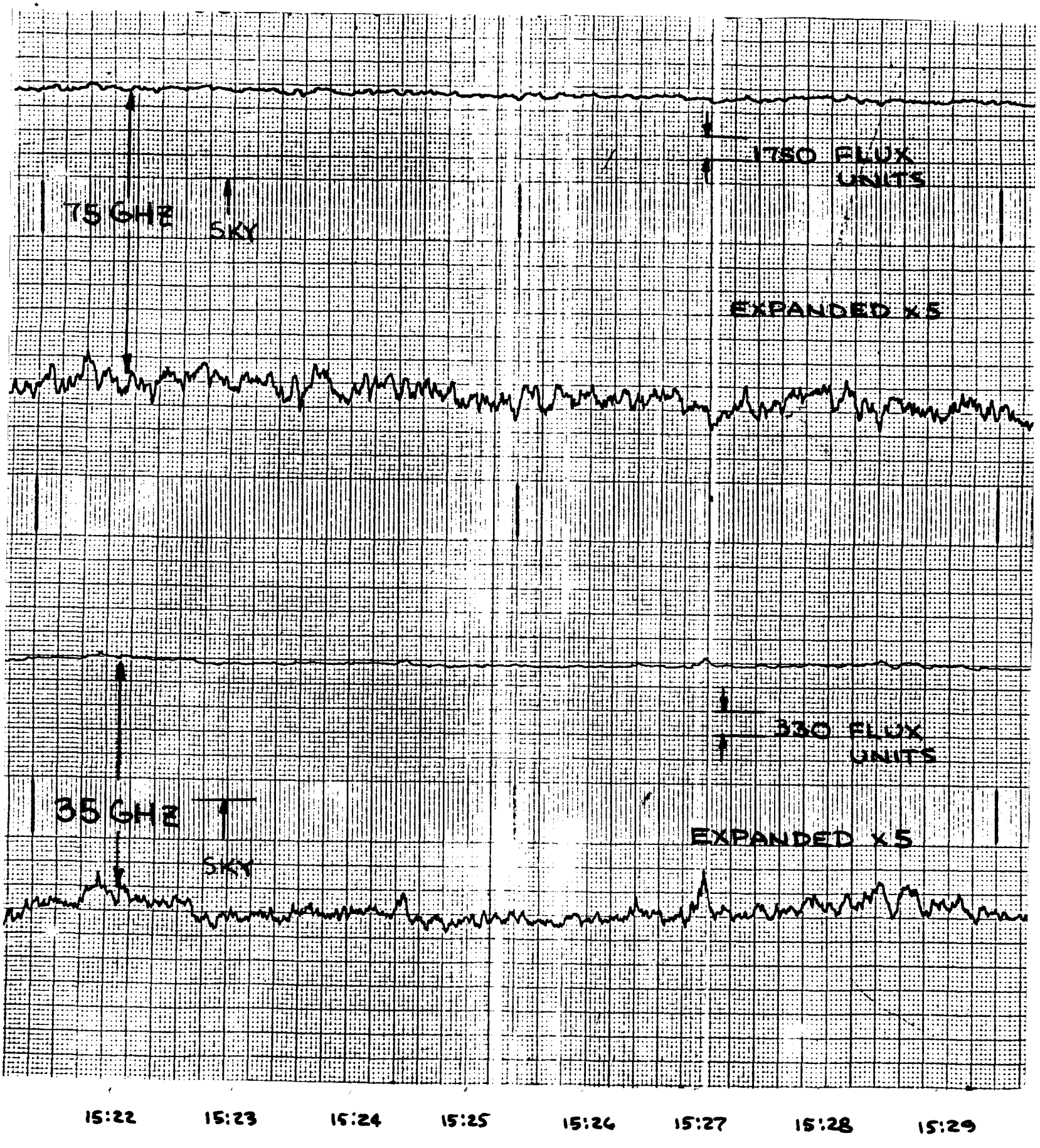

FIGURE 2-28

SOLAR ACTIVITY - JUNE 27

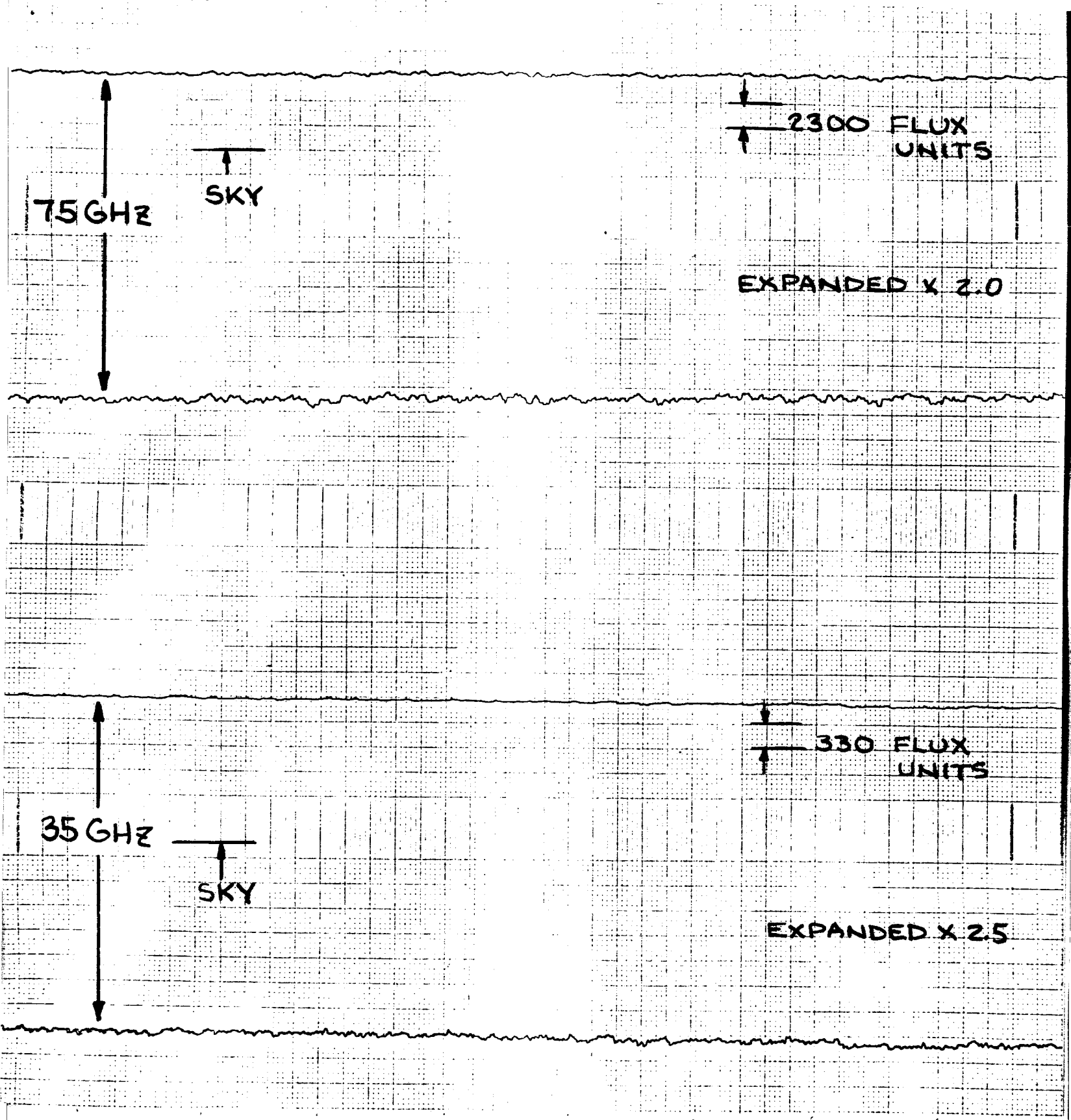

FIGURE 2-29

SOLAR ACTIVITY - JUNE 27

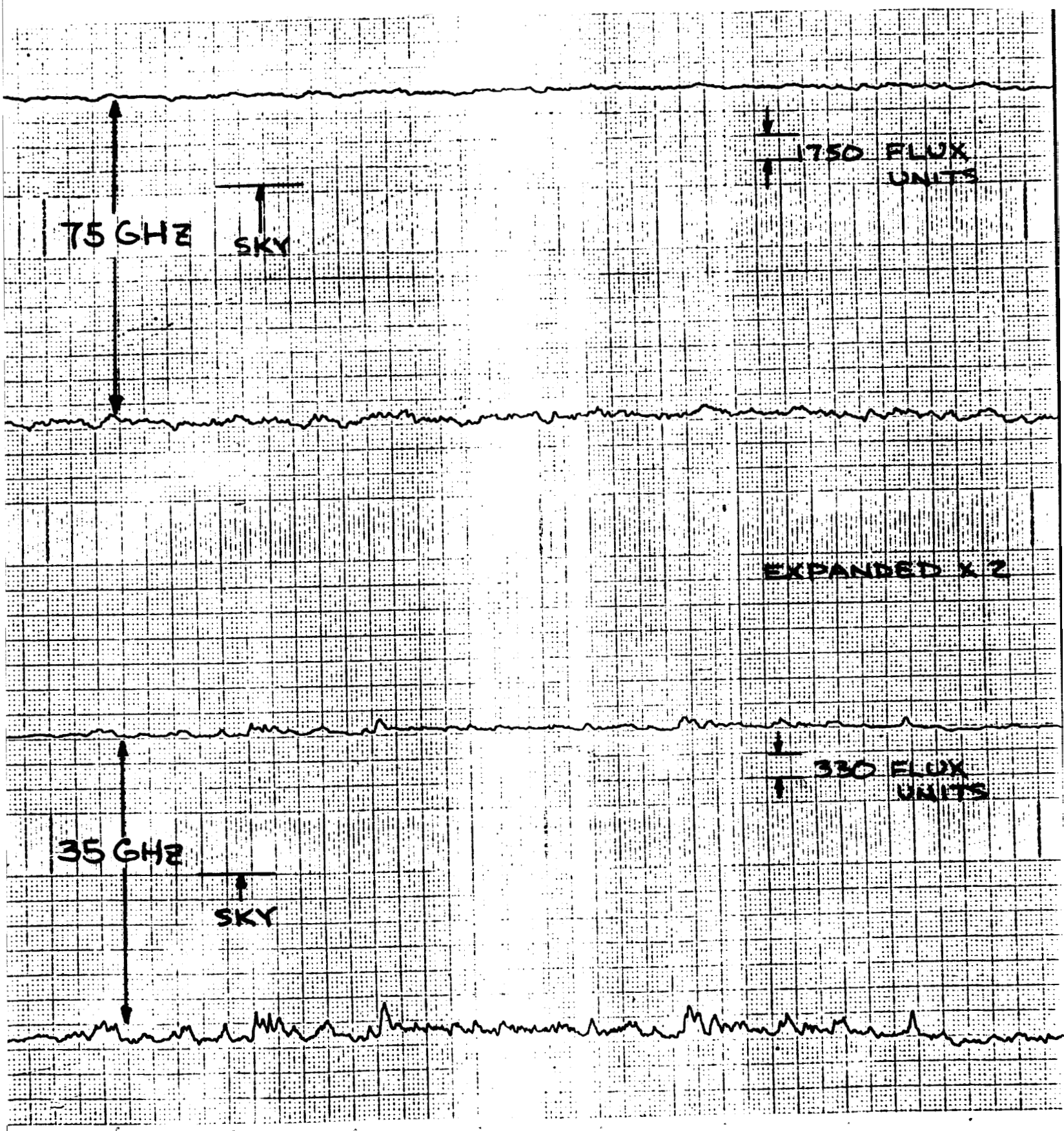

3.0 ATMOSPHERIC EFFECTS

A considerable amount of effort was expended in an attempt to discriminate against atmospheric contamination of the sun signal level. The problem was approached both analytically and with instrumentation techniques. In the latter area, we elected to introduce a comparison horn in a manner such that the atmospheric reradiation component would be cancelled insofar as its contribution to the output indicator reading. There is no known way to cancel the attenuation component, however, its effect on the received signal may be reduced considerably by using a feedback network which operates on the sensed level of the reradiation component. The reradiation component feedback approach was not implemented, since the prime objective of the effort was accumulation of solar data. The investigation of this technique is worthy of consideration, however, it should be noted that the sensor which provides the feedback signal must be very carefully calibrated, quite stable, and in many respects, meet the requirements of an absolute temperature measuring device. Techniques in this area were also analytically investigated and a fundamental approach established. Implementation in hardware form was not undertaken for the previously mentioned reason.

The two atmospheric characteristics of concern are attenuation and reradiation. The reradiation component as noted previously was cancelled by an "antenna beam comparison technique." Our effort was then directed to the determination of the time function of atmospheric opacity.

Analytical Approach

Our analytical approach was directed to an understanding of the physical phenomena and the derivation of appropriate correction factors for the measured signal intensity, obtained by separate measurement of meteorological parameters (temperature and relative humidity) at the time of observation.

Attenuation of microwave energy by atmospheric gases is due, primarily to molecular absorption by oxygen and water vapor. These two gases are capable of interacting with and absorbing microwave energy by virtue of the permanent electric dipole of the water molecule and the permanent magnetic dipole moment of the oxygen molecule. Other natural atmospheric gases have negligible effects. The microwave absorption, due to atmospheric oxygen is caused by magnetic dipole resonances of the molecule near 115 GHz and 60 GHz. For water vapor, one line occurs at approximately 22 GHz and one at approximately 184 GHz. In addition, there is a vast array of lines in the near-millimeter region. The skirts of these absorption bands extend through the frequency region of interest and even exhibit a noticeable effect at the lower microwave frequencies.

The absorption caused by molecular transitions has been analyzed by many researchers. The Van Vleck-Weisskopf Equation (1945) has accounted most closely to observed absorption characteristics. This equation contains two sets of parameters. The first establishes the frequency of each absorption line and is obtained either from a knowledge of energy levels or by measurement. The second describes the width of the absorption maxima.

The water vapor concentration of the atmosphere, in general, exhibits an exponential decrease with altitude and makes a negligible contribution at altitudes above approximately 10 km. The water vapor attenuation rates at altitudes other than sea-level reflect this decrease. The horizontal attenuation at any altitude is then related to the sea-level value by an expression of the form:

$$A_{(h,\lambda)} = A_{(o,\lambda)_{H_2O}} EXP(-Kh) \qquad (3\text{-}1)$$

where:

h = the vertical distance above the surface in units of distance.

$A(h,\lambda)_{H_2O}$ = the horizontal attenuation rate in units of length at altitude .

$A(0,\lambda)_{H_2O}$ = the horizontal attenuation rate at sea level.

K = an empirical constant.

Weger** through a reiterative curve filtering process determined the value for the constant $K = 0.5$ which gives a good approximation for a standard maritime Polar Atmosphere with h expressed in kilometers.

Atmospheric oxygen content is dependent upon partial pressure and temperature, and hence is also altitude dependent. Weger has shown that oxygen attenuation in the region near a resonance line at an altitude h in kilometers can be described by the decaying exponential function:

$$A_1(h,\lambda) = A_i(0,\lambda)_{O_2} \; EXP\,(0.0886) \qquad (3\text{-}2)$$

In the wings of a resonance line, the exponential relation is:***

$$A_2(h,\lambda)_{O_2} = A_2(0,\lambda)_{O_2} \; EXP\,(-0.183h) \qquad (3\text{-}3)$$

Oxygen and water vapor attenuation at various altitudes has been reported by Talbert and Dickinson.**** These values as a function of frequency are shown in

---

* Std. Maritime Polar Atmos. "Handbook of Geophysics", Ref. Ed., U.S.A.F., ARDC, AFRD, GRD, New York, MacMillan Co., 1961.

** Weger, E., "The Atmospheric Background Apparent Temperature at Absorption Maxima of Water Vapor and Oxygen in the Microwave Region," Nortronics Technical Report No. 10041, July 1962.

*** Weger, E., Booth, T.L., "Final Report on Feasibility Study of Target Radiometry," Westinghouse Electrical Corporation, 26 June 1959.

**** Talbert, C.W., Dickinson, R.M., "Calculated Values of Absorption Due to Water Vapor and Oxygen in the Millimeter Spectrum," EERL Dept. No. 6-42, University of Texas, February 20, 1961.

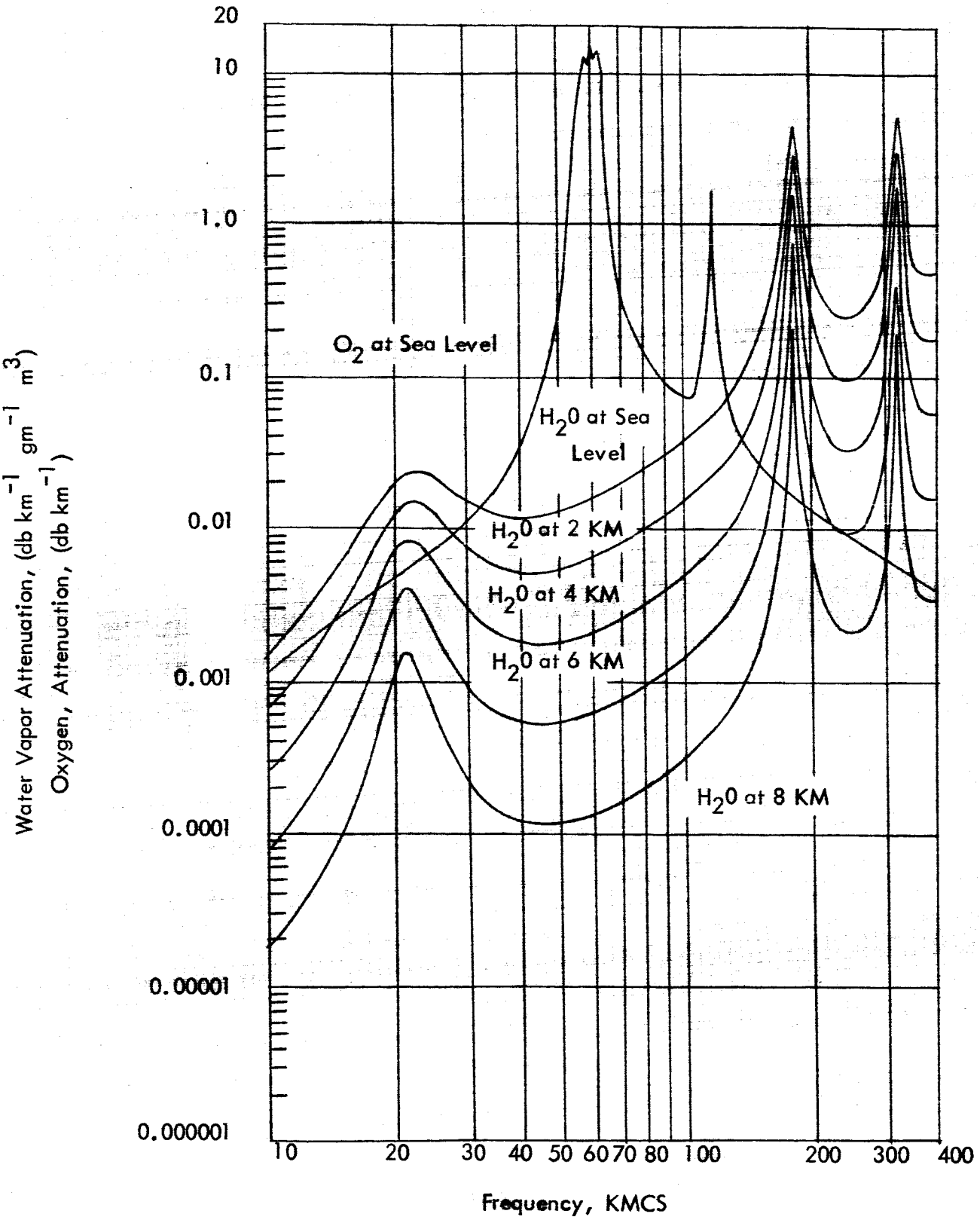

FIGURE 3-1. OXYGEN AND WATER VAPOR ATTENUATION FOR VARIOUS ELEVATIONS IN THE EARTH'S ATMOSPHERE

Figure 3-1. It should be noted that the water vapor attenuation rates shown in Figure 3-1 are given in units of db km^{-1} gm^{-1} m^3. Hence they must be multiplied by the water vapor density at each corresponding altitude and converted from the db notation into numericals to obtain the actual horizontal water vapor attenuation rate, $A(h, \lambda)$, as indicated in the previous expressions.

Considering now the effect of atmospheric attenuation on the observed flux intesity of an exo-atmospheric source, note that the received power can be represented in temperature units by the relationship:

$$\Phi A = K T_A \tag{3-4}$$

or:

$$T_A = \frac{\Phi A}{K \beta} \tag{3-5}$$

where:

K	=	Boltzmann's Constant
β	=	the frequency (cps) bandwidth of the receiver
T_A	=	the equivalent black-body temperature in degrees Kelvin
Φ	=	the intensity of the radiation in watts per unit area

From the solution of the electromagnetic wave equation, the intensity or power density at a point, r (for a wave moving in the slant range direction r), is in the steady state:

$$\Phi_r = \Phi_{r_o} EXP\left(-\int_{r_o}^{r} A_{(r)}\, dr\right) \tag{3-6}$$

where Φ_r is the intensity (watts per unit area) at r_o, at time zero and the integration is taken over the path from source to the sensor. Thus, the intensity of the traveling wave of radiation is exponentially attenuated, where $A_{(r)}$ is the attenuation coefficient of the

atmosphere in reciprocal units of length and r is the distance traveled. In general, $A_{(r)}$ is assumed to include all mechanisms (e.g., scattering and absorption).

Thus, the apparent temperature of the radiation at any point r, is directly proportional to the intensity at that point and:

$$T_{(r)} = T_{o(r_o)}\ EXP\left(-\int_{r_o}^{r} A(r,\lambda)\,dr\right) \qquad (3\text{-}7)$$

The integral $\int_{r_o}^{r} A_{(r,\lambda)}\,dr$ is the total attenuation over the path, therefore, $\exp\left(\int A_{(r,\lambda)}dr\right)$ is a measure of the total loss and may be written:

$$L = EXP\left(\int_{r_o}^{r} A_{(r,\lambda)}\,dr\right) \qquad (3\text{-}8)$$

For $L \geq 1$, it is convenient to express the loss in decibels, where:

$$L_{(db)} = 10\,LOG_{10}\,L = (10\,LOG_{10}e)\int A_{(r,\lambda)}dr \qquad (3\text{-}9)$$
$$= 4.343\int A_{(r,\lambda)}dr$$

In terms of the exponential decay coefficient, τ, path opacity:

$$\tau_{(r,\lambda)} = \int_{o}^{r} A_{(r,\lambda)}dr = 0.23\,L_{(r,\lambda)_{db}} \qquad (3\text{-}10)$$

The value of $A_{(h,\lambda)}$ may be written in terms of the sea level attenuation rate as:

$$A_{(h,\lambda)} = A_{(0,\lambda)}\ EXP(-Kh) \qquad (3\text{-}11)$$

hence:

$$L_{V(db)} = 4.343\, A_{(0,\lambda)} \int_0^h EXP(-Kh)\,dh \qquad (3\text{-}12)$$

where K is a constant in reciprocal units of length and the unit of length is considered to be the incremental vertical distance over which a prescribed value of the horizontal absorption coefficient is essentially constant, i.e,, horizontally stratified layers are assumed.

Thus:

$$L_{V(db)} = \frac{-4.343\, A_{(0,\lambda)}}{K} \left[1 - EXP(-Kh)\right] \qquad (3\text{-}13)$$

where the attenuation rate is given in db per unit of height (Δh). The attenuation ($A_{(0,\lambda)}$db) from Equation 3-13 is:

$$A_{(0,\lambda)_{db}} = \frac{-4.343\, A_{(0,\lambda)}}{K} \left[1 - EXP(-K\Delta h)\right] \qquad (3\text{-}14)$$

or:

$$A_{(0,\lambda)} = \frac{-0.23K\, A_{(0,\lambda)db}}{\left[1 - EXP(-K\Delta h)\right]} \qquad (3\text{-}15)$$

therefore:

$$L_{V(db)} = A_{(0,\lambda)_{db}} \left[\frac{1 - EXP(-Kh)}{1 - EXP(-K\Delta h)}\right] \qquad (3\text{-}16)$$

For large values of h, the total water vapor attenuation through the atmosphere can be calculated using Weger's value for $K = 0.5$ and Δ h of 1 km, as:

$$L_{V(db)} = A_{(0,\lambda)_{db}} \left[\frac{1}{1 - EXP(-0.5)} \right]$$

$$\approx 2.5\, A_{(0,\lambda)_{db}} \qquad (3\text{-}17)$$

where: $A_{(0,\lambda)_{db}}$ is determined as a function of frequency from the data of Talbert and Dickinson (Figure 3-1). It should be noted here that the factor of 2.5 indicated by Equation 3-17 is in agreement with the findings of A. O'Brian.* He concluded from a graphical integration of attenuation rates normalized to the sea-level rate, and plotted as a function of altitude that the total water vapor attenuation over a vertical path through the atmosphere is approximately 2.5 times the sea-level rate.

In a similar manner, the total oxygen absorption is:

$$L_{V_1(db)O_2} = A_{1(0,\lambda)_{db}} \left[\frac{1}{1 - EXP(-0.0886)} \right]$$

$$= 11.6\, A_{1(0,\lambda)_{db}} \qquad (3\text{-}18)$$

$$L_{V_2(db)O_2} = A_{2(0,\lambda)_{db}} \left[\frac{1}{1 - EXP(-0.183)} \right]$$

$$= 6\, A_{2(0,\lambda)_{db}} \qquad (3\text{-}19)$$

Since the total vertical attenuation is the sum of the water vapor and oxygen "losses" in db, the opacity is given by the relationship:

$$\tau_V = 0.23\, L_{V(db)} \qquad (3\text{-}20)$$

*A. O'Brian, "Atmospheric Attenuation at Microwave Frequencies," Ewen Knight Report.

From geometrical considerations, the slant range distance r is:

$$r = h \csc \Theta_H = h \sec \Theta_Z \tag{3-21}$$

and:

$$dr = dh \sec \Theta_Z \tag{3-22}$$

where: Θ_H is the elevation angle of observation measured from the horizon and Θ_Z is the angle measured from the zenith.

The atmospheric loss factor as a function of viewing angle, assuming a flat earth and horizontally stratified homogeneous atmospheric condition, is obtained by multiplying the db loss in the vertical direction by csc Θ_H or sec Θ_Z, e.g.:

$$L_{(r)} = EXP\left(\sec \Theta_Z \int_0^h A(h,\lambda)\, dh\right) \tag{3-23}$$

or:

$$L_{(r)_{db}} = 4.343 \int A(h,\lambda)\, dh \sec \Theta_Z = L_{(V)_{db}} \sec \Theta_Z \tag{3-24}$$

and:

$$\tau_r = 0.23\, L_{(V)_{db}} \sec \Theta_Z \tag{3-25}$$

From Equation 3-25, one can obtain a first order prediction of the atmospheric loss over any path through the atmosphere from knowledge of the sea-level water vapor content and the assumed exponential decay which describes the assumed water vapor content distribution with altitude for the existing weather conditions. A family of "k" values could, of course, be determined for various weather classes. This type of information is not useful, however, except where radio-sonde data is available. Calculated attenuation values are valid only on clear, "well-behaved" days.

Using the sea-level attenuation rates of Talbert and Dickinson, and the multiplication factors in Equation (3-17) and (3-19), the expected vertical attenuations at 35 Gc/s are:

(a) Oxygen attenuation = 0.12 db or 2.76×10^{-2} in units of opacity.

(b) Water vapor attenuation = 0.026 db/gm/M^8 or 0.006/gm/M^2, where gm/M^3 refers to 1 gram of pure water vapor per cubic meter of air.

These calculated values are consistent with those used by other investigators.

Oxygen attenuation is assumed to be constant at 0.12 db or 2.76×10^{-2} in units of opacity.

Water vapor attenuation is proportional to water vapor density in grams per cubic meter. The density of water vapor, P_W in grams per cubic meter is:

$$P_W = 216.68 \frac{e_W}{T} \tag{3-26}$$

where:

e_W = the water vapor pressure measured in millibars

T = the absolute temperature in degrees Kelvin

By introducing the appropriate constant of proportionality (0.006/gm/M^3), the expression for the water vapor opacity takes the form:

$$\tau_{H_2O} = 1.3 \frac{e_W}{T} \tag{3-27}$$

In general, the water vapor content is quite variable. Values between 1/gm/M^3 in winter and 20 gm/M^3 in summer are not uncommon. A value of 7.5 gm/M^3 is assumed for the standard atmosphere. Using the value of 7.5 gm/M^3 leads to a total opacity of:

$$\tau = \tau_{O_2} + \tau_{H_2O} = 0.0276 + 0.006 \times 7.5 = 0.073 \tag{3-28}$$

The presence of clouds and other atmospheric products can cause the total value to increase by an order of magnitude or more over that calculated above. In general, high values of τ will be associated with variable weather conditions typical of cloudy or overcast days. Under these conditions, a reliable prediction of attenuation by surface water vapor measurements is not obtained. A cloud cover monitor was used to great advantage during the program. Under scattered cloud conditions, this parallel recording of optical solar intensity easily identified those time periods when a cloud entered the ray path from the sun to the sensor.

To aid in the data reduction process, tabular values of the function $e^{\tau \sec \theta_z}$ were prepared for increments of 1 degree in zenith angle of observation covering the range of meridian crossing angles of the sun for the observing site. Values of τ in increments of 0.01 over the range from 0.03 to 0.15 were included in the Figure 3-2.

Referring to Figure 3-2, note that the correction varies from 17% to 43% under weather conditions where $\tau = 0.15$. Data obtained on days where τ exceeded 0.11 were, in general, eliminated from the monthly published values.

Empirical Determination of τ

During the first four-months of the observing period, an intensive effort was directed to an empirical determination of τ, obtained directly from the daily record of the observed antenna temperature as a function of the zenith angle of observation. The approach was predicated on the reasoning that the antenna temperature obtained when observing the sun may be expressed in the form:

$$T_A - T_{ATmos.} = (T_S - T_{ATmos.}) \, EXP(-\tau_{(r)}) \qquad (3\text{-}29)$$

or:

$$T_A = T_S \, EXP(-\tau_{(r)}) + T_{ATmos.} \left[1 - EXP(-\tau_{(r)})\right] \qquad (3\text{-}30)$$

ATMOSPHERIC CORRECTIONS FOR MERIDIAN CROSSING OF SUN, BOSTON LATITUDE

Dec. Angle	.03 Sec Θ_z e	.04 Sec Θ_z e	.05 Sec Θ_z e	.06 Sec Θ_z e	.07 Sec Θ_z e	.08 Sec Θ_z e	.09 Sec Θ_z e	.10 Sec Θ_z e	.11 Sec Θ_z e	.12 Sec Θ_z e	.13 Sec Θ_z e	.14 Sec Θ_z e	.15 Sec Θ_z e
-23	1.0744	1.1050	1.1270	1.1542	1.1821	1.2110	1.2410	1.2703	1.3015	1.3325	1.3643	1.3980	1.4320
-22	1.0716	1.0965	1.1223	1.1486	1.1752	1.2012	1.2306	1.2599	1.2882	1.3190	1.3492	1.3810	1.4130
-21	1.0690	1.0930	1.1180	1.1430	1.1684	1.1950	1.2220	1.2498	1.2778	1.3061	1.3359	1.3640	1.3959
-20	1.0666	1.0898	1.1136	1.1380	1.1625	1.1880	1.2138	1.2400	1.2677	1.2950	1.3222	1.3502	1.3819
-19	1.0645	1.0868	1.1100	1.1330	1.1570	1.1812	1.2061	1.2320	1.2578	1.2833	1.3113	1.3380	1.3678
-18	1.0625	1.0842	1.1056	1.1290	1.1520	1.1752	1.1991	1.2238	1.2490	1.2748	1.3001	1.3275	1.3540
-17	1.0605	1.0815	1.1128	1.1249	1.1470	1,1696	1.1930	1.2160	1.7405	1.2652	1.2901	1.3162	1.3419
-16	1.0587	1.0791	1.1000	1.1210	1.1428	1.1647	1.1870	1.2100	1.2325	1.2568	1.2805	1.3060	1.3300
-15	1.0571	1.0768	1.0970	1.1178	1.1382	1.1600	1.1824	1.2038	1.2258	1.2490	1.2720	1.2960	1.3200
-14	1.0556	1.0748	1.0944	1.1142	1.1346	1.1552	1.1762	1.1978	1.2194	1.2419	1.7642	1.2878	1.3110
-13	1.0542	1.0728	1.0918	1.1112	1.1307	1.1501	1.1717	1.1920	1.2138	1.2347	1.2570	1.2792	1.3019
-12	1.0527	1.0710	1.0895	1.1082	1.1272	1.1471	1.1670	1.1870	1.2078	1.2280	1.2499	1.2708	1.2938
-11	1.0516	1.0695	1.0875	1.1058	1.1249	1.1440	1.1632	1.1828	1.2016	1.2231	1.2443	1.2653	1.2860
-10	1.0504	1.0675	1.0852	1.1032	1.1212	1.1398	1.1589	1.1778	1.1970	1.2170	1.2370	1.2578	1.2780
- 9	1.0490	1.0660	1.0831	1.1005	1.1182	1.1362	1.1549	1.1731	1.1921	1.2118	1.2223	1.2502	1.2708
- 8	1.0480	1.0646	1.0814	1.0984	1.1159	1.1339	1.1512	1.1693	1.1881	1.2065	1.2200	1.2456	1.2645
- 7	1.0470	1.0633	1.0796	1.0964	1.1135	1.1304	1.1482	1.1660	1.1838	1.2021	1.2216	1.2400	1.2592
- 6	1.0461	1.0620	1.0780	1.0944	1.1110	1.1279	1.1450	1.1622	1.1800	1.1980	1.2160	1.2342	1.2503
- 5	1.0453	1.0607	1.0765	1.0925	1.1090	1.1252	1.1420	1.1590	1.1762	1.1939	1.2116	1.2299	1.2479
- 4	1.0444	1.0596	1.0750	1.0907	1.1068	1.1228	1.1390	1.1558	1.1730	1.1898	1.2072	1.2247	1.2425
- 3	1.0436	1.0850	1.0737	1.0890	1.1046	1.1204	1.1362	1.1530	1.1692	1.1860	1.2030	1.2203	1.2380
- 2	1.0428	1.0750	1.0724	1.0874	1.1037	1.1182	1.1339	1.1500	1.1660	1.1725	1.1990	1.2160	1.2330
- 1	1.0420	1.0640	1.0710	1.0859	1.1100	1.1160	1.1318	1.1472	1.1632	1.1790	1.1955	1.2122	1.2295
0	1.0414	1.0556	1.0700	1.0845	1.0993	1.1142	1.1292	1.1450	1.1601	1.1761	1.1920	1.2083	1.2250
+ 1	1.0407	1.0546	1.0689	1.0831	1.0976	1.1123	1.1271	1.1426	1.1529	1.1730	1.1890	1.2050	1.2210
+ 2	1.0401	1.0537	1.0678	1.0819	1.0961	1.1106	1.1250	1.1406	1.1552	1.1707	1.1860	1.2050	1.2172
+ 3	1.0396	1.0530	1.0667	1.0805	1.0945	1.1080	1.1236	1.1380	1.1530	1.1678	1.1828	1.1980	1.2140
+ 4	1.0389	1.0522	1.0658	1.0794	1.0933	1.1072	1.1215	1.1360	1.1507	1.1650	1.1800	1.1952	1.2110
+ 5	1.0384	1.0516	1.0649	1.0788	1.0919	1.1059	1.1199	1.1340	1.1484	1.1628	1.1778	1.1920	1.2078
+ 6	1.0379	1.0508	1.0640	1.0773	1.0907	1.1044	1.1180	1.1322	1.1462	1.1603	1.1752	1.1898	1.2048
+ 7	1.0375	1.0502	1.0632	1.0762	1.0895	1.1030	1.1169	1.1305	1.1441	1.1582	1.1730	1.1870	1.2019
+ 8	1.0370	1.0496	1.0625	1.0754	1.0885	1.1016	1.1150	1.1290	1.1427	1.1568	1.1708	1.1850	1.1990
+ 9	1.0366	1.0490	1.0616	1.0744	1.0874	1.1005	1.1138	1.1270	1.1408	1.1542	1.1682	1.1822	1.1963
+10	1.0362	1.0484	1.0610	1.0734	1.0863	1.0993	1.1122	1.1258	1.1391	1.1523	1.1660	1.1800	1.1942
+11	1.0357	1.0479	1.0603	1.0723	1.0853	1.0982	1.1112	1.1241	1.1372	1.1510	1.1645	1.1779	1.1920
+12	1.0353	1.0474	1.0596	1.0720	1.0845	1.0970	1.1100	1.1228	1.1360	1.1490	1.1625	1.1762	1.1895
+13	1.0350	1.0470	1.0591	1.0710	1.0835	1.0960	1.1089	1.1215	1.1348	1.1473	1.1610	1.1742	1.1880
+14	1.0347	1.0464	1.0585	1.0705	1.0827	1.0950	1.1078	1.1202	1.1330	1.1462	1.1590	1.1722	1.1860
+15	1.0344	1.0460	1.0578	1.0697	1.0820	1.0942	1.1069	1.1191	1.1319	1.1445	1.1578	1.1709	1.1839
+16	1.0341	1.0456	1.0574	1.0692	1.0812	1.0934	1.1058	1.1180	1.1306	1.1431	1.1562	1.1691	1.1822
+17	1.0338	1.0451	1.0568	1.0686	1.0804	1.0925	1.1046	1.1170	1.1292	1.1418	1.1547	1.1672	1.1803
+18	1.0334	1.0448	1.0564	1.0680	1.0798	1.0916	1.1370	1.1158	1.1282	1.1416	1.1532	1.1660	1.1790
+19	1.0332	1.0446	1.0560	1.0675	1.0792	1.0910	1.1300	1.1150	1.1270	1.1396	1.1520	1.1649	1.1778
+20	1.0329	1.0441	1.0556	1.0670	1.0786	1.0904	1.1220	1.1142	1.1262	1.1383	1.1510	1.1632	1.1762
+21	1.0327	1.0438	1.0551	1.0665	1.0780	1.0895	1.1150	1.1133	1.1252	1.1372	1.1500	1.1622	1.1742
+22	1.0324	1.0435	1.0547	1.0660	1.0775	1.0890	1.1050	1.1124	1.1274	1.1362	1.1488	1.1610	1.1732
+23	1.0323	1.0433	1.0543	1.0655	1.0770	1.0884	1.1000	1.1117	1.1237	1.1358	1.1476	1.1600	1.1720

FIGURE 3-2

Since:

$$L_{(r)} = EXP(\tau_r) \tag{3-31}$$

Then:

$$T_A = \frac{T_S}{L_r} + \left(1 - \frac{1}{L_r}\right) T_{ATMOS.} \tag{3-32}$$

where:

$T_{ATMOS.}$ = the mean temperature along the observing path through the atmosphere

T_S = the effective antenna temperature contributed by the sun in the absence of the atmosphere

The first term in Equation (3-32) is the attenuated sun temperature, the second is the "reradiated" atmospheric temperature.

Since an expanded beam comparison technique was used, the "reradiation" term was cancelled and the expression for the observed antenna temperature was then:

$$T_A = K_S \left(\frac{T_S}{L_r}\right) = K_S T_S EXP(-\tau_{(r)})$$

$$= K_S T_S EXP(-\tau_V \sec \theta_Z) \tag{3-33}$$

where K_S is a system constant. Normalizing the expression to the internal noise calibration source T_{cal}:

$$\frac{T_A}{T_{CAL}} = K_S \left(\frac{T_S}{T_{CAL}}\right) EXP(-\tau_V \sec \theta_Z) \tag{3-34}$$

Redefining the system constant such that:

$$\frac{K_S T_S}{T_{CAL}} = \frac{n K_S' T_S}{T_{CAL}} = \frac{n T_{A_O}}{T_{CAL}} \equiv 1 \qquad (3\text{-}35)$$

then:

$$K_S = n K_S' = \frac{T_{CAL}}{T_S} \qquad (3\text{-}36)$$

where K_S' is the reciprocal of receiver system gain factor ($K_S' = T_{AO}/T_S$) and is independently determined. The quantity n is the numeric required to adjust the intercept of the log plot of Equation (3-36) to unity, i.e.,

$$LOG_e \frac{T_A}{T_{CAL}} = LOG_e \left(\frac{K_S' T_S}{T_{CAL}}\right) - \tau_V \sec \theta_Z \qquad (3\text{-}37)$$

Variations in the reciprocal of n provide a measure of the variations in the normalized value of T_S. That is:

$$\frac{\left(\frac{1}{n}\right)}{\left(\frac{T_S}{T_{CAL}}\right)} = \frac{\left(\frac{T_{A_O}}{T_{CAL}}\right)}{\left(\frac{T_S}{T_{CAL}}\right)} = K_S' \, EXP\left(-\tau_V \sec \theta_Z\right) \qquad (3\text{-}38)$$

The value of T_{AO}/T_{CAL} is determined by interpolation of the measured data points to a "best fit" plot of Equation (3-38) at $\sec \theta_Z = 0$.

$$LOG_e\left(\frac{T_A}{T_{CAL}}\right) = LOG_e\left(\frac{K_S' T_S}{T_{CAL}}\right) - \tau_V \sec \theta_Z \qquad (3\text{-}39)$$

The path opacity is determined by normalizing the plot to a unity intercept. The functional relationship between Θ_Z and transit time of the sun is:

$$\cos \Theta_Z = \sin \phi \sin \delta + \cos \phi \cos \delta \cos H \qquad (3\text{-}40)$$

where:

Θ_Z = zenith angle of observation

ϕ = the latitude of the observing site

δ = the declination of the source

H = the local hour angle with respect to the source $= \pi t / 12$

t = time from transit in hours

Thus:

$$t = \frac{12}{\pi} \sec^{-1} \left[\frac{\cos \phi \cos \delta}{\cos \Theta_Z - \sin \phi \sin \delta} \right] \qquad (3\text{-}41)$$

The effect of a time varying atmospheric attenuation can be derived by assuming that the attenuation varies linearly with time in the form:

$$\tau = \tau_o + \left| \frac{\Delta \tau}{\Delta t} \right| \left| \frac{12}{\pi} \right| \sec^{-1} \left| \frac{\cos \phi \cos \delta}{\cos \Theta_Z - \sin \phi \sin \delta} \right| \qquad (3\text{-}42)$$

where: $\Delta \tau / \Delta t$ = the rate at which the opacity is changing.

The expression for the attenuation ratio under this condition becomes:

$$\log_e \left(\frac{T_A}{K_S' T_S} \right) = - \left[\tau_o + \left| \frac{12}{\pi} \right| \left| \frac{\Delta \tau}{\Delta t} \right| \sec^{-1} \left| \frac{\cos \phi \cos \delta}{\cos \Theta_Z - \sin \phi \sin \delta} \right| \right] \qquad (3\text{-}43)$$

$$LOG_e\left(\frac{T_A}{K_S' T_S}\right) = \left[-\tau_o + \left(\frac{12}{\pi}\right)\left(\frac{\Delta\tau}{\Delta t}\right) H_{(RADIANS)} \right] \qquad (3\text{-}44)$$

It is apparent that if the attenuation changes linearly at a rate of $-\Delta\tau/\Delta t$, and data are taken over a sizeable range of sec θ_Z on either side of transit, then the average of pre- and post-transit values will provide an indication of the true attenuation at transit as well as the contribution to effective antenna temperature provided by the sun. An interpolation of the morning data only, would give a high sun temperature and the interpolation of the afternoon data only would give a low sun temperature. The reverse would be true for an attenuation change rate of $+\Delta\tau/\Delta t$.

The gross effect of averaging data on a cloudy day leads to an apparent decrease in attenuation as the sun is tracked to transit and an increase in attenuation as it is tracked from transit to sunset, since there is a higher probability of viewing through a cloud at small values of θ_Z.

Several graphical plots of the observed data were made over a period of three months. The results were very discouraging except on days of relatively clear stable weather conditions. Under these conditions, close agreement was found with the previously described technique used for computing τ directly from measured values of temperature and relative humidity. After several unsuccessful attempts to arrive at methods by which a high level of confidence could be assigned to the method of empirical measurement of τ, the technique was abandoned and all data thereafter was reduced in accord with correction factors determined from temperature and humidity measurements at the site.

4.0 EQUIPMENT DESCRIPTION

The solar patrol telescope consists of an Antenna Complex and a Control and Data Readout Console. The antenna complex is a modified SCR-584 Radar Van. Modifications include: equatorial mounting of the SCR-584 antenna pedestal and incorporation of dual parabolic antennas and RF Heads which comprise the sensor portion of the radiometric receivers. The antenna and mount are contained within a 12-foot diameter air-supported radome attached to the top of the van. Pressurizing blowers are located within the van. Personnel access is provided via an air lock chamber immediately inside the van door.

Pyramidal horns are used as the primary feeds for the parabolic secondary reflectors at both frequencies. The antennas are linearly polarized parallel to the local meridian when the mount is in the "transit position".

A photograph of the Antenna Complex with radome removed is shown in Figure 4-1.

The video signal output of each radiometer is fed by an underground cable between the Antenna Complex to the Control and Data Readout Console which is located in the Ewen Knight Laboratory. This Console contains all controls necessary for the operation of the antenna, axis position readout indicators for the antenna, antenna programming circuitry as well as the IF amplification and video signal processing portions of each radiometer channel.

A photograph of the Control and Data Readout Console in its original configuration is shown in Figure 4-2. The dual channel strip chart recorder was replaced in April 1966 by a six-channel unit provided on loan by NASA-ERC.

The original intent was to preprogram the mount for automatic start on three successive days of observation. Circuitry is included in the system for achieving this function. The accuracy of the clock mechanism however is not adequate to achieve precise positioning since

the positioning requirement was increased by a factor of 2 over that originally anticipated by use of antennas whose apertures are twice the original design diameters. The 35 GHz system utilizes a 4-foot antenna aperture providing a 3 db beam angle resolution of 0.5^{o}. The 75 GHz system is currently equipped with a 2-foot diameter antenna aperture providing a beam angle of 0.45^{o}.

The sensitivity of the 35 GHz system has been consistently 1.5°K rms for a post-detection integration time constant of 1 sec. The 75 GHz system in its recently modified form has provided a consistent rms sensitivity of 3°K for a post-detection integration time constant of three seconds. The original design was predicated on integration time constants of ten seconds at both frequencies, however, the detection of ESB suggested reduction of the time constants to the values noted above.

FIGURE 4-1
MILLIMETER ANTENNA COMPLEX WITH RADOME REMOVED

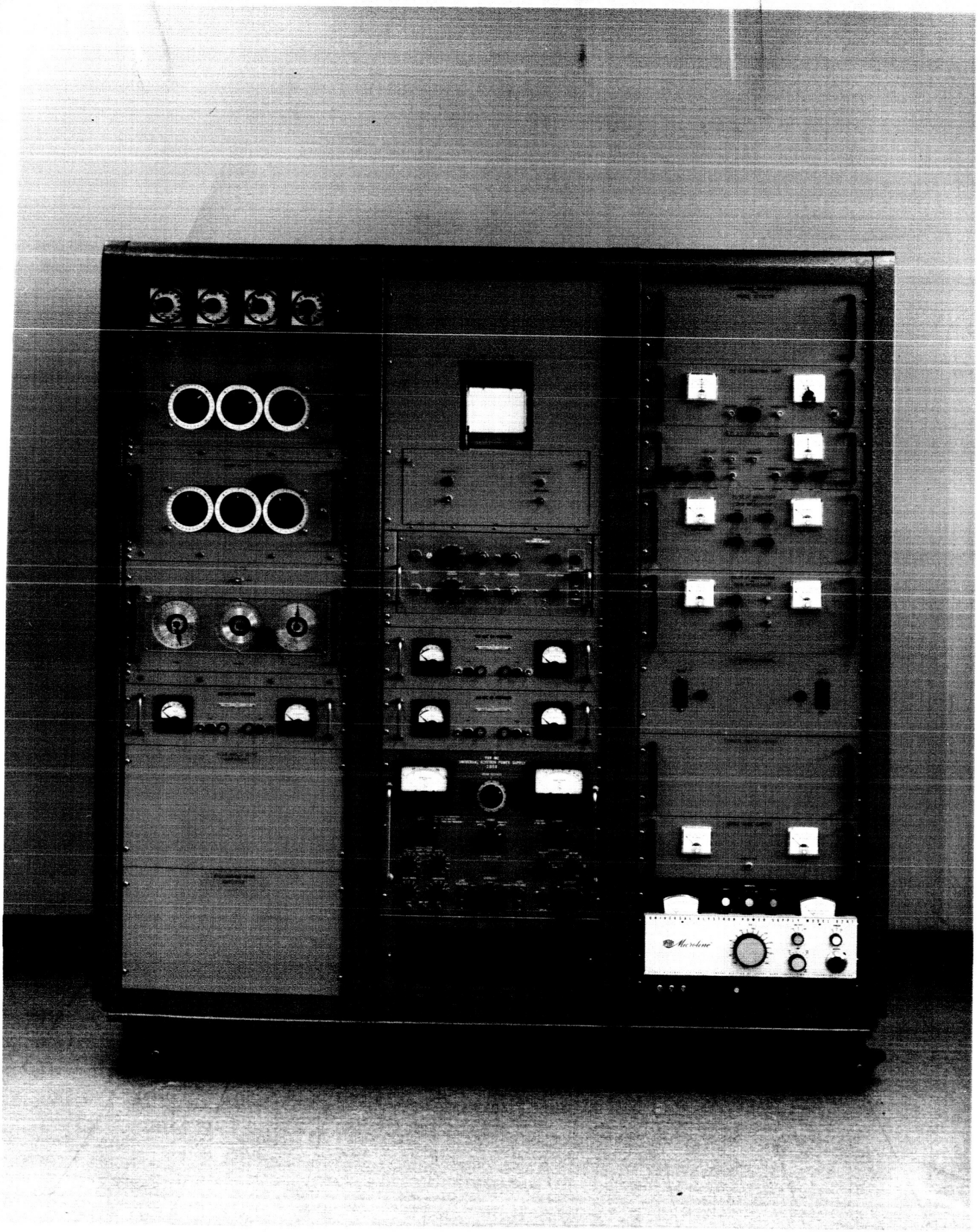
Microlume

FIGURE 4-2
CONTROL AND DATA READOUT CONSOLE

5.0 OBSERVING PROCEDURES

It is difficult to establish the most appropriate observing procedure for the detection of an undefined phenomena at the outset of an observing program. As might have been anticipated, the operating procedure was revised on numerous occasions throughout the one-year period of observation. Each change reflected added experience with the equipment as well as the solar phenomena under investigation. The most recent revision in the observing procedure was introduced early in May 1966 to accommodate methods for accumulating optimum data, utilizing the 6-channel recorder coupled with concentration on detection of ESB phenomena.

The chart presentation provides a time marker on the right-hand margin indicating one minute and 30-minute time intervals. Data channel records beginning with the one adjacent to the time marker are:

35 GHz Expanded Scale - 2.5 x the "Normal Scale" value with zero suppression to provide an average deflection of 10 to 15 millimeters from the right side of the chart recording, with an increase in solar intensity corresponding to a deflection to the left.

35 GHz Normal Scale - Full scale deflection from sky zero to the sun level corresponding to a nominal value of 40 millimeters with zero suppression to 15 millimeters from the right-side of the chart paper.

75 GHz Expanded Scale - 2 x the Normal Scale value with zero suppression to an average value of 15 mm from the right-side of the channel recording, with an increase in solar intensity corresponding to a deflection to the left.

75 GHz Normal Scale - Full scale deflection from sky zero to the sun level corresponding to a nominal value of 40 millimeters with zero suppression to 15 mm from the right-side of the chart paper.

Cloud Cover Monitor - Zero cloud level x, clear day, set at approximately 5 mm from the left side of the chart recording, with night-time level set near 1 millimeter from the right side of the chart recording.

(Minor modifications of the procedure on a day to day basis are based on observer judgement).

To chart paper rate is set at 25 mm per minute (1.5 meters per hour). At the beginning of each two-hour period (starting at 7:15 A.M. EST), the pen indicator on the "Normal Scale" for both channels is adjusted for a 5 mm deflection from the right side of the chart recording. The sun level is set at approximately 40 mm of deflection to the left from sky zero. Internal noise source calibration signals are then inserted simultaneously in the comparison arm of both radiometers, providing a negative deflection (to the right) to obtain a measure of the ratio of the signal level to the calibration level. The calibration sources are then extinguished. When the indicator pens return to their original sun level, the zero or sky level is suppressed off-scale to the right to bring the average indicator deflection on both channels to a level of 15 mm from the right side of each chart. This accomodates the measure of a burst increase up to 85% above the quiet sun level. This "headroom" corresponds to 1,700 flux units at 35 GHz and 6,000 flux units at 75 GHz.

The expanded channels at both frequencies are zero suppressed to an average level of 15 mm from the right-hand side of their respective chart recordings.

The antenna position is carefully adjusted in both declination and hour angle to assure that a peak intensity is received on both channels.

The antenna is then positioned forward of the sun (west in hour angle), and a drift scan obtained to verify sky zero, average sun level, expanded scale gain, and symmetry of peak intensities on all channels. For this drift scan, zero suppression is removed on both Normal Channels.

REFERENCES

1. R. J. Coates, J.E. Gibson, and J. P. Hagen, "The 1954 Eclipse Measurement of the 8.6 MM Brightness Distrib ution, "Astrophysical Journal, vol. 128, pp. 406-415, September 1958.

2. R.J. Coates, "A Model of the Chromosphere from Millimeter Wavelength Observations," Astrophysical Journal, vol. 128. pp. 83-91, July 1958.

3. R. J. Coates, "Measurements of Solar Radiation and Atmospheric Attenuation at 4.3 Millimeters Wavelength," Proc. IRE, vol. 46, pp. 122-126, January 1958.

4. H. Tanaka and T. Kakinuma, "The Relation Between the Spectrum of Slowly Varying Component of Solar Radio Emission and Solar Proton Event, " Rept. Ionosphere Space Res. Japan, vol. 18 pp 32-44, No. 1, 1964.

5. J. Copeland, "Radio Observations of the Moon and Venus at 8.6 MM Wavelength, "Ewen Knight Corporation Doc # 1088, Contract No. NASw-593.

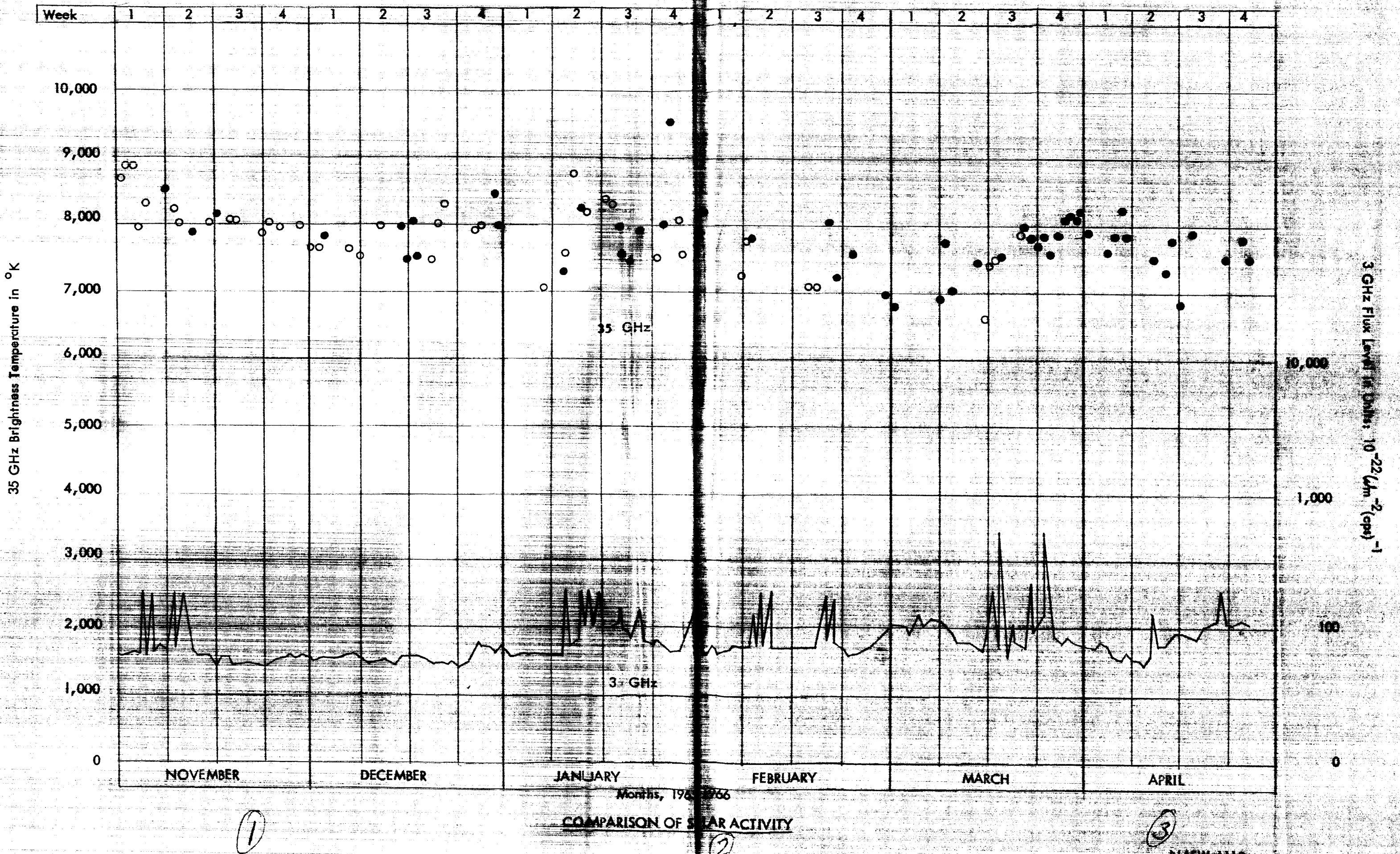

COMPARISON OF SOLAR ACTIVITY

NASW-1118

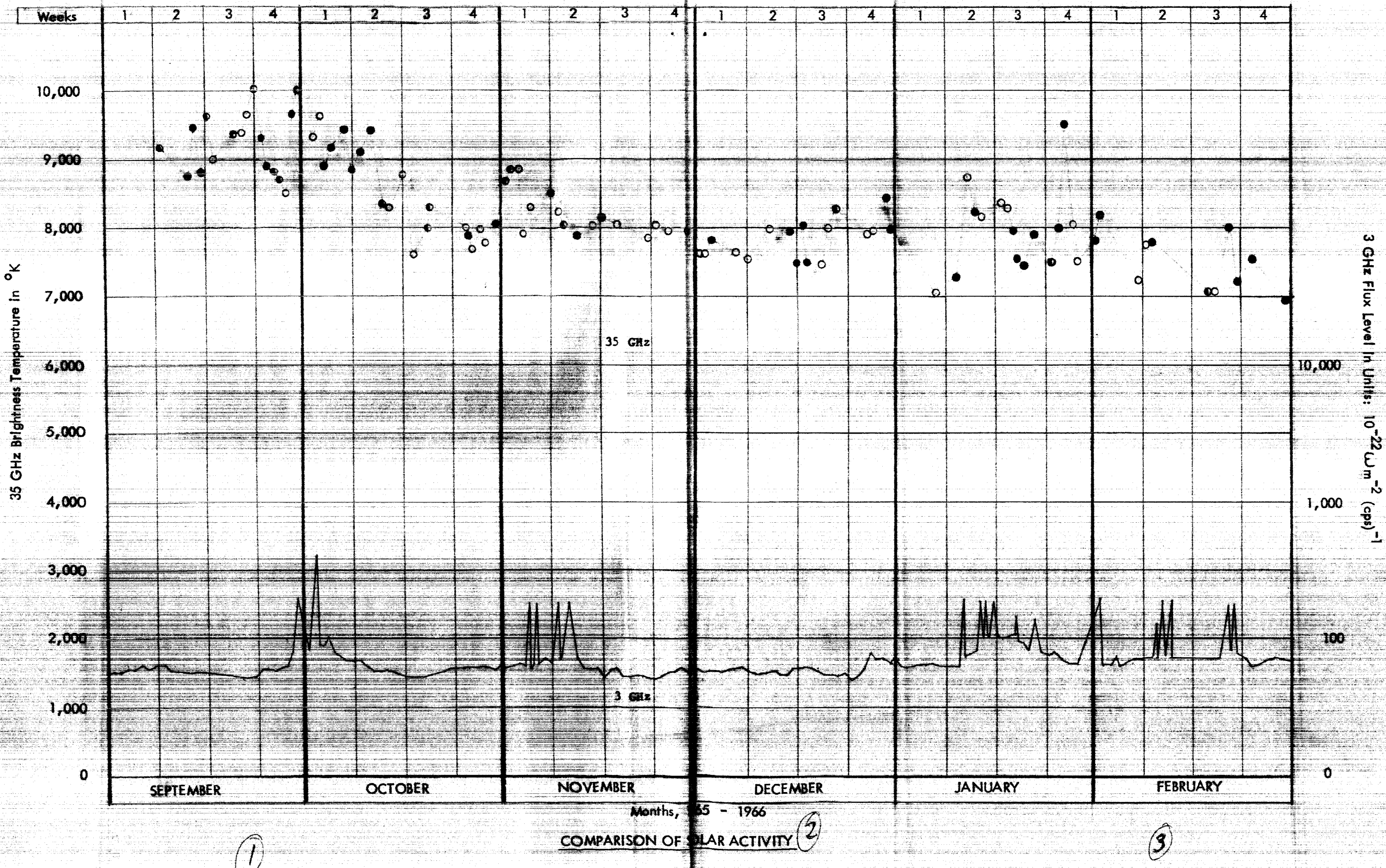

COMPARISON OF SOLAR ACTIVITY (2)

(1) (3)